Spontaneous Synchronization of Josephson Junctions and Fiber Lasers

A Thesis
Presented to
The Academic Faculty

by

Denis Tsygankov

In Partial Fulfillment
of the Requirements for the Degree
Doctor of Philosophy

School of Physics
Georgia Institute of Technology
August 2005

Spontaneous Synchronization of Josephson Junctions and Fiber Lasers

Approved by:

Dr. Kurt Wiesenfeld, Advisor
School of Physics
Georgia Institute of Technology

Dr. Turgay Uzer
School of Physics
Georgia Institute of Technology

Dr. Predrag Cvitanović
School of Mathematics
Georgia Institute of Technology

Dr. Rigoberto Hernandez
School of Chemistry and Biochemistry
Georgia Institute of Technology

Dr. Michael F. Schatz
School of Physics
Georgia Institute of Technology

Date Approved: 15$^{\text{th}}$ July 2005

ACKNOWLEDGEMENTS

First of all I would like to thank my adviser, Kurt Wiesenfeld, who made possible my scientific maturity and the creation of this thesis. Aside from being a great scientist, he was the best mentor I could ever imagine. Giving me the freedom of an independent researcher, he unostentatiously guided me through my work. Every talk we had for the last four years was extremely helpful both for my theoretical progress and the development of proper scientific thinking. From him I could always find support, understanding and encouraging criticism regardless of the craziness of my new idea.

A part of my thesis is devoted to the study of coupled fiber lasers, which I did in parallel with a postdoctoral fellow, Slaven Peles, who has worked on some other aspects of the same problem. I had many useful conversations with Slaven and I would like to acknowledge his help and willingness to collaborate.

Being a member of the Center for Nonlinear Science community, I also had the support and attention of its leader, Predrag Cvitanović, who has been doing a great job managing the friendly working environment in our center.

I would also like to thank Andrew Zangwill, who was one of the best lecturers I have ever met, making my comprehensive examination a substantially easier task after a year of working hard on his homework assignments. Besides, he was a tireless graduate coordinator readily assisting me with any problem. I also thank him for financial support during my last semester at Georgia Tech.

Finally, I would like to express my sincere gratitude to all members of my thesis committee, who agreed to review my work, which might not be the easiest mission in the world considering the number of tedious calculations included. I assure them that they were necessary for me to gain a full understanding of the phenomena I observed during my research.

My last words of appreciation go to all the professors, postdocs and students that I met in the School of Physics and who made my years at Georgia Tech enjoyable and memorable.

TABLE OF CONTENTS

LIST OF FIGURES

SUMMARY

This work is devoted to the study of the phenomenon of spontaneous synchronization in systems of coupled nonlinear oscillators. The first chapter provides a step by step introduction to the basic concepts associated with oscillations, nonlinearity, coupling, collective dynamics and corresponding phenomena, especially synchronization. Examples from diverse natural and technological systems are given in order to demonstrate the importance of an understanding of such phenomena.

However, the main focus of the following chapters is on a special type of oscillator array with a non-trivial dynamical coupling. Although such systems are quite common, they have been studied relatively little. Most researchers typically consider models with direct coupling of some nature. In contrast, this work dials with nonlinear oscillators coupled through a dynamical object, which can provide a resonant structure or other benefits for the overall synchronization. Two contemporary experimental systems considered in the thesis are particularly interesting from this perspective.

Chapter 2 is devoted to the problem of Josephson junctions embedded in a transmission line. It is a transmission line that plays the role of dynamical coupling. This chapter includes introductory sections with historical background and detailed derivations of all necessary equations, which are then used to provide theoretical description of the system. One of the most interesting results of this chapter is a new pairing phenomenon, which is explained by both analytical and numerical analysis.

Another interesting phenomenon of weak-link synchronization is presented in chapter 3 in the context of a system of coupled fiber lasers. In this case the dynamical coupling is provided by the oscillators themselves. Basically, this is a hybrid system of qualitatively different oscillators. This new phenomenon can be potentially important for systems where conventional direct coupling fails to produce a synchronized state due to intrinsic variations of oscillator parameters.

Although the Josephson transmission line and coupled fiber lasers are very different systems, both of them demonstrate the advantages of dynamical coupling and corresponding resonant structures, which will hopefully motivate further fundamental studies in this field as well as useful industrial application.

CHAPTER I

INTRODUCTION

1.1 Nonlinear Oscillators

Many processes evolving in the real world can be understood as an oscillatory behavior in one way or another. From the theoretical point of view, oscillation is a basic concept expressed in terms of various differential equations and iterated maps to model diverse physical problems [1, 2].

Practical problems in physics can be described by linear equations only in rare situations. Usually a nonlinear approach is required for description of a real physical system. Though quantum mechanical wave functions obey the superposition principle, very often the description in terms of wave functions requires infinite dimensionality, which makes the problem as hard as nonlinear ones. Actually, many finite-dimensional nonlinear problems can be adequately represented as infinite-dimensional linear systems by some transformation. As a rule, linearization of a nonlinear process leads to a correct description of this system only locally in phase space. A linear description is a matter of exceptional cases; generic systems in nature are rather nonlinear.

Many different oscillating systems have in common the property of keeping their own rhythm of oscillations even after being isolated. This rhythm must be maintained by some internal source of energy that compensates for the dissipation, and it is determined by properties of the system itself. These oscillators are called autonomous and belong to a class of nonlinear problems known as self-sustained oscillations [3].

The principal features of self-sustained oscillators modeling natural phenomena are dissipation, stability and nonlinearity. There are some systems in nature, such as orbiting planets or vibrating molecules, that can be accurately described as conservative systems. But in most cases the dissipation of system energy takes place because of electrical resistance, mechanical friction or some other process. Thus, such an oscillation would eventually

decay without a constant energy supply. The most important difference between dissipative and conservative systems is the stability of oscillations with respect to small perturbations. From the mathematical point of view, the stability in dissipative systems is a result of phase volume decrease, which is not the case for conservative systems that preserve the initial phase volume and, consequently, have no attractors. The key concept in the theory of self-sustained oscillators is the stable limit cycle, and an essential ingredient for maintaining limit cycle oscillations is nonlinearity. As a rule, linear systems with periodic oscillations are conservative. Moreover, linear systems that have an energy source but no dissipation or visa versa cannot have a limit cycle, but only growing or decaying solutions.

There are many examples of nonlinear self-sustained oscillators. One of the most studied is the driven Van der Pol oscillator [4]:

$$\ddot{x} - \gamma(1 - x^2)\dot{x} + \omega_0^2 x = g\cos(\omega_D t). \tag{1}$$

It has a dissipation term, which is negative for small amplitudes, supplying energy to the system, and positive for large amplitudes. Therefore, spontaneous self-sustained oscillations can be observed even without periodic driving. Van der pol and van der Mark studied a simple electronic circuit where the negative dissipation was provided by a negative resistance region in the I-V characteristic of a neon tube. When this oscillator is driven at a frequency which is different from its free oscillation frequency, the nonlinear phenomenon of frequency locking is observed.

Another well-known nonlinear oscillator used to model various physical, engineering and even biological problems is the Duffing oscillator [5, 6]:

$$\ddot{x} + \gamma\dot{x} \pm \omega_0^2 x + \beta x^3 = g\cos(\omega_D t), \tag{2}$$

which provides a demonstration of several interesting phenomena such as nonlinear resonance, bifurcations, hysteresis and secondary resonances. The driven Duffing oscillator also shows chaotic behavior.

Such a rich variety of interesting phenomena and complex behavior that has no counterpart in linear systems provides a strong motivation for studying nonlinear self-sustained

oscillators.

1.2 Coupled Nonlinear Oscillators

Many systems, both natural and artificial, consist of oscillating components interacting with each other and producing a collective behavior in the form of complex spatio-temporal patterns. Researchers have been studying cooperative behavior of interacting nonlinear oscillators in relation to different phenomena such as nonlinear waves, collective transport, clustering and synchronization. Systems that produce such behavior include: arrays of Josephson junctions, central pattern generators in biological systems, arrays of coupled lasers, communication systems via chaotic oscillators, charge-density waves, chemical reactions and cardiac tissue, competing species in population dynamics, thin film fabrication, bubble behavior in fluidization and mixing processes, fireflies that emit rhythmic light pulses, earthquakes, and active nonlinear antenna and radar systems [7, 8, 9, 10, 11].

This thesis is devoted to the detailed study of Josephson junction and fiber laser arrays, but in this introduction I would also like to describe briefly several other systems mentioned above.

A number of unusual nonlinear phenomena can be generated by inherently nonlinear systems of active antennas. Over the years, researchers have developed extensive analysis and new control techniques to manipulate these dynamical systems. Active antenna and radar systems consist of coupled nonlinear cells, such as van der Pol oscillators, interacting with each other dynamically, to form an amplitude and phase pattern creating a specific beam characteristic. In contrast, traditional antenna and radar systems consist of passive linear elements that act independently, and they require a lot of external components, such as steering mechanisms and phase shifters, to control the beam position and shape [12, 13, 14].

The study of earthquake faults is very important [15, 16, 17, 18], but a deep understanding of such complex phenomena as earthquakes is a serious challenge for physicists and mathematicians. The most spectacular feature of earthquakes is that they occur over an enormous range of scales. The observed distribution of sizes of seismic activity is a

power law over more than ten orders of magnitude. This power-law distribution of event sizes is known as the Gutenberg-Richter law. It is one of the most fundamental discoveries in the field of seismology. Earthquake faults occur as a result of frictional instabilities in the upper ten kilometers of the Earth crust. Accumulated over hundreds of years, stress is then suddenly relieved in a stick-slip fashion. Tectonic plates move in response to large-scale convective flows in the mantle.

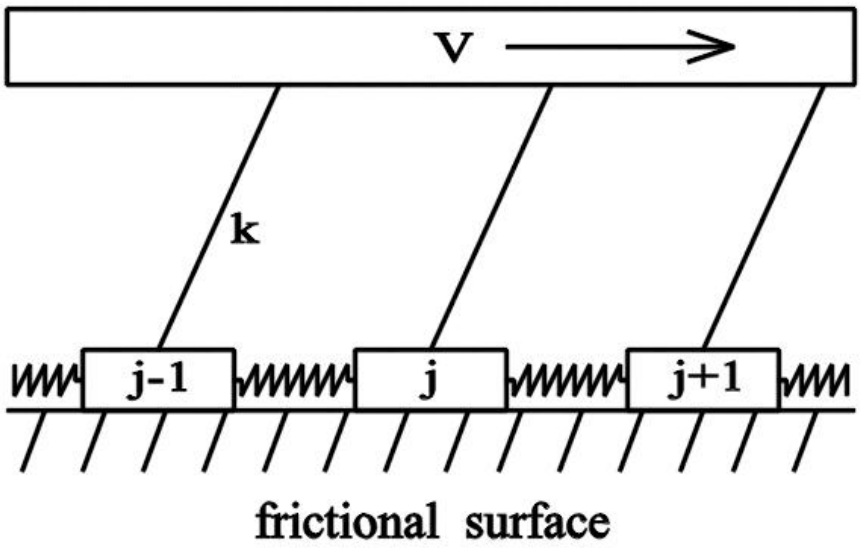

Figure 1: Schematic of the Burridge-Knopoff model.

In 1967 Burridge and Knopoff proposed a simple nontrivial model of earthquakes [19]. They introduced a chain of blocks harmonically interacting with their nearest neighbors. These blocks represent a lubricant between sliding surfaces. Each block interacting with the lower surface by a phenomenological dry-friction law, but the interaction with the upper surface is modelled by springs. The upper surface moves horizontaly with very small constant velocity V, called the sliding velocity (See Fig. 1):

$$\ddot{x_j} + F_{fric}(\dot{x}) = x_{j+1} - 2x_j + x_{j-1} + k(Vt - x_j), \tag{3}$$
$$F_{fric}(V) = \frac{\text{sign}(V)}{1 + 2\alpha|V|}.$$

Though this spring-block model is spatially uniform and has no built in irregularities or

added noise, it has a deterministically chaotic dynamics and behavior that is quite similar to the behavior of real earthquake faults. Most important is that the model produces spatially localized earthquake events with a broad spectrum of scales from small to large. These earthquake events relocate stress from one point to another, but they do not relieve stress in the whole system. The model also shows large spatially extended events that have epicenters of strong slipping pulses, which then propagate along the fault and unload the stress on large parts of the system. The small events fit a power-law size distribution similar to the Guntenberg-Richter law. But the large events occur randomly on a time period of the order of loading time. After Bak, Tang and Wiesenfeld discovered that crustal faults exhibit self-organized criticality [20, 21], the behavior of nontrivial spring-block models of earthquake fault regained the attention of the scientific community.

Chemical oscillations have been present in nature since the beginning of the existence of life. Actually, living organisms have hundreds of chemical oscillators. However, the study of nonlinear chemical dynamics in general and oscillating chemical reactions in particular is a relatively young discipline [1, 22]. Chemical oscillations are different from, for example, the traditional pendulum in that they never pass through their equilibrium point. Therefore, a chemical reaction oscillates in a far-from-equilibrium regime and should be described by non-equilibrium thermodynamics. The model of diffusively coupled cells turns out to be a useful approximation of a continuous medium. In principle, this approximation can be made as accurate as required. The dynamics of chemical oscillators and other diffusive systems have been successfully described by such reaction-diffusion models. The best known and studied oscillating reaction is the Belousov-Zhabotinsky reaction [23]. If we isolate a small element of this chemical solution from the whole medium, it will still produce limit cycle oscillations. This suggests that the behavior of the total system can be understood as the collective dynamics of diffusively coupled limit cycle oscillators.

Obviously, systems in the real world such as in living organisms are never ideally homogeneous. They always have spatial structures of some sort. Naturally, the behavior of identical oscillators interacting through a short-range diffusive coupling exhibits ordered motions of different types (modes). Indeed, since the interaction range is finite, any local

event will affect distant points of the medium with some time delay. As a result, the dynamics of distributed systems produce various kinds of coherent modes in the form of chemical waves [24]. For instance, tho classical wave patterns observed in the Belousov-Zhabotinsky reaction are expanding target waves and rotating spiral waves [25, 26, 27].

These are just a few well-known examples of systems successfully modelled by coupled nonlinear oscillators, that can generate an amazing range of behaviors such as entrainment, quenching (oscillator death) [28, 29], rhythmogenesis, birhythmicity, compound and complex oscillations, and chaos. However, the main focus of this thesis is the phenomenon of synchronization.

1.3 Synchronization of Coupled Nonlinear Oscillators

For decades considerable attention has been devoted to the problems of coordinated motion of interacting autonomous units [3, 30]. Research efforts in diverse disciplines such as ecology, control theory, statistical physics, social sciences, and computer graphics have been devoted to the study of collective behavior of a large number of dynamical units without a centralized individual control. Examples of such coordination can be observed in collections of autonomous robots or vehicles as well as in crowds of people, flocks of birds, schools of fish and so on.

1.3.1 Synchronization in Social and Natural Sciences

Synchronization as an adjustment of rhythms due to an interaction is an example of the emergence of a coherence between initially irregular oscillations of coupled self-sustained units. The phenomenon of synchronization is represented in nature on a great range of scales from electrons and photons to planets and galaxies. Synchronization can be observed among lifeless objects as well as among living organisms, including creatures of widely different complexity from fireflies to humans. It is quite natural to expect intelligent organization or some centralized rule, enforced on oscillating elements, to be responsible for any kind of coordinated behavior. Actually, this is not always the case, though such systems indeed exist in nature. For example, we all live experiencing the cycle of day and night. Consequently, human beings and other species have daily variations in their physiology, which

affect their behavior as well [31, 32, 33]. These changes are not simply a direct response to the environmental conditions, but rather an adjustment of internal temporal cycles of the organism to the external day and night rhythm. This internal temporal mechanism, known as a biological clock, regulates the timing of various processes in the organism in accordance with the 24-hour cycle of the physical environment. The biological clock is also responsible for the coordination of the internal processes themselves. Therefore, the survival of an organism strongly depends on its ability to synchronize internal rhythms to each other and to the external environment.

But synchronization is not necessarily a good thing; it can have destructive consequences for human beings. For example, external periodic signals of a specific frequency might have dangerous effects on electrical rhythms in the human brain. This kind of scenario occurred with Japanese children during an episode of Pokemon on December 16, 1997, when they watched an explosion of bright colors flashing at 12 Hz for five seconds [34, 35, 36]. Hundreds of children got instantly sick with symptoms like seizure, breathing problems and vomiting. Flashing red, white and blue lights apparently produced strong optical stimulation, which triggered so called photosensitive epilepsy [37]. This type of epilepsy is understood as a synchronization disorder, when light pulses repeated at a particular frequency entrain the firing neurons in the human brain. There are many other examples of undesirable synchronization in social life including the emergence of fads, mobs and traffic jams, which we all experience on a daily basis.

Another example of synchronization in the human brain is the mind itself [38]. Though an understanding of how neural activity forms our thoughts is still quite primitive, scientists believe that neural synchrony is responsible for such processes as face recognition or word memorization. Experiments show that during these acts of cognition millions of firing neurons lock in-phase, forming an oscillating signal at 40 Hz for a short period of time, and then a new pattern of neurons synchronizes for the next act. From this perspective, memory, perception, and cognition are the result of a sequence of synchronized states among large collections of distributed neurons.

Very surprising examples of synchronization phenomena come from spontaneous cooperation of a large number of oscillating units, when they do not have any centralized pacemakers controlling the rhythm of every agent. This scenario can be observed on the riverbanks in Southeast Asia, when millions of fireflies manage to organize their flashing in phase [39, 40]. This type of synchronization is not a consequence of any external rhythm imposed on independent fireflies. Instead, individual insects adjust their own rhythms in accordance with flashing of surrounding fireflies, so that overall synchronization spontaneously emerge after a short period of time, and then it is maintained for a long time.

Fortunately, we do not have to travel Southeast Asia each time we want to enjoy that kind of phenomenon. The same type of synchronization occurs in our hearts. The sinoatrial node is a cluster of about 10000 pacemaker cells, which collectively generate a rhythm to control beating of the rest of the heart [41]. These pacemaker cells are self-sustained oscillators and produce electrical rhythm even if they are isolated from the node. Nature is using synchronization to provide a reliable pace by spontaneous cooperation of thousands of oscillating cells, so that the failure of a few cells does not affect the functioning of the whole system.

Synchronization phenomena are quite common among other living organisms too. For example, cicadas hide themselves underground for almost two decades before they simultaneously start their short mating season [42]. Male fiddler crabs attract the attention of a female by waving their huge claws in unison [43]. It was also observed that human females communicating on a daily basis (i.e. roommates, coworkers, sisters or just close friends) exhibit the phenomenon of menstrual synchronization [44]. In this case coupling is probably provided by pheromones - odorless chemicals, that transmit synchronizing signals from one person to another [45, 46].

1.3.2 Synchronization in Engineering

The first time the phenomenon of synchronization was observed and described by Christiaan Huygens in the seventeenth century. He discovered the synchronization of two pendulum

clocks coupled through a common support [47, 48]. After some transient time the pendulums started to move in opposite directions with the same frequency. Huygens accurately described his observations and suggested that this anti-phase synchronization was established because of the movement of the beam, which the pendulums were hanging from. The original intention of the Huygens' experiment with clocks was to determine the longitude during a sea trial.

Later in the nineteenth century the discovery of synchronization in acoustic systems was made by Lord Rayleigh [49], when he observed that two distinct organ-pipes start to sound in unison if they are similar enough. He also discovered quenching, which is the suppression of oscillations occurring when the coupling becomes too strong.

With the development of radio and electrical engineering the study of synchronization reached a new level. Eccles and Vincent showed that two coupled generators oscillate with the same frequency even though their natural frequencies were different before the interaction was turned on [50]. Shortly after that, Appleton and van der Pol developed the first theoretical analysis of this phenomenon [51, 52]. They proved that a weak external signal of some frequency entrains the oscillations of a generator with a slightly different frequency. This research was of particular significance since triode generators were the main elements of radio devices. Over time scientists realized that various systems exhibiting synchronization phenomena obey some universal laws despite the differences in the nature of the nonlinearity, coupling and dynamics of the individual elements.

Modern technology has many examples of useful implications of synchronization. For instance, the coherent laser beam is a combined light of trillions of atoms synchronized the emitting in phase [53]. Superconductivity occurs when an ensemble of Cooper pairs spontaneously form the synchronized state, known as a Bose-Einstein condensate, and passes through a metal carrying electrical current without resistance [54]. Josephson junctions (simple devices that consist of two superconductors separated by a thin insulating layer) are used for the most sensitive detectors of magnetic field [55]. Indeed, superconducting quantum interference devices (SQUIDs), which rely on the synchronization of two Josephson junctions, measures magnetic fields 100 billion times weaker than the Earth's field.

The power grid is also an example of the implementation of synchronization. It consists of thousands of generators interconnected with each other to form one huge generator with all component units rotating in synchrony [56, 57].

For centuries the solution of the longitude problem has required the existence of accurate enough clocks. In our day atomic clocks allow one to determine position anywhere on the Earth to within meters [58]. The global positioning system (GPS), which is roughly a system of several distinct synchronized atomic clocks, is widely used to calculate the fastest routes for fire-trucks and ambulances, to find locations of rental cars, for precise farming, and even for blind landing of airplanes in heavy fog [59].

Despite some progress in the understanding of synchronization phenomena and their important applications in technology, the study of synchrony has not lost its relevance in our day, and many questions in the context of different practical compound systems still have to be answered.

CHAPTER II

JOSEPHSON JUNCTIONS IN A TRANSMISSION LINE

The topic of this chapter is an array of Josephson junctions coupled through a transmission line. The first three sections provide the background essential for an understanding of the basic system elements and their properties. Specifically, in Section 2.1 I describe the Josephson effect and different types of devices whose operation is based on the supercurrent phenomenon. A simplified derivation of the principal equations is provided as well.

The next section introduces the concept of Josephson junction arrays and their synchronization due to a conventional global coupling architecture. This section also summarizes the results obtained by various research teams who have studied this system.

Another principal element of the system of interest is a transmission line, introduced in the Section 3. A brief historical review of the field is provided with a detailed derivation of the equations governing the dynamics of an electrical transmission line.

The model for the dynamics of Josephson junction embedded in a transmission line is given in the Section 4, where the analysis of the system is based on a perturbation technique; first, in a general form, and then in a special case of equally-spaced junctions. Additional symmetry of the problem allows one to obtain a full analytical solution and investigate a particular synchronized state in different regimes, including the transition from relatively small frequencies to high ones.

The theoretical analysis of the resonant architecture of the Josephson transmission line with an arbitrary positioning of the junctions leads to a new phenomenon: the creation of inert oscillator pairs. This is described in the last section of this chapter.

2.1 Josephson Junction

The discovery of the peculiar properties of tunnelling between superconductors has led to the development of many useful applications.

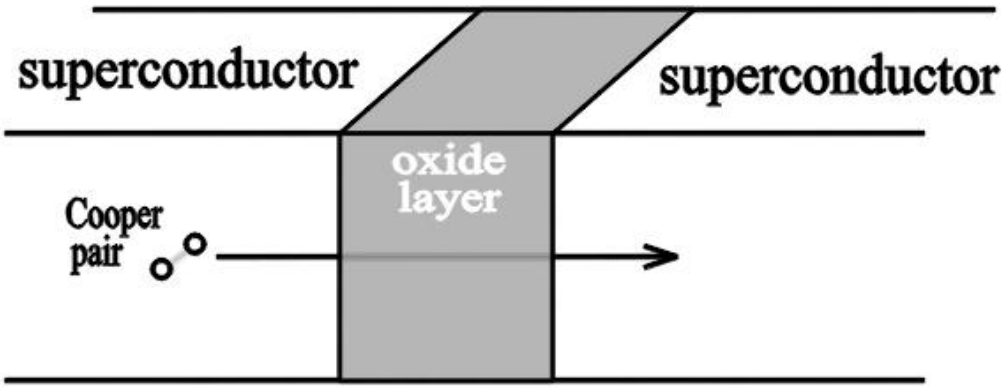

Figure 2: Schematic of a Josephson junction (SIS).

In 1962 a graduate student at Cambridge University, Brian Josephson, suggested that a weak electrical contact between two superconductors (see Fig. 2) should produce a phenomenon, the supercurrent I_s, which is a part of total electrical current passing through the contact [60]. Later this weak electrical contact was called a Josephson junction [61, 62]. Josephson derived a specific relationship between the supercurrent and the voltage across the junction from the main principles of quantum mechanics, so that the formula explicitly contains the Planck's constant [63].

The next year Josephson's prediction was experimentally confirmed [64], which triggered an extensive study of the Josephson effect and other related processes with a goal to understand the underlying physical laws, as well as necessary and sufficient conditions for its observation in the laboratory. Later Brian Josephson was awarded the Nobel Prize for his discovery. The importance of the Josephson effect went well beyond its interest in the field of superconductivity. Based on Josephson junctions, researchers have developed new devices with surprising features useful in many areas such as medicine, physics, biology and chemistry, as well as radio-astronomy and metrology. Thus, the Josephson effect turned

out to be very important for both fundamental and applied studies [65].

Let me give here a rather simple physical picture of the phenomenon and then demonstrate the classical derivation of the Josephson equations [66, 67, 68]. Suppose we have two superconductors placed close to each other. If the distance between them is large enough, then the Cooper pairs in each superconductor are described by a macroscopic wave function $\psi_{1,2}$, which can be written as

$$\psi_i = |\psi_i(\vec{r})| \exp\{i[\theta_i(\vec{r}) - \frac{2\mathcal{E}_F}{\hbar}t]\},$$

where $\mathcal{E}_F$ is the Fermi energy and $\theta_i(\vec{r})$ are the phases of the wave functions and defined up to an arbitrary constant [69]. In this case the phases are independent and unrelated. When we reduce the distance between superconductors, the wave functions start to penetrate the barrier and this couples the condensates on each side. As a result, coupling reduces the total system energy, while the energy associated with coupling increases. When the coupling energy becomes larger than thermal fluctuations, the phases get locked and Cooper pairs start to flow from one superconductor to the other one without energy loss. This scenario occurs even if we apply a voltage across the junction. But in this case, the wave function phases are not locked, instead they slip relative to each other at a rate proportional to the voltage.

A simple way to describe the dynamics of the interacting wave functions in each superconductor of a Josephson junction is:

$$\begin{aligned} i\hbar\frac{\partial\psi_1}{\partial t} &= U_1\psi_1 + \kappa\psi_2, \\ i\hbar\frac{\partial\psi_2}{\partial t} &= U_2\psi_2 + \kappa\psi_1, \end{aligned}$$

where $U_{1,2}$ are the energies of the wave functions, and κ characterizes the coupling strength between them. Since the voltage source V is applied across the junction, then $U_2 - U_1 = -2eV$ and, therefore:

$$\begin{aligned} i\hbar\frac{\partial\psi_1}{\partial t} &= +eV\psi_1 + \kappa\psi_2, \\ i\hbar\frac{\partial\psi_2}{\partial t} &= -eV\psi_2 + \kappa\psi_1. \end{aligned}$$

The next step is to express the wave function in terms of the pair density and the phase: $\psi_k = n_k^{1/2} \exp(i\theta_k)$ so that

$$\frac{i\hbar}{2\sqrt{n_1}}\frac{\partial n_1}{\partial t} - \hbar\sqrt{n_1}\frac{\partial \theta_1}{\partial t} = eV\sqrt{n_1} + \kappa\sqrt{n_2}e^{i(\theta_2-\theta_1)},$$
$$\frac{i\hbar}{2\sqrt{n_2}}\frac{\partial n_2}{\partial t} - \hbar\sqrt{n_2}\frac{\partial \theta_2}{\partial t} = -eV\sqrt{n_2} + \kappa\sqrt{n_1}e^{-i(\theta_2-\theta_1)}.$$

Separating real and imaginary parts, one gets

$$\frac{\partial n_1}{\partial t} = \frac{2\kappa}{\hbar}\sqrt{n_1 n_2}\sin\phi, \tag{4}$$
$$\frac{\partial n_2}{\partial t} = -\frac{2\kappa}{\hbar}\sqrt{n_1 n_2}\sin\phi, \tag{5}$$
$$\frac{\partial \theta_1}{\partial t} = -\frac{eV}{\hbar} - \frac{\kappa}{\hbar}\sqrt{\frac{n_2}{n_1}}\cos\phi, \tag{6}$$
$$\frac{\partial \theta_2}{\partial t} = \frac{eV}{\hbar} - \frac{\kappa}{\hbar}\sqrt{\frac{n_1}{n_2}}\cos\phi, \tag{7}$$

where $\phi = \theta_2 - \theta_1$.

It is assumed that there is a current in the circuit, containing the Josephson contact, so that the change of pair density does not create an imbalance between the electrons and the ions in the superconductors. The density of the current I flowing through the contact is proportional to the time derivative of the pair charge density, $2en$. Hence, from Eq.(4) one finds the first Josephson expression

$$I = I_c \sin\phi, \tag{8}$$

where I_c is the critical current. In this analysis the value of κ was not specified. Thus, I_c cannot be estimated in this way. However, with a microscopic theory the critical current density was found to be

$$J_c = \frac{G_n}{A}\left(\frac{\pi\Delta(T)}{2e}\right)\tanh\frac{\Delta(T)}{2k_BT},$$

where $\Delta(T)$ is the temperature dependent gap parameter, G_n is the tunnelling conductance and A is the junction area [70].

The evolution of the phase difference of the junction can be found by subtracting Eq.(6) from Eq.(7), and then equating n_1 and n_2, so that

$$\frac{\partial \phi}{\partial t} = \frac{2e}{\hbar}V, \tag{9}$$

which is the second Josephson relation.

In the case when V is a dc voltage, Eq.(9) gives $\phi = \frac{2e}{\hbar}Vt + \phi_0$ and therefore, from Eq.(8) one obtains

$$I = I_c \sin(\omega_J t + \phi_0),$$

where

$$\omega_J = \frac{2e}{\hbar}V = 303.9 \cdot 10^{13} \left(\frac{Hz}{V}\right) \cdot V.$$

is the frequency of the ac-current, flowing through the Josephson contact.

One of the applications of Josephson junctions (SQUID) was mentioned in the introduction with respect to synchronization. Extremely high frequencies of the supercurrent provide other important applications, especially in digital circuits. Indeed, the Josephson junction can switch from a state with zero voltage in a matter of a few picoseconds. Thus, the junction can be used in logic circuits and memory cells. It was demonstrated experimentally that memory cells based on the junctions perform state changes in times $\ll$100 ps. Potentially, these high speed and low power digital circuits can be very useful for signal processors and high-performance computers [71].

So far I have described the current which is produced by the flow of the Cooper pairs. In reality, the current through the Josephson contact usually consists of several components, only one of which is the supercurrent.

First of all, if I take into account very small but non-zero temperatures T, then I should consider thermal motion of charges with energies of the order of $k_B T$. This motion makes some pairs break apart, which would form a finite density of single electrons. Actually, the properties of these electrons are not exactly the same as those in normal metals, because of the influence of the superconducting condensate. For this reason they are called quasiparticles. Nevertheless, the IV-dependence of the apparent normal current I_N is very close to the usual Ohm's law:

$$I_N = \frac{V}{R_J},$$

where the parameter R_J is known as the normal resistance of the junction.

Another contribution to the net current comes when the voltage across the junction is

not constant ($\dot{V} \neq 0$). In this case the displacement current I_D appears in the circuit. This current effectively sums with the other currents, though formally it does not flow through the Josephson contact itself. The displacement current can be expressed in terms of the junction capacitance C_J in the usual form:

$$I_D = C_J \dot{V}.$$

The capacitance depends on the geometry of the junction, its size, and it is the same as the capacitance of the contact in the normal state.

Collecting all mentioned components of the total current, one gets

$$I = I_s(\phi) + I_N(V) + I_D(\dot{V}),$$

which can be written in the form of a differential equation for the equivalent circuit element (see Fig. 3):

$$I = I_c \sin(\phi) + \frac{V}{R_J} + C_J \frac{dV}{dt}. \tag{10}$$

Using Eq(9), one obtains an expression describing the evolution of the junction phase difference:

$$\frac{\hbar C_J}{2e}\ddot{\phi} + \frac{\hbar}{2eR_J}\dot{\phi} + I_c \sin\phi = I. \tag{11}$$

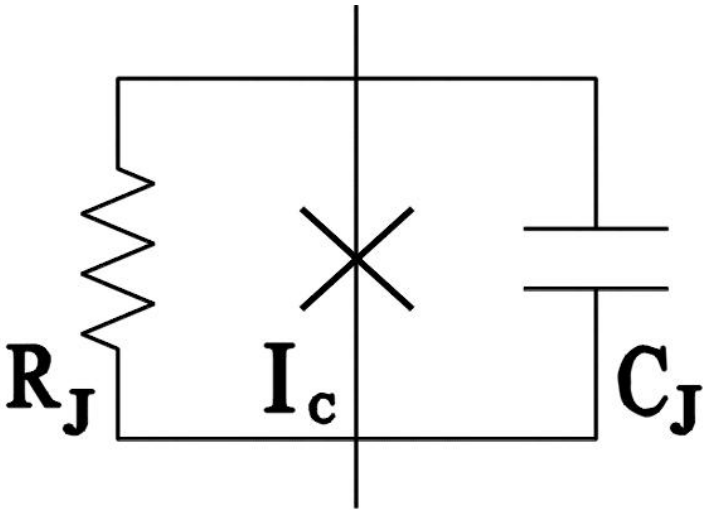

Figure 3: Equivalent circuit of a Josephson junction.

In the previous analysis I described a tunnel junction of the SIS type. This is a junction which consists of two superconductors (S) and a thin insulating layer (I) in between. Usually,

vacuum-deposited superconducting films are used for this type of junction, and the oxide of the lower electrode serves as the insulator. When the thickness of the oxide layer is about ten to thirty atomic sizes, the electrons penetrate from one electrode to the other with a small non-zero probability, $p \sim 10^{-5} - 10^{-3}$, due to quantum tunnelling, while the insulator provides the energy barrier.

It turns out that the Josephson relations can be observed in a whole family of devices that exhibit a Cooper pair current. The so called weak link (SNS sandwich) is an example of such a device. This consists of superconductors separated by a normal metal (N), semimetal or even another weak superconductor. Although the structure and fabrication of these contacts are very similar to the SIS sandwiches, their properties are quite different. The fact that the superconducting condensate of the pairs conserves the amplitude and the phase in a normal metal at a depth of the order of the coherence length is known as the proximity effect, which is responsible for creating the supercurrent I_s in the SNS contacts. Indeed, if the thickness of a link layer is about a coherence length, then the wave functions of the superconductors can still interact and produce a current proportional to $\sin\phi$. Typical superconductors have a coherence length of the order of hundreds of nanometers, which is much greater than the thickness of the usual oxide layers. Therefore, weak links have relatively small specific capacitance C/A.

I should also mention one more type of Josephson junction - the point contacts. The important feature of point contacts is that their fabrication technology is very simple. Actually, in order to make the contact one just needs to press a sharply pointed superconducting needle against a flat surface of another superconductor with some sort of adjusting mechanism. If the pressure is small, the superconductors are separated by the oxide layer covering their surfaces. But if the pressure is strong enough, the oxide layer breaks and forms an irreproducible complex system of microshorts between the superconductors. These point contacts exhibit the same dynamical behavior as the sandwich-type Josephson junctions.

2.2 Josephson Junction Arrays

Arrays of Josephson junctions represent a very interesting and important example of coupled non-linear oscillators.

The interest in such systems is motivated by their intriguing physical properties such as phase transitions, macroscopic quantum phenomena, locking and chaos, which are attractive from the perspective of many physical and biological problems. Moreover, Josephson junction arrays are important from the technological point of view due to the production of useful electronic devices with unique properties, for example, Josephson voltage standards, fast logic elements, photofluxonic detectors, hyperfrequency cryodevices and vortex-flow transistors [72, 73, 74, 75, 76, 77, 78].

Modern electronic circuits may consist of hundreds of Josephson junctions with parameters that can be identical to within a few per cent of their average values. The discovery of high-temperature superconductors increased the interest in such devices even more because of their potential to work at liquid nitrogen temperatures.

Milliwatt output power and small linewidths (< 1MHz) at frequencies of the order of hundreds of GHz are the usual requirements for some applications in metrology , astronomy and high-speed electronics. Josephson junctions are very attractive as potential microwave sources in a unique range of frequencies, because typical Josephson oscillations have frequencies up to several hundreds gigahertz. However, single junctions have very low power outputs, and impedances which do not match typical loads. This produces a problem for practical implementations of single Josephson junctions. Fortunately, arrays of Josephson contacts have sufficient output power (> 0.1mW) and useful impedance for most applications, if the junctions in these arrays are phase-locked. Therefore, one-dimensional and two-dimensional arrays of phase-locked junctions can provide high-amplitude fast oscillations with narrow linewidth to a matched load. However, the locking mechanism requires the study of the complex nonlinear dynamics produced by many interacting units and, consequently, many degrees of freedom.

An array of globally coupled junctions is an important class of Josephson junction arrays. The situation when each cell is coupled to all others with the same strength can happen in

the context of electrical circuits as well as in some laser and classical mechanical systems.

While studying large populations of self-sustained oscillators, Winfree discovered that synchronization occurs in a way similar to a thermodynamic phase transition [79]. Later Kuramoto proposed an exactly solvable model of coupled oscillators with distributed natural frequencies and confirmed Winfree's observation [1, 80]. Since the Kuramoto model was analytically tractable, it stimulated a lot of theoretical progress [81, 82] but had no connection with any experimental system. Later Wiesenfeld et al. showed that the Josephson junction array shunted by a load and subjected to a bias current I_b is a practical realization of the Kuramoto model [83].

In this case the array length was assumed to be much smaller than the radiation wavelength. The coupling was described by Kirchhoff's laws and understood as the interaction between the oscillating junctions and the ac-current in the external load [84, 85, 86]. For example, if the load consists of a series of resistance, capacitance and inductance (see Fig. 4), then the described system can be modelled with the following equations:

$$\frac{\hbar C_J}{2e}\ddot{\phi}_i + \frac{\hbar}{2eR_J}\dot{\phi}_i + I_c \sin\phi_i + I = I_b, \tag{12}$$

$$L\ddot{I} + R\dot{I} + \frac{1}{C}I = \frac{\hbar}{2e}\sum_{i=1}^{N}\ddot{\phi}_i. \tag{13}$$

Such problems with global coupling belong to the one of the simplest classes of many body systems because of a high degree of symmetry. As a rule, there are three types of periodic solutions for any array of globally coupled identical oscillators. The first solution corresponds to an in-phase state, when all oscillators produce the same waveform, and when they also oscillate in phase with each other. Another solution represents a state when all N oscillators have the same waveform with period T, but each waveform has a T/N phase shift with respect to the next closest wave form. This state is called a splay state or an antiphase state or ponies on a merry-go-round. All other states are considered to be out of phase. This solution is usually a mixture of in-phase and antiphase states [87, 88].

Systems with a large number of antiphase states can be used in applications as a high content addressable memory [89]. Indeed, 11 identical oscillators may produce $10! = 3628800$ antiphase states, while for a binary system, there would be only $2^{11} = 2048$ states.

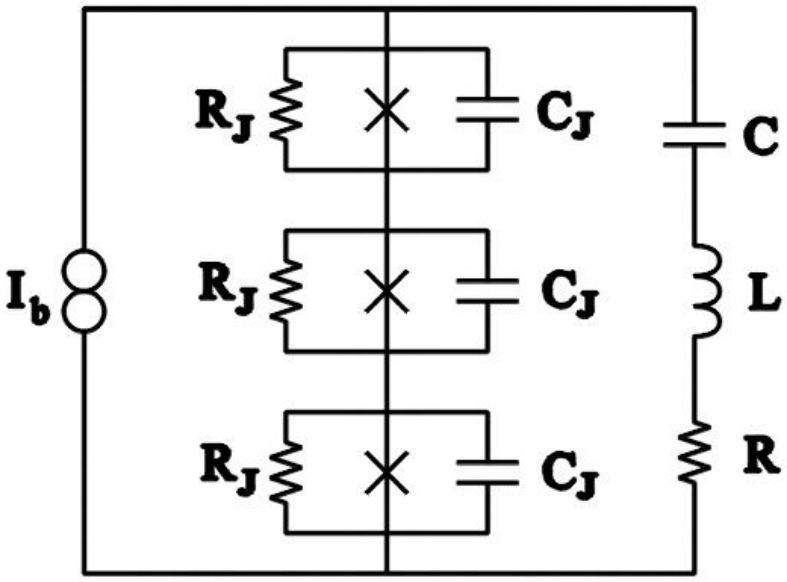

Figure 4: Circuit schematic for the shunted Josephson array.

Thus, memory elements based on antiphase states would have sufficiently larger capacity.

Several authors analytically studied Eqs.(12,13) [90, 91, 92]. It was shown that for a purely resistive load, weak coupling, and capacitance-free junctions ($C_J = 0$) these equations are integrable [93]. Later, researchers showed that this integrability was destroyed by a slight variation in the individual junction parameters. Wiesenfeld and Swift analytically proved that identical Josephson contacts with negligible capacitance and small coupling exhibit stable synchronous solution when the load is inductive [86]. This solution becomes unstable if the load is predominantly capacitive. Other authors have also obtained this result with a different mathematical approach [94]. The threshold between the stable and unstable regimes corresponds to the resonance case, when the load frequency $\frac{1}{\sqrt{LC}}$ coincides with the Josephson junction frequency. However, computer simulations showed that the stability of the synchronous solution strongly depends on the junction capacitance even when it is very small: $\beta \equiv \frac{2eR_j^2 C_J I_c}{\hbar} \ll 1$. Chernikov and Schmidt developed a powerful perturbation method which allows one to take into account arbitrarily large values of both β and the coupling strength, $\alpha \equiv \frac{\hbar}{e\ell L I_c}$ [95]. Moreover, their results are in very good agreement the direct numerical calculations.

2.3 Transmission Line

In situations when frequencies are low, circuit theory gives a proper description of the dynamics of electronic components interconnected by inactive wires. However, when frequencies become large enough, the circuit approach fails for two reasons. The first reason is that the energy stored in electronic components produces electromagnetic fields in the space around them, and the fields of different reactive components start to overlap. The second reason is that wires are actually reactive components themselves, and they store energy too. Therefore, the separation of the circuit into individual reactive components interconnected by non-reactive wires is just an approximation, which is called the lumped circuit limit. The speed of light in vacuum is finite and is about 30 cm per nanosecond, which imposes an obvious limitation, because it is the maximum speed with which any event can propagate in a circuit. When frequencies are very high, such as in the case of Josephson junctions, the linear dimensions of the circuit can be sufficiently larger than the wavelength of the oscillations. Thus, for a proper description of these distributed circuit systems one has to take into account the impedance properties of the wires, that is consider the wires as a transmission line [96, 97].

The first electrical transmission line came into existence in 1747, when William Watson showed that using the Earth as a conductor electric current can be sent through a wire. Based on this result the idea of a telegraph was proposed in 1753. However, the development of the overland telegraph took almost a century. The first telegraph cable connecting Calais and Dover was constructed in 1851. This coaxial cable consisted of a central wire surrounded by insulation typically made of gutta-percha. Extra layers of tarred hemp and steel armoring were also used to protect the insulator and strengthen the cable. In turn, the armoring was protected from corrosion by a tarred jute tape. Eventually the idea of very long cables including a 2000 mile long transatlantic cable, led to the necessity of a theoretical analysis of the signal propagation in transmission lines [98].

The first mathematical description for coaxial cables was developed by William Thomson in 1854. He took into account ohmic losses in the wires by considering a resistance per unit length R. The Kirchhoff laws applied to an infinitesimal length of the cable give the following

result (see details at the end of this section):

$$\frac{\partial V}{\partial x} = -RI, \tag{14}$$

$$\frac{\partial I}{\partial x} = -C\frac{\partial V}{\partial t}, \tag{15}$$

where $V = V(x,t)$ is the voltage along the cable and $I = I(x,t)$ is the current in it. Substituting I from Eq.(14) into Eq.(15), one obtains the diffusion equation:

$$\frac{\partial V}{\partial t} = \frac{1}{RC}\frac{\partial^2 V}{\partial x^2}.$$

In 1858 the first transatlantic cable went into operation, but the cable insulator degraded in a few weeks, because it was not suitable for operating voltages as high as 2000 volts. An earlier attempt, in 1857, had also failed because the cable broke and was lost. Nevertheless, the 1858 cable allowed one to send the first message across the ocean and receive it on the other side in several seconds, while the fastest conventional way to deliver messages in those days was by boat, which usually took about 10 days.

In 1865 another attempt to span the ocean was made with a new type of cable, but it also broke about one third of the way across the Atlantic. This cable was repaired the next year and became the first successfully operated transatlantic cable. It was operated at low voltages. The cable was 3593 km long, weighted 5080 tons, and had Thomson's mirror galvanometer as a signal detector.

It was Oliver Heaviside who corrected Thomson's equations (14,15) by considering the conductance G of the insulator due to its leakage [99]. In 1876 Heaviside took also into account the inductance L of the cable and derived final and correct transmission line equations:

$$\frac{\partial V}{\partial x} = -L\frac{\partial I}{\partial t} - RI, \tag{16}$$

$$\frac{\partial I}{\partial x} = -C\frac{\partial V}{\partial t} - GV. \tag{17}$$

These linear equations can be uncoupled to obtain individual equations for the current and voltage:

$$\frac{\partial^2 V}{\partial x^2} - LC\frac{\partial^2 V}{\partial t^2} - (RC + GL)\frac{\partial V}{\partial t} - GRV = 0, \tag{18}$$

$$\frac{\partial^2 I}{\partial x^2} - LC\frac{\partial^2 I}{\partial t^2} - (RC + GL)\frac{\partial I}{\partial t} - GRI = 0. \tag{19}$$

These expressions are known as the telegraphers equations. Eqs. (16,17) were obtained by Heaviside from circuit principles, while James Maxwell was developing his electromagnetic vector field theory [100]. A few year later, Heaviside applied Maxwell's theory to the transmission line problem as well.

Since the first cables were operated by an ordinary telegraph key, so that signal frequencies were low (10 Hz), the inductive properties of the line and losses due to insulation leakage could be ignored. For this reason Thomson's equations (14,15) gave a good approximation for the signal transmission. However, at high frequencies both inductive effects and losses become very important. For example, the typical attenuation in a cable, just due to resistive losses, were of the order of 0.1 dB/km at high frequencies.

In 1956, cables with repeaters were used to make the first transatlantic cable with voice transmission. This cable was able to carry 36 telephone conversations. In 1988 the first optical-fiber cable allowed one to transmit 8000 simultaneous conversations across the ocean [101].

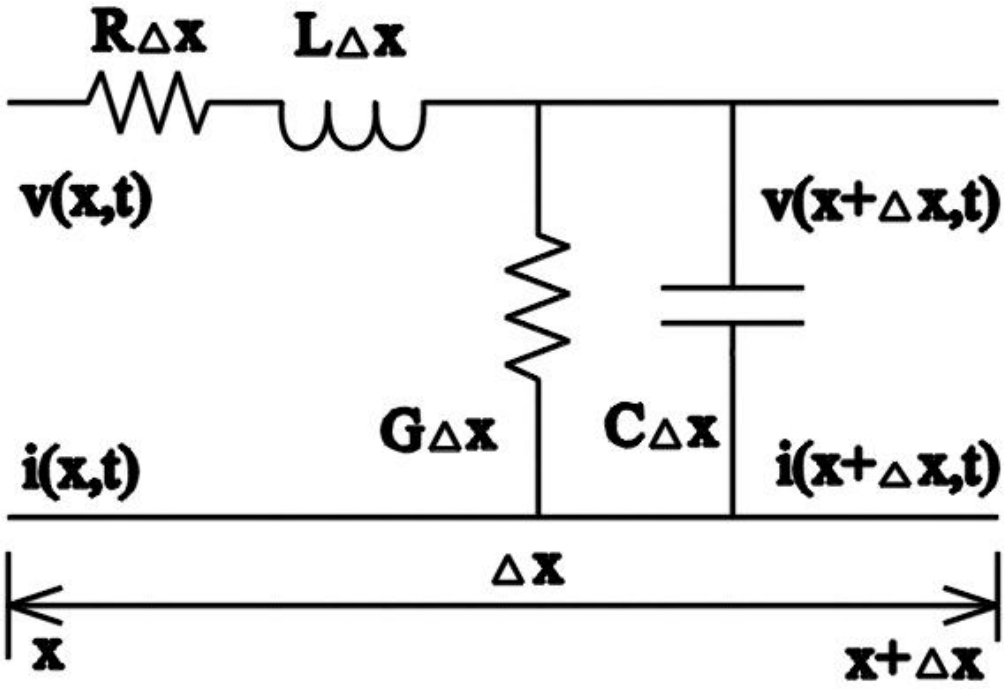

Figure 5: Equivalent circuit of an element of a transmission line with a length of Δx.

As was mentioned above, the description of the circuit with parameters distributed

throughout a transmission line gives a good approximation for the line dynamics. Let me consider a segment of the line with the length Δx, represented by the equivalent circuit as shown in Fig. 5. Using Kirchhoff's voltage law for this circuit, one finds the equation:

$$V(x,t) - R\Delta x\, I(x,t) - L\Delta x \frac{\partial I(x,t)}{\partial t} - V(x+\Delta x,t) = 0,$$

which can be written as

$$\frac{V(x+\Delta x,t) - V(x,t)}{\Delta x} = -RI(x,t) - L\frac{\partial I(x,t)}{\partial t}.$$

Now taking the limit $\Delta x \to 0$ one obtains the first transmission equation (16):

$$\frac{\partial V(x,t)}{\partial x} = -RI(x,t) - L\frac{\partial I(x,t)}{\partial t}.$$

In order to get the other equation, one should apply Kirchhoff's current law to the segment, so that

$$I(x,t) - G\Delta x\, V(x+\Delta x,t) - C\Delta x \frac{\partial V(x+\Delta x,t)}{\partial t} - I(x+\Delta x,t) = 0,$$

which is equivalent to the expression:

$$\frac{I(x+\Delta x,t) - I(x,t)}{\Delta x} = -GV(x+\Delta x,t) - C\frac{\partial V(x+\Delta x,t)}{\partial t}.$$

Finally, I let $\Delta x \to 0$ and get the second transmission equation (17):

$$\frac{\partial I(x,t)}{\partial x} = -GV(x,t) - C\frac{\partial V(x,t)}{\partial t}.$$

The characteristic impedance (that is the ratio between the voltage and the current) for both lossy and lossless transmission lines does not depend on the line length. It can be expressed in terms of L, R, C, and G as

$$Z_0 = \sqrt{\frac{R+i\omega L}{G+i\omega C}}.$$

In other words the impedance depends only on the properties of the metal of the conductor, the dielectric material of the insulator, and the geometry of the line cross-section.

2.4 Josephson Transmission Line

Almost all theories developed so far to study synchronization and phase locking in Josephson junction arrays use the lumped approach. These theories require feedback through an external load for phase locking. However, as was explained in the previous section, when arrays are pushed to larger numbers of junctions and higher operating frequencies, lumped circuit theories break down. When the wavelength of the emitted radiation becomes smaller than the spatial extent of the array, new physical aspects become important which are ignored in the lumped limit [102, 103, 104, 105, 106, 107]. Actually, experimentalists have tried to take advantage of the fact that spatial positioning of the elements is important in the high frequency regime. Han et al. and Booi and Benz demonstrated that clustering junctions at strategic locations along the wire connecting them can increase the emitted power [108, 109]. This strategy is based on a simple physical picture where the clusters lie at antinodes of a particular standing wave of the junction-free wire.

Despite its importance, our present theoretical understanding of synchronization in the high-frequency regime is relatively primitive. Detailed spatiotemporal information is unavailable from experiments on real Josephson arrays. Models of Josephson junctions coupled to a single-mode resonant cavity, which picks up some of the character of the distributed problem, have also been studied [105, 110, 111, 112], but as will be shown in the next section, the single-mode approach may not properly represent the behavior of the current in a transmission line.

One goal of this thesis is to make the first step towards a physical and mathematical understanding of spontaneous synchronization in a Josephson transmission line. To do this, I consider a current biased transmission line interrupted by N identical junctions [102, 113]. A nice feature of the load free system is that in the low-frequency limit the junctions are dynamically uncoupled. In this sense, the system is ideally suited for exploring those new dynamical features that emerge only at higher frequencies.

In this section I consider mainly equally-spaced junctions and frequencies that allow me to study Josephson transmission lines in the high-frequency limit, and also in the intermediate regime for better understanding of the transition from lumped to distributed behavior.

In the next section I will show results for even higher frequencies and will allow arbitrary positioning of the junctions.

Mathematically, the distributed problem is more difficult to analyze than the corresponding lumped one, since the governing dynamical equations have much lower symmetry. One consequence is the absence of a perfectly synchronized state in which all oscillators have precisely the same output at all times. This raises the question of what dynamical state(s) to track and how high a degree of synchronization can be achieved even in principle.

To analyze the problem I apply a perturbation technique which has proven to be very useful in earlier studies on lumped arrays [95, 114]. The calculation leads to the identification of the synchronized dynamical state, and the development of an N-dimensional map, which I use to explore the stability of this state. Numerical simulations of the full dynamical system are used both as a check of the analytic results and as a means of exploring the dynamics where the most-synchronized state is unstable.

Let me begin by setting up the problem and putting it in a form suitable for the method of analysis. The perturbation scheme I use leads to somewhat lengthy algebraic expressions, but since the idea of the calculation and its structure are simple, it is worthwhile to discuss the main features before presenting the detailed calculation.

Consider a wire of length ℓ interrupted by identical Josephson junctions at positions $x_1, x_2, ..., x_N$. A constant bias current I_b is maintained at one end of the line and removed at the other. At low frequencies, the current within the wire is spatially uniform and equal to the value at its ends. At higher frequencies, the wire becomes an active dynamical entity, and can be modelled as a transmission line of inductance per unit length L and capacitance per unit length C.

The partial differential equation governing the dynamics of the Josephson transmission line can be determined by considering the finite element representation shown in Fig. 6. Each inductor-capacitor segment represents a short length Δx of the wire. Some segments also contain a Josephson junction in series with the inductor. We assume that each junction is small enough that it can be treated as a lumped element, although the system as a whole is spatially extended. Current conservation implies

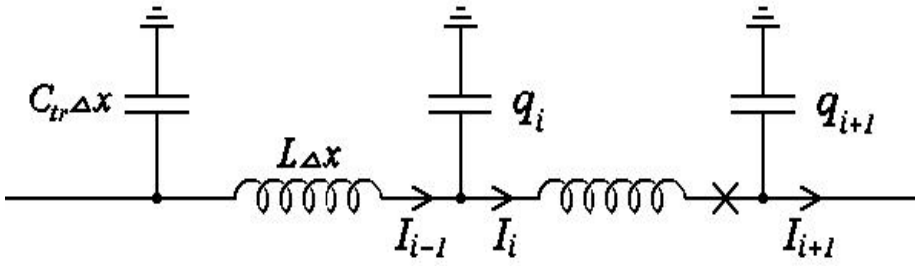

Figure 6: Finite-element schematic of a piece of the transmission line. The "X" denotes a Josephson junction. In the piece shown, only one of the segments contains a junction.

$$I_{i-1} = \dot{q}_i + I_i, \tag{20}$$

where q_i is the charge on the i^{th} capacitor, I_i is the current in the i^{th} inductor, and the overdot denotes differentiation with respect to time. Equating voltage drops of two paths from node i to ground yields

$$\frac{q_i}{C\Delta x} = L\Delta x\dot{I}_i + \frac{q_{i+1}}{C\Delta x} + \frac{\hbar}{2e}\dot{\Phi}_j\delta_{i,i_j}, \tag{21}$$

where, as before, $\hbar$ is Planck's constant divided by 2π, e is the magnitude of the electronic charge and Φ_j is the difference in the phase of the macroscopic quantum wave function across the j^{th} junction. The Kronecker delta is used to include the voltage drop across the j^{th} Josephson junction if it happens to appear in segment i of the transmission line; for example, if the 3^{rd} junction appears in the 89^{th} segment, $i_3 = 89$. Combining Eqs.(20) and (21) gives

$$v^2\frac{I_{i+1} - 2I_i + I_{i-1}}{\Delta x^2} = \ddot{I}_i + \frac{\hbar}{2eL\Delta x}\ddot{\Phi}_j\delta_{i,i_j}, \tag{22}$$

where I have used $v^2 = 1/(LC)$. Passing to the limit $\Delta x \to 0$ yields an equation for the current $I(x,t)$

$$\frac{\partial^2 I}{\partial t^2} - \upsilon^2 \frac{\partial^2 I}{\partial x^2} + \sum_{j=1}^{N} \frac{\hbar}{2eL} \ddot{\Phi}_j \delta(x - x_j) = 0. \tag{23}$$

The boundary conditions are

$$I(0,t) = I(\ell,t) = I_b.$$

Meanwhile, since the current through the j^{th} junction is $I(x_j,t)$, we have from Eq.(11)

$$\frac{\hbar C_J}{2e} \ddot{\Phi}_j + \frac{\hbar}{2eR_J} \dot{\Phi}_j + I_c \sin\Phi_j = I(x_j,t). \tag{24}$$

Recall that C_J, R_J, and I_c are the junction capacitance, resistance, and critical current, respectively.

To put these in dimensionless form, I first make the rescalings

$$\begin{aligned} x_j &\rightarrow r_j \ell, \\ t &\rightarrow \frac{\hbar}{2eRI_c} t, \\ I &\rightarrow I_c I, \end{aligned}$$

so that from Eqs.(23,24) one gets

$$\frac{\partial^2 I}{\partial t^2} - \frac{\hbar^2 \upsilon^2}{4e^2 \ell^2 R^2 I_c^2} \frac{\partial^2 I}{\partial r^2} + \sum_{j=1}^{N} \frac{\hbar}{2e\ell I_c L} \ddot{\Phi}_j \delta(r - r_j) = 0, \tag{25}$$

$$\beta \ddot{\Phi}_j + \dot{\Phi}_j + \sin\Phi_j = I(r_j,t), \tag{26}$$

where $\beta = \frac{2eCI_cR^2}{\hbar}$.

The next step is to turn the partial differential equation into a set of ordinary differential equations by expanding $I(r,t)$ in spatial modes. A convenient choice is to use the eigenfunctions for the unloaded transmission line, so that

$$I = I_b + \sum_{k=1}^{\infty} A_k(t) \sin(\pi k r). \tag{27}$$

It is easy to see that this automatically satisfies the boundary conditions, for arbitrary values of the $\{A_k\}$. Expand the δ-function in the same basis:

$$\delta(r - r_j) = \sum_{k=1}^{\infty} 2 \sin(\pi k r_j) \sin(\pi k r), \tag{28}$$

so that Eqs.(25,26) become

$$\ddot{A}_k + c^2 k^2 A_k + \alpha \sum_{j=1}^{N} \ddot{\Phi}_j \sin(\pi k r_j) = 0 \tag{29}$$

and

$$\beta \ddot{\Phi}_j + \dot{\Phi}_j + \sin \Phi_j = I_b + \sum_{k=1}^{\infty} A_k \sin(\pi k r_j), \tag{30}$$

where

$$c = \frac{\pi \hbar \upsilon}{2e\ell R I_c}, \quad \alpha = \frac{\hbar}{e\ell L I_c},$$

and A_k, I_b, t, β are dimensionless.

I am going to construct a perturbation expansion based on the small parameter $b = \frac{1}{I_b}$, so one more rescaling is needed: $t \to \frac{1}{I_b} \cdot t$ and $A_k \to I_b \cdot A_k$. Hence, the governing system of equations becomes

$$\ddot{A}_k + \tilde{c}^2 k^2 A_k + \tilde{\alpha} \sum_{j=1}^{N} \ddot{\Phi}_j \sin(\pi k r_j) = 0, \tag{31}$$

$$\tilde{\beta} \ddot{\Phi}_j + \dot{\Phi}_j + b \sin \Phi_j = 1 + \sum_{k=1}^{\infty} A_k \sin(\pi k r_j), \tag{32}$$

where $\tilde{c} = cb$, $\tilde{\alpha} = \alpha b$, and $\tilde{\beta} = \frac{\beta}{b}$.

I expect the following perturbation method to be consistent if

$$b \ll 1, \tilde{\alpha}, \tilde{\beta}, \tilde{c}^2. \tag{33}$$

Let me estimate these coefficients. Taking typical experimental values of a junction, $I_c \sim 100\mu A$, $R \sim 1\Omega$, $C \sim 1pF$, and of a transmission line, $l \sim 100\mu m$, $L \sim 10^{-8} H/m$, $C_{tr} \sim 10^{-8} F/m$, one finds that $\upsilon = \frac{1}{\sqrt{LC_{tr}}} \sim 10^8 m/s$, $\beta \sim 0.1$, $\alpha \sim 10$, $c \sim 10$. Thus, I will use the values $b = 0.05$, $\beta = 0.5$, α and c from ~ 10 to ~ 100 when displaying numerical results later on, in keeping with the condition (33). I note in passing that the characteristic frequency of the solution of Eq.(32) is

$$\omega_o = \frac{2eRI_c}{\hbar b} \sim 10^{11} Hz.$$

In the next subsection, I will develop an analytic calculation based on a small b expansion. Specifically, I assume that

$$A_k = A_k^{(0)} + bA_k^{(1)} + b^2 A_k^{(2)} + \ldots, \tag{34}$$

$$\Phi_k = \Phi_k^{(0)} + b\Phi_k^{(1)} + b^2 \Phi_k^{(2)} + \ldots. \tag{35}$$

Since b is the coefficient of the only nonlinear term, the expansion reduces the problem to a set of linear equations, which allows me to get an explicit representation of the solution.

The structure of the solutions is as follows. To lowest order, the junction phases Φ_j increase at a constant rate. In the familiar pendulum analogy for Josephson junctions, this corresponds to pendulums which overturn with uniform angular velocity. To this order, there are no voltage oscillations and the transmission line modes are inactive. The first order corrections merely introduce oscillations at the overturning frequency. The crucial interactions show up in second order, and govern the stability of the state in which the junction oscillations are synchronized.

In fact, I find a family of solutions which depend on the initial values of the junction phases, and this allows me to derive an N-dimensional return map involving the N phases, and it is this map that I use to investigate dynamical stability. Note that this map is not a bona fide Poincare return map since it doesn't explicitly involve the other phase space coordinates. Nevertheless, I expect it to be a good approximation to the dynamics after an initial transient time, as the other dynamical variables are effectively slaved by the N phase variables. This expectation is borne out by direct comparisons between the analytic solution and numerical simulations of the full set of equations.

2.4.1 Perturbation analysis

To lowest order equations (31) and (32) are

$$\ddot{A}_k^{(0)} + \tilde{c}^2 k^2 A_k^{(0)} + \tilde{\alpha} \sum_{j=1}^{N} \ddot{\Phi}_j^{(0)} \sin(\pi k r_j) = 0,$$

$$\tilde{\beta} \ddot{\Phi}_j^{(0)} + \dot{\Phi}_j^{(0)} = 1 + \sum_{k=1}^{\infty} A_k^{(0)} \sin(\pi k r_j).$$

One can readily identify the following N-parameter family of steady state solutions where the junction phases overturn at a constant rate,

$$A_k^{(0)} = 0 \qquad \text{and} \qquad \Phi_j^{(0)} = t + \theta_j,$$

where the θ_j are constants. One might wonder whether there are also uniformly overturning solutions but with non-zero $A_k^{(0)}$. Indeed, there can be: for example if all of the junctions are placed at nodes of a particular spatial mode, say $k = K$, then there are solutions with $A_K(t) \sim \sin(\tilde{c}Kt)$ and all other $A_k = 0$. These solutions persist indefinitely only because I have assumed that the transmission line is perfectly lossless, and for this reason I ignore them in the ensuing analysis. (Including a small amount of damping in the line would result in more complicated expressions later on without any compensating insight.)

To first order in b,

$$\ddot{A}_k^{(1)} + \tilde{c}^2 k^2 A_k^{(1)} + \tilde{\alpha} \sum_{j=1}^{N} \ddot{\Phi}_j^{(1)} \sin(\pi k r_j) = 0, \tag{36}$$

$$\tilde{\beta}\ddot{\Phi}_j^{(1)} + \dot{\Phi}_j^{(1)} + \sin(t + \theta_j) = \sum_{k=1}^{\infty} A_k^{(1)} \sin(\pi k x_j). \tag{37}$$

The solution of Eqs.(36,37) can be found in the form

$$A_k^{(1)} = c_k \sin t + d_k \cos t, \tag{38}$$

$$\Phi_k^{(1)} = a_k \sin t + b_k \cos t. \tag{39}$$

Let me substitute Eqs.(38,39) into Eqs.(36,37) and in each equation equate separately the terms proportional to $\sin t$ and $\cos t$. This yields four sets of equations for the coefficients a_j, b_j, c_j, d_j,

$$c_k(1 - \tilde{c}^2 k^2) + \tilde{\alpha} \sum_{j=1}^{N} a_j \sin(\pi k r_j) = 0, \tag{40}$$

$$d_k(1 - \tilde{c}^2 k^2) + \tilde{\alpha} \sum_{j=1}^{N} b_j \sin(\pi k r_j) = 0, \tag{41}$$

$$-\tilde{\beta} a_j - b_j + \cos\theta_j = \sum_{k=1}^{\infty} c_k \sin(\pi k r_j), \tag{42}$$

$$-\tilde{\beta}b_j + a_j + \sin\theta_j = \sum_{k=1}^{\infty} d_k \sin(\pi k r_j). \tag{43}$$

Multiplying Eq.(42) by $\tilde{\beta}$ and subtracting the result from Eq.(43) gives, upon solving for a_j,

$$a_j = \frac{1}{1+\tilde{\beta}^2}(\tilde{\beta}\cos\theta_j - \sin\theta_j) + \frac{1}{1+\tilde{\beta}^2}\sum_{k=1}^{\infty}(d_k - \tilde{\beta}c_k)\sin(\pi k r_j), \tag{44}$$

whereas multiplying Eq.(43) by $\tilde{\beta}$ and adding the result to Eq.(42) leads to an expression for b_j:

$$b_j = \frac{1}{1+\tilde{\beta}^2}(\tilde{\beta}\sin\theta_j + \cos\theta_j) - \frac{1}{1+\tilde{\beta}^2}\sum_{k=1}^{\infty}(\tilde{\beta}d_k + c_k)\sin(\pi k r_j). \tag{45}$$

Let $S_{k'k} = \sum_{j=1}^{N}\sin(\pi k' r_j)\sin(\pi k r_j)$. Then substituting Eqs.(44,45) into Eqs.(40,41) gives

$$\begin{aligned} c_k(1-\tilde{c}^2k^2) \quad &+ \quad \frac{\tilde{\alpha}}{1+\tilde{\beta}^2}\sum_{j=1}^{N}(\tilde{\beta}\cos\theta_j - \sin\theta_j)\sin(\pi k r_j) \\ &+ \quad \frac{\tilde{\alpha}}{1+\tilde{\beta}^2}\sum_{k'=1}^{\infty}(d_{k'} - \tilde{\beta}c_{k'})S_{k'k} = 0, \end{aligned}$$

$$\begin{aligned} d_k(1-\tilde{c}^2k^2) \quad &+ \quad \frac{\tilde{\alpha}}{1+\tilde{\beta}^2}\sum_{j=1}^{N}(\tilde{\beta}\sin\theta_j + \cos\theta_j)\sin(\pi k r_j) \\ &- \quad \frac{\tilde{\alpha}}{1+\tilde{\beta}^2}\sum_{k'=1}^{\infty}(\tilde{\beta}d_{k'} + c_{k'})S_{k'k} = 0. \end{aligned}$$

This calculation is good for any spatial distribution of junctions. But now I specialize to the important case of equally-spaced junctions: $r_j = \frac{j}{N+1}$, where $j = 1, 2, \ldots, N$. Then $S_{k'k} = \frac{N+1}{2}\delta_{k'k}$, and the last expressions decouple in k. Then it is straightforward to solve them, with the following result

$$c_k = P\sum_{j=1}^{N}\frac{\tilde{\beta}H + M_k}{M_k^2 + H^2}\sin\theta_j \sin\left(\frac{\pi k j}{N+1}\right) + P\sum_{j=1}^{N}\frac{H - \tilde{\beta}M_k}{M_k^2 + H^2}\cos\theta_j \sin\left(\frac{\pi k j}{N+1}\right),$$

$$d_k = -P\sum_{j=1}^{N}\frac{\tilde{\beta}H + M_k}{M_k^2 + H^2}\cos\theta_j \sin\left(\frac{\pi k j}{N+1}\right) + P\sum_{j=1}^{N}\frac{H - \tilde{\beta}M_k}{M_k^2 + H^2}\sin\theta_j \sin\left(\frac{\pi k j}{N+1}\right),$$

where

$$M_k \equiv 1 - \tilde{c}^2 k^2 - \tilde{\beta} H,$$
$$P \equiv \frac{2H}{N+1},$$
$$H \equiv \frac{\tilde{\alpha}(N+1)}{2(1+\tilde{\beta}^2)}.$$

Finally, substituting this back into Eqs.(44,45), I get:

$$\begin{aligned} a_j &= \frac{P}{\tilde{\alpha}}(\tilde{\beta}\cos\theta_j - \sin\theta_j) \\ &+ \frac{P^2}{\tilde{\alpha}}\sum_{i=1}^{N}\sum_{k=1}^{\infty}\frac{H(1-\tilde{\beta}^2) - 2\tilde{\beta}M_k}{M_k^2 + H^2}\sin\theta_i \sin\left(\frac{\pi k i}{N+1}\right)\sin\left(\frac{\pi k j}{N+1}\right) \\ &- \frac{P^2}{\tilde{\alpha}}\sum_{i=1}^{N}\sum_{k=1}^{\infty}\frac{M_k(1-\tilde{\beta}^2) + 2\tilde{\beta}H}{M_k^2 + H^2}\cos\theta_i \sin\left(\frac{\pi k i}{N+1}\right)\sin\left(\frac{\pi k j}{N+1}\right), \end{aligned}$$

$$\begin{aligned} b_j &= \frac{P}{\tilde{\alpha}}(\tilde{\beta}\sin\theta_j + \cos\theta_j) \\ &- \frac{P^2}{\tilde{\alpha}}\sum_{i=1}^{N}\sum_{k=1}^{\infty}\frac{H(1-\tilde{\beta}^2) - 2\tilde{\beta}M_k}{M_k^2 + H^2}\cos\theta_i \sin\left(\frac{\pi k i}{N+1}\right)\sin\left(\frac{\pi k j}{N+1}\right) \\ &- \frac{P^2}{\tilde{\alpha}}\sum_{i=1}^{N}\sum_{k=1}^{\infty}\frac{M_k(1-\tilde{\beta}^2) + 2\tilde{\beta}H}{M_k^2 + H^2}\sin\theta_i \sin\left(\frac{\pi k i}{N+1}\right)\sin\left(\frac{\pi k j}{N+1}\right). \end{aligned}$$

The second order expansion of Eqs.(31,32) gives

$$\ddot{A}_k^{(2)} + \tilde{c}^2 k^2 A_k^{(2)} + \tilde{\alpha}\sum_{j=1}^{N}\ddot{\Phi}_j^{(2)}\sin(\pi k r_j) = 0, \tag{46}$$

$$\tilde{\beta}\ddot{\Phi}_j^{(2)} + \dot{\Phi}_j^{(2)} + \cos(t+\theta_j)\Phi_j^{(1)} = \sum_{k=1}^{\infty} A_k^{(2)}\sin(\pi k r_j). \tag{47}$$

Now, the third term on the left hand side of Eq.(47) is equal to the sum of a constant term plus second harmonic terms. Thus, the solution is of the form

$$\Phi_j^{(2)} = -\langle b\cos(t+\theta_j)\Phi_j^{(1)}\rangle t + E_j\sin 2t + F_j\cos 2t, \tag{48}$$

$$A_k^{(2)} = G_k\sin 2t + H_k\cos 2t, \tag{49}$$

where the angular bracket denotes a time average over one period. In subsection 2.4.3, where I consider the stability of solutions, it will turn out that I won't need explicit expressions

for the coefficients E_j, F_j, G_j, and H_j. On the other hand, the stability hinges crucially on the coefficient of the term proportional to t, which is:

$$\langle \cos(t+\theta_j)\Phi_j^{(1)}\rangle = \frac{1}{2}(b_j\cos\theta_j - a_j\sin\theta_j)$$
$$= \frac{P}{2\tilde{\alpha}} - \frac{P^2}{2\tilde{\alpha}}\sum_{i=1}^{N}\sum_{k=1}^{\infty}\frac{H(1-\tilde{\beta}^2)-2\tilde{\beta}M_k}{M_k^2+H^2}\cos(\theta_j-\theta_i)\sin\left(\frac{\pi k i}{N+1}\right)\sin\left(\frac{\pi k j}{N+1}\right)$$
$$+\frac{P^2}{2\tilde{\alpha}}\sum_{i=1}^{N}\sum_{k=1}^{\infty}\frac{M_k(1-\tilde{\beta}^2)+2\tilde{\beta}H}{M_k^2+H^2}\sin(\theta_j-\theta_i)\sin\left(\frac{\pi k_i}{N+1}\right)\sin\left(\frac{\pi k j}{N+1}\right). \quad (50)$$

2.4.2 Synchronized State

In this subsection I explore the characteristics of the obtained solution to first order in b in the case when $\theta_j = \theta$, for all j. As noted previously, this system does not admit the type of fully symmetric inphase state that is found in many lumped circuit problems. However, the solution with $\theta_j = \theta$ is the synchronized state in the sense that, in the limit $b \to 0$, this is the solution branch which coincides with the inphase state. As one will see, the waveforms for this state can line up virtually perfectly even though the amplitudes can differ substantially from one oscillator to the next.

It is convenient to introduce the following notation

$$\sigma_{ij} = P\sum_{k=1}^{\infty}\frac{H(1-\tilde{\beta}^2)-2\tilde{\beta}M_k}{M_k^2+H^2}\sin\left(\frac{\pi k i}{N+1}\right)\sin\left(\frac{\pi k j}{N+1}\right), \quad (51)$$

$$\rho_{ij} = P\sum_{k=1}^{\infty}\frac{M_k(1-\tilde{\beta}^2)+2\tilde{\beta}H}{M_k^2+H^2}\sin\left(\frac{\pi k i}{N+1}\right)\sin\left(\frac{\pi k j}{N+1}\right). \quad (52)$$

Then I can rewrite the coefficients a_j and b_j in the form

$$a_j = \frac{P}{\tilde{\alpha}}\left[(\tilde{\beta}-\sum_{i=1}^{N}\rho_{ij})\cos\theta - (1-\sum_{i=1}^{N}\sigma_{ij})\sin\theta\right], \quad (53)$$

$$b_j = \frac{P}{\tilde{\alpha}}\left[(\tilde{\beta}-\sum_{i=1}^{N}\rho_{ij})\sin\theta + (1-\sum_{i=1}^{N}\sigma_{ij})\cos\theta\right]. \quad (54)$$

Note that as $k \to \infty$, the terms in Eqs.(51,52) tend to zero as $\frac{1}{k^2}$. Hence, for numerical purposes I can consider finite sums choosing $k_{\max}$ big enough for any required accuracy.

Next, I define an order parameter which represents the degree of synchronization of the array. The quantity of direct physical interest is the voltage across a junction which is proportional to $\dot{\Phi}$. To first order in the perturbation expansion I have

$$\dot{\Phi}_j = 1 + b\dot{\Phi}_j^{(1)} + O(b^2) = 1 + b(a_j \cos t - b_j \sin t) + O(b^2).$$

To study the effects of phase locking, I write this as

$$\dot{\Phi}_j = 1 + be_j \sin(t + f_j) + O(b^2),$$

so that a natural order parameter is

$$p = | < \exp(if_j) > | = \left| \frac{1}{N} \sum_{j=1}^{N} \exp(if_j) \right|. \tag{55}$$

I want to express f_j in terms of the derived quantities σ_{ij}, ρ_{ij}. Equating the last two expressions for $\dot{\Phi}_j$ gives

$$f_j = -\arctan \frac{a_j}{b_j} \tag{56}$$

and so, in view of Eqs.(53,54)

$$\begin{aligned} \tan f_j &= \frac{(1 - \sum_i \sigma_{ij}) \sin\theta - (\tilde{\beta} - \sum_i \rho_{ij}) \cos\theta}{(1 - \sum_i \sigma_{ij}) \cos\theta + (\tilde{\beta} - \sum_i \rho_{ij}) \sin\theta} \\ &= \frac{\tan\theta - \tan\tilde{\theta}_j}{1 + \tan\theta \tan\tilde{\theta}_j} = \tan(\theta - \tilde{\theta}_i), \end{aligned}$$

where for the moment I have introduced the quantity

$$\tan\tilde{\theta}_j = \frac{\tilde{\beta} - \sum_i \rho_{ij}}{1 - \sum_i \sigma_{ij}}.$$

Finally, I get the desired formula for the phase of the voltage waveform

$$f_j = \theta - \arctan \frac{\tilde{\beta} - \sum_i \rho_{ij}}{1 - \sum_i \sigma_{ij}}. \tag{57}$$

Meanwhile, the amplitude of the voltage waveform is

$$e_j = \sqrt{a_j^2 + b_j^2} = \frac{P}{\tilde{\alpha}} \sqrt{(\tilde{\beta} - \sum_i \rho_{ij})^2 + (1 - \sum_i \sigma_{ij})^2}. \tag{58}$$

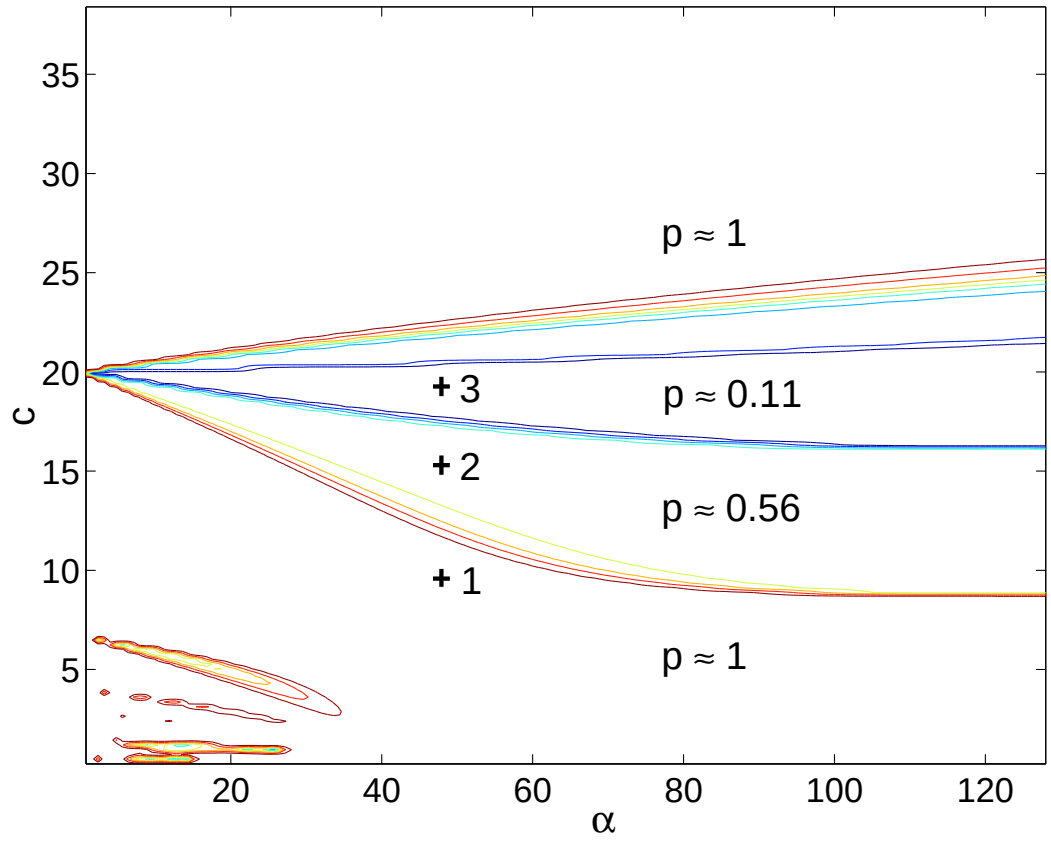

Figure 7: Contour plot of the order parameter, p, as a function of α and c using the analytic result Eq.(55). Here $b = 0.05$, $\beta = 0.5$, $n = 10$, $k_{max} = 40$. The symbols 1, 2 and 3 indicate the points of the parameter space that I used for the following Figs. 8, 9, and 10 correspondingly.

The order parameter Eq.(55) is equal to one when all of the voltage waveforms line up and it tends to zero if the waveform phases f_j are randomly distributed on the interval $[-\pi, +\pi]$. Fig. 7 shows the dependence of p on α and c. There are regions where the order parameter is approximately 1 (to within a few percent), where it is relatively small (~ 0.1) and where it has intermediate values. The next three figures demonstrate the behavior of the solution $\dot{\Phi}_j$ in these different regions of parameter space. Also shown in these figures are the corresponding results generated from direct numerical integration of the nonlinear differential equations (31,32). These are in good agreement with the analytically derived

solution.

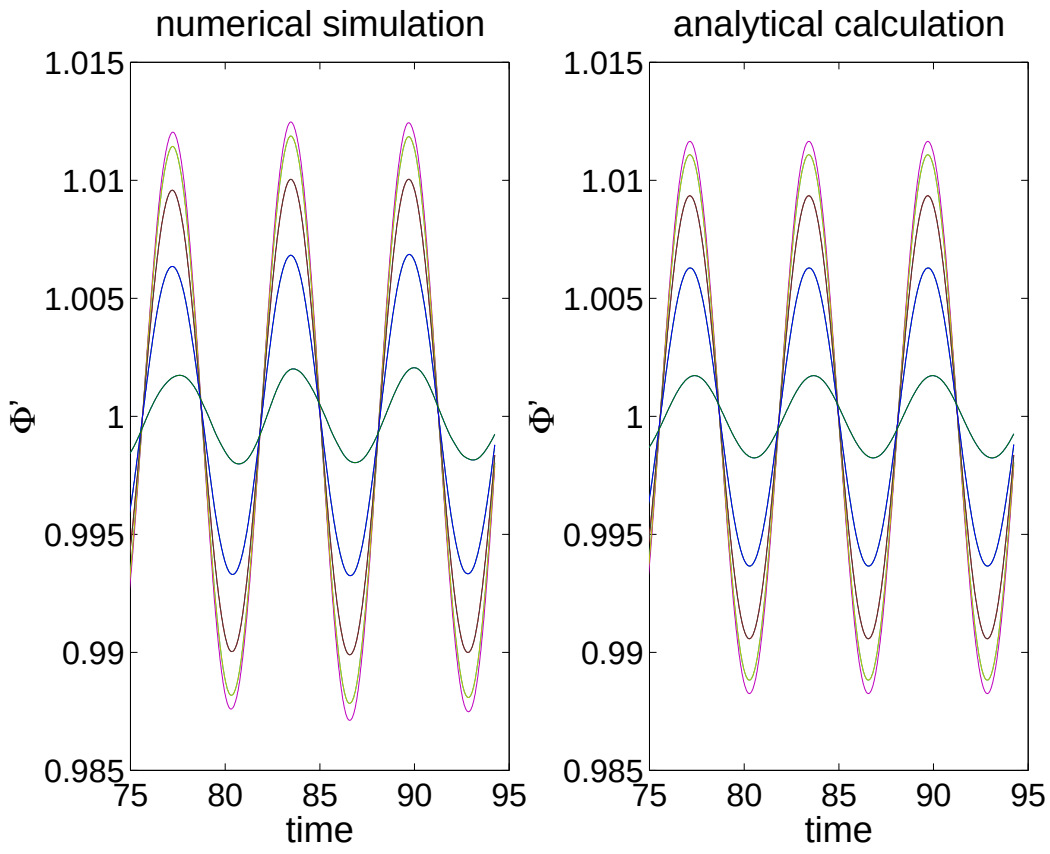

Figure 8: Functions $\dot{\Phi}_j(t)$ corresponding to the point 1 on Fig.7 ($\alpha = 48$, $c = 9.6$) from the region with $p \approx 1.00$. Although there are 9 junctions, only 5 curves are seen since the waveforms of junctions symmetrically located about the midpoint are identical.

2.4.3 Stability of the Synchronized State

Through second order, the solution for Φ_j is

$$\Phi_j(t) = t + \theta_j + b(a_j \sin t + b_j \cos t) - b^2(\langle \cos(t+\theta_j)\Phi_j^{(1)}\rangle t + E_j \sin 2t + F_j \cos 2t) + O(b^3).$$

From Eqs.(50,51,52), I obtain

$$\langle \cos(t+\theta_j)\Phi_j^{(1)}\rangle = \frac{P}{2\tilde{\alpha}}\left(1 - \sum_i \sigma_{ij}\cos(\theta_j - \theta_i) + \sum_i \rho_{ij}\sin(\theta_j - \theta_i)\right).$$

Hence, evaluating this at $t = 0$ and $t = 2\pi$ leads to, :

$$\Phi_j(2\pi) = \Phi_j(0) + 2\pi\left(1 - \frac{b^2 P}{2\tilde{\alpha}} + \frac{b^2 P}{2\tilde{\alpha}}\sum_{i=1}^{N}\sigma_{ij}\cos[\Phi_j(0) - \Phi_i(0)] - \right.$$
$$\left. - \frac{b^2 P}{2\tilde{\alpha}}\sum_{i=1}^{N}\rho_{ij}\sin[\Phi_j(0) - \Phi_i(0)]\right),$$

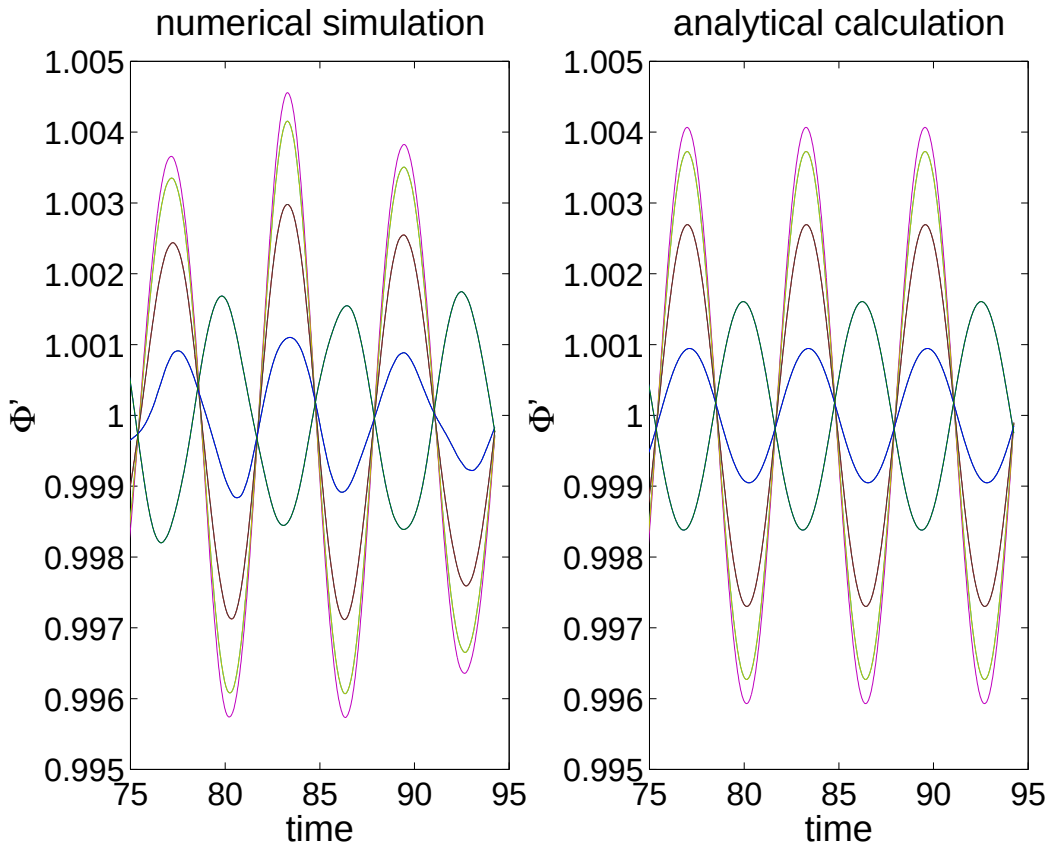

Figure 9: Functions $\dot{\Phi}_j(t)$ corresponding to the point 2 on Fig.7 ($\alpha = 48$, $c = 15.6$) from the region with $p \approx 0.56$.

where I have used the fact that $\Phi_j(0) = \theta_j + O(b)$. I can view this as an N-dimensional map for the phase dynamics. The fact that it involves "only" N variables is significant, since this is much smaller than the phase space dimension of the original problem. In effect, the map treats the other degrees of freedom as being slaved to the junction phases.

Consider now orbits that are infinitesimally close to the synchronized solution I identified previously, so that $\theta_j = \theta + \delta\theta_j$, where $|\delta\theta_j| \ll |\theta|$. Then one gets $\Phi_j = \Phi_j^0 + \delta\Phi_j$, where

$$\Phi_j^0(2\pi) = \Phi^0(0) + \left(2\pi - \frac{\pi b^2 P}{\tilde{\alpha}} + \frac{\pi b^2 P}{\tilde{\alpha}} \sum_{i=1}^{N} \sigma_{ij}\right), \tag{59}$$

$$\delta\Phi_j(2\pi) = \delta\Phi_j(0) - \frac{\pi b^2 P}{\tilde{\alpha}} \sum_{i=1}^{N} \rho_{ij}(\delta\Phi_j(0) - \delta\Phi_i(0)), \tag{60}$$

with $\Phi^0(0) = \theta$ and $\delta\Phi_j(0) = \delta\theta_j$. Now I ask whether the perturbations grow or shrink.

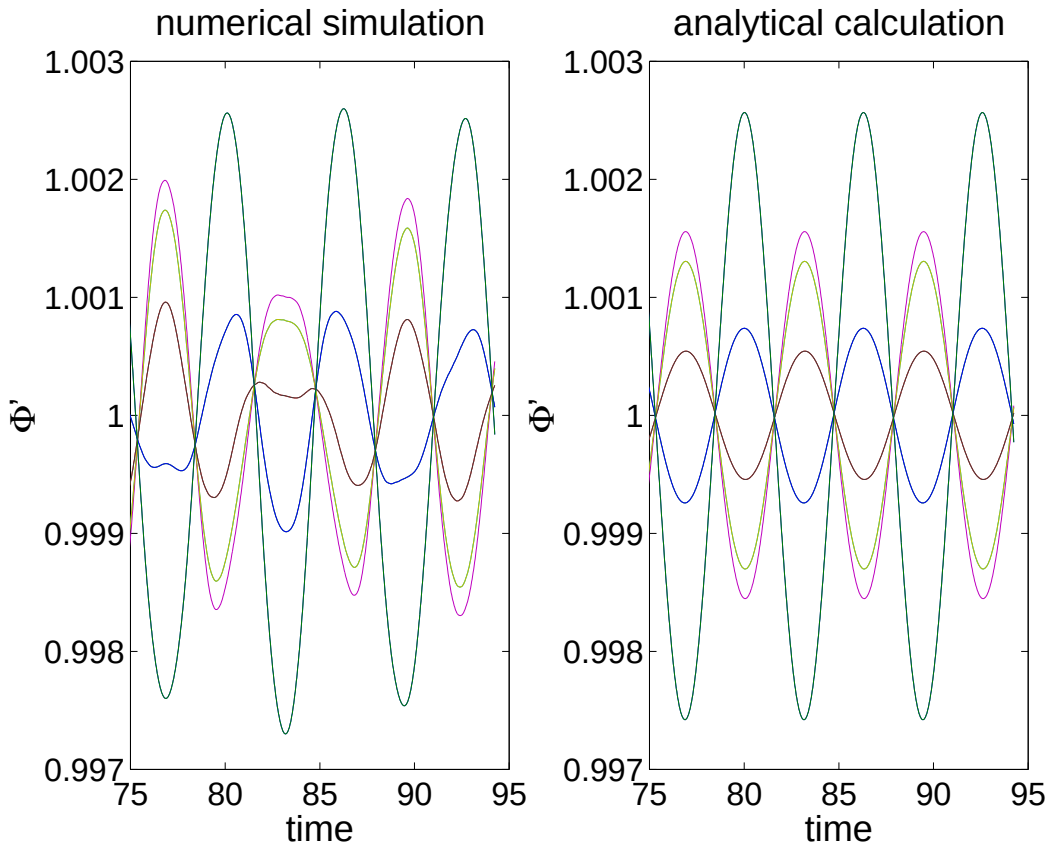

Figure 10: Functions $\dot{\Phi}_j(t)$ corresponding to the point 3 on Fig.7 ($\alpha = 48$, $c = 19.2$) from the region with $p \approx 0.11$.

One can rewrite Eq.(60) in matrix form:

$$\delta\overrightarrow{\Phi}(2\pi) = \mathbf{T}\delta\overrightarrow{\Phi}(0),$$

where

$$\mathbf{T}_{ij} = \delta_{ij}\left(1 - \frac{\pi b^2 P}{\tilde{\alpha}}\sum_m \rho_{mj}\right) + \frac{\pi b^2 P}{\tilde{\alpha}}\rho_{ij}. \tag{61}$$

If I denote by λ_m the eigenvalue of this matrix which has the largest magnitude, the stability condition is $\lambda_m < 1$.

Fig. 11 summarizes the behavior of λ_m over the (α, c)-parameter plane. I can identify four qualitatively different regions of parameters space. Region (I) corresponds to a resonant regime, with both λ_m and the order parameter p varying in a complicated fashion. The next section will be devoted exclusively to this region. Region (II) corresponds to an unstable regime, with the minimum eigenvalue of $\mathbf{T}_{ij}$ equal to one and all the other eigenvalues

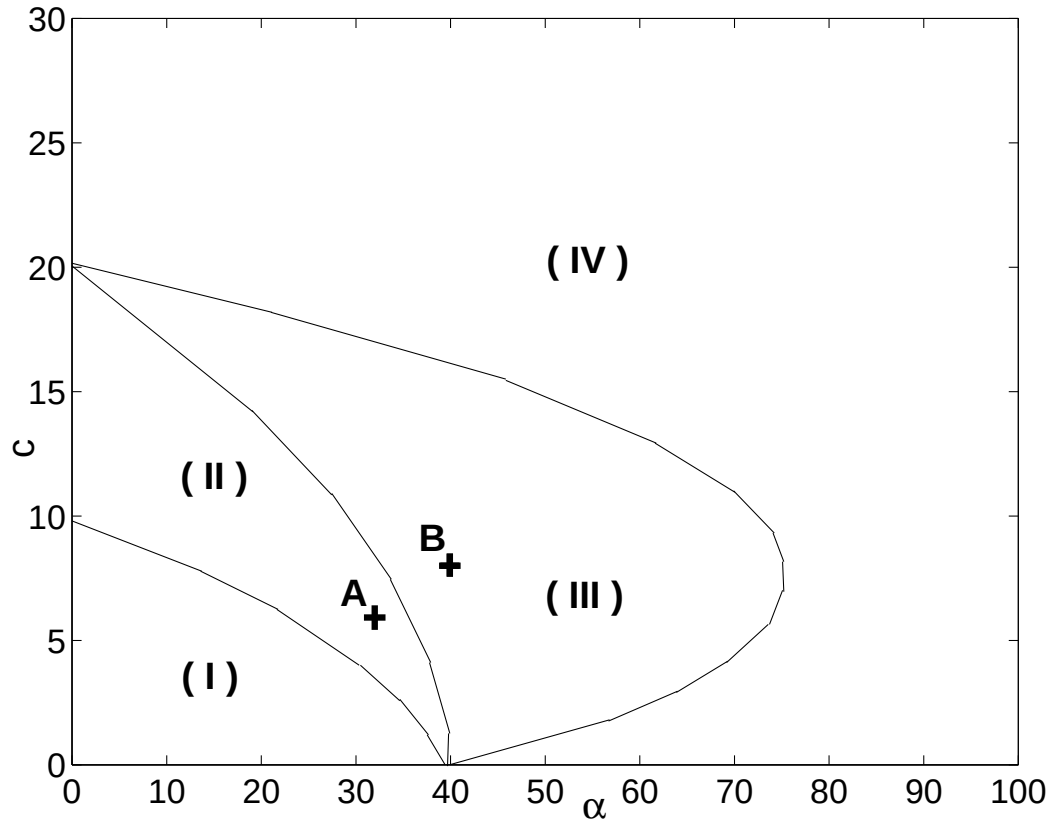

Figure 11: Schematic (based on the contour plot of the maximum eigenvalue of $\mathbf{T}_{ij}$ as a function of α and c for $b = 0.05$, $\beta = 0.5$, $n = 10$, $k_{max} = 40$), identifying qualitatively different regions of parameter space.

greater than one. Region (III) corresponds to a stable regime where the maximum eigenvalue is equal to one and all the other eigenvalues are less than one. Region (IV) also corresponds to a stable regime, but it is qualitatively different from region (III) by virtue of the fact that all of the eigenvalues here are close to one, so that this is a region of very weak stability.

Figures 12 and 13 demonstrate the behavior of the solution with parameters taken from opposite sides of the stability threshold. Fig. 12 corresponds to the point A in region (II), so that the initially perturbed solution never tends to the synchronized state $\dot{\Phi}_j^0$. Fig. 13 corresponds to the point B in region (III) where the initially perturbed solution converges to the inphase state.

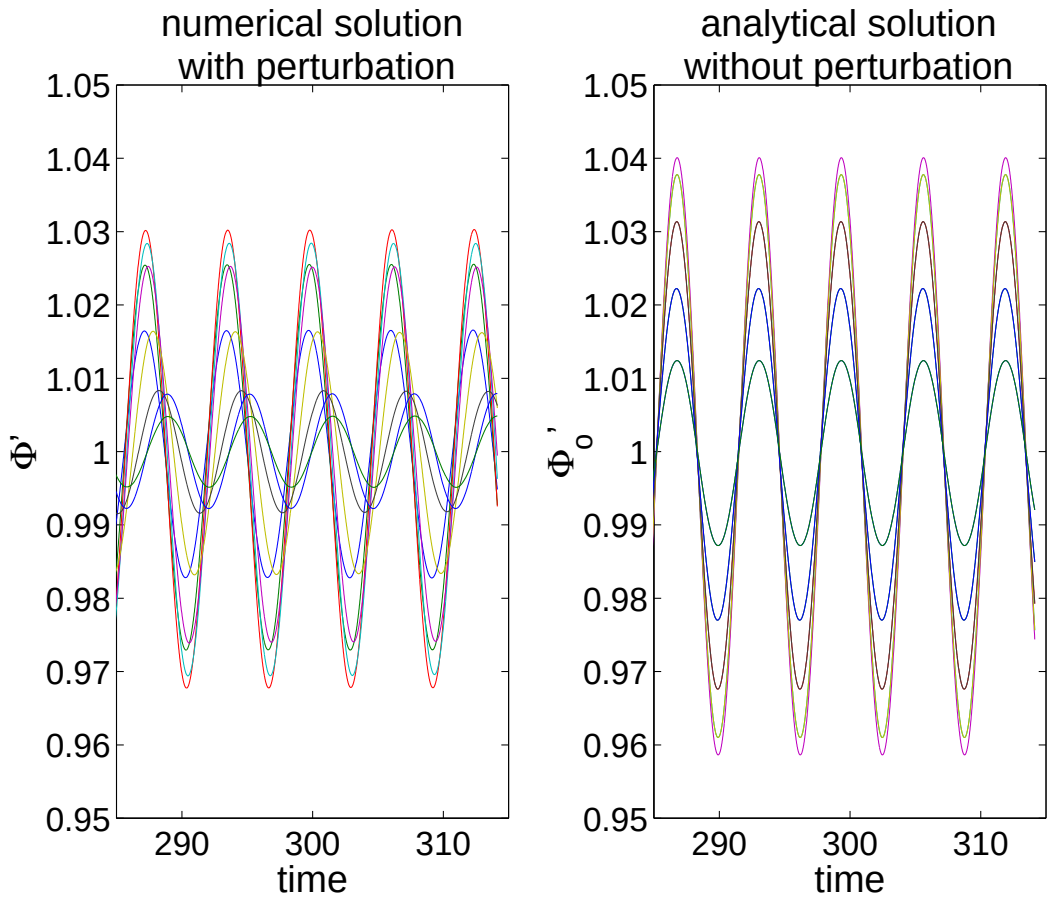

Figure 12: Functions $\dot{\Phi}_j(t)$ and $\dot{\Phi}_j^0(t)$ corresponding to the point A on Fig.11 ($\alpha = 32$, $c = 6.00$: unstable regime).

2.4.4 Discussion

My primary motivation was to develop some fundamental theoretical understanding of the synchronization dynamics when the spatial extent of the array is a significant factor. As a practical matter, this is an important issue if arrays are to produce greater power levels and operate at very high frequencies, since in this case the system gets pushed out of the lumped circuit limit. I have chosen a relatively simple situation to underscore the new physics that "turns on" in this regime. By considering a series array without an additional load, I have isolated the new coupling effects; without them (i.e. at low frequencies) the junctions are dynamically uncoupled, and no synchronization – inphase, splay phase, or otherwise – is possible.

One property of the distributed system is that the totally synchronized state is not a

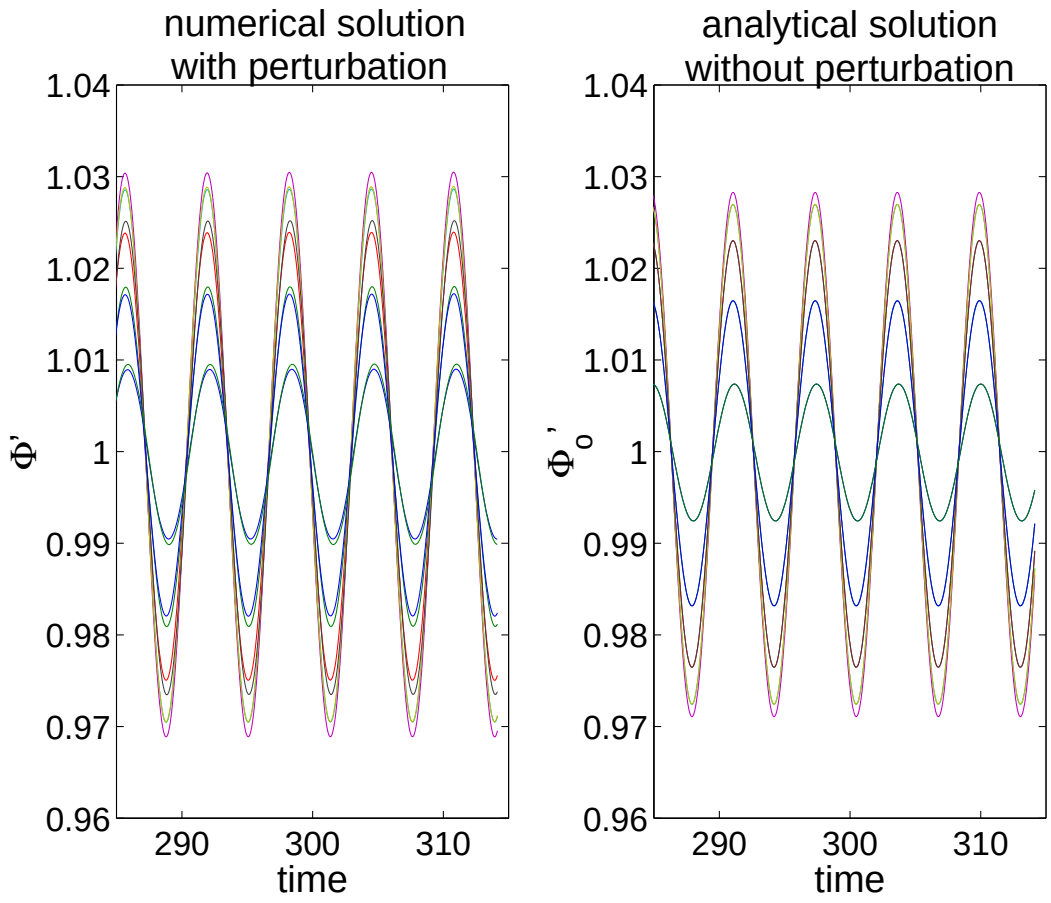

Figure 13: Functions $\dot{\Phi}_j(t)$ and $\dot{\Phi}^0_j(t)$ corresponding to the point B on Fig.11 ($\alpha = 40$, $c = 8.16$: stable regime).

possible solution. This makes the problem more subtle to study than the corresponding load-coupled lumped arrays, where the high degree of symmetry of the inphase state can be exploited. One nice feature of the perturbation expansion I employed is that it naturally identifies a highly synchronized solution, which may be thought of as the continuation of the solution branch containing the totally synchronized state. It is this state whose properties I analyzed.

Another interesting and somewhat unexpected result is that the array can show significant synchronization even when the most-synchronized state is unstable. The contour plot Fig. 7 summarizes this aspect of the problem. It is consistent with the stability diagram Fig. 11, and in some respects is equally useful. I also found a large region of parameter space where the most-synchronized state is stable but only very weakly so, and presumably

in this regime the coherence would be easily corrupted by the presence of quenched disorder and dynamical noise.

One obviously interesting variation of the problem is to consider spatially clustered junctions, an architecture which experiments have shown can result in significantly higher output powers than arrays in which the junctions are equally spaced [108, 109, 102](see the next section). This presents a great challenge for the theorist, since a non-uniform spacing of junctions lowers the symmetry of the problem still further.

A natural question to ask is whether the results are sensitive to weak disorder. I have presented results only for the case where the junctions are identical and equally spaced. The question of disorder deserves careful and systematic investigation, and I have not undertaken such a study. As a general rule, in regions of parameter space where the synchronized state is attracting, one expects the system behavior to be robust with respect to the addition of at least a small amount of disorder. Indeed, if the attractors are hyperbolic – the usual case except at bifurcation points – one is guaranteed that the attractors persist and vary continuously with arbitrary changes in the parameter values. To test this, I have run numerical simulations for the system (Eqs. 31,32) including a 5% spread in the parameters β_j and x_j, where β_j involves the junction parameters and x_j is the junction position. The behavior is not greatly changed: for example, for the conditions in Fig. 8, the disorder has a negligible effect on phase synchronization, and introduces variations of about 2% in the amplitudes. One might expect the most significant changes to occur at the stability boundary of the synchronized state, and in the region where the synchronized state is (in the ideal case) only weakly stable.

Finally, I point out that the same considerations which motivated the present work also apply to other physical realizations of coupled oscillator arrays. Of particular note are arrays of semiconductor oscillators which are being used to implement new strategies for power combining, beam steering, and beam shaping [115, 116, 117, 118, 119]. These arrays typically operate in the distributed-coupling limit in direct analogy with the Josephson system I studied here. The spatial variations of current in the stripline connecting the array elements acts as an intermediary which couples the various oscillators. Just as in

the Josephson problem, the various desirable dynamical states are highly synchronized. An analysis carried out along the lines here could determine which stripline conditions would be most favorable for achieving the target attractors.

2.5 Pairing Phenomenon

In this section, I describe a new phenomenon that arises in a particular architecture of an array of localized nonlinear oscillators coupled via the linear wave equation. Since I was first drawn to consider this problem by experimental schemes [108, 109] which use a resonant cavity architecture, where the spatial separation of the elements are matched to a particular normal mode of the transmission line and the junctions' temporal frequency is matched to that of the normal mode, in my analysis I do not make any assumptions about junction positions a priori, as I did in the previous section.

In my simulations, I find that pairs of oscillators very quickly synchronize (inphase), but that the synchronized pairs behave as though they are uncoupled [120]. This behavior is attracting: during the initial (transient) period, the various elements exhibit complicated interactions. Wiesenfeld has suggested the following analogy: roughly, the behavior is akin to a gas of interacting monatomic atoms which form a nearly inert gas of diatomic molecules.

Before starting the calculations, I will demonstrate the pairing effect in a specific case. Once again, let me consider a transmission line interrupted by N identical Josephson junctions. A constant current I_b is applied, which causes voltage oscillations in the individual junctions, and these drive the transmission line in turn. The dynamics is described by the system of dimensionless differential equations (31,32)

$$\ddot{A}_k + \tilde{c}^2 k^2 A_k + \tilde{\alpha} \sum_{j=1}^{N} \ddot{\Phi}_j \sin(\pi k r_j) = 0,$$

$$\tilde{\beta}\ddot{\Phi}_j + \dot{\Phi}_j + b \sin\Phi_j = 1 + \sum_{k=1}^{\infty} A_k \sin(\pi k r_j),$$

with the boundary conditions $I(0,t) = I(1,t) = 1$ and where Φ_j is the difference in the phase of the macroscopic quantum wave function across the j^{th} junction, and $A_k(t)$ are the

amplitudes of the transmission line spatial modes:

$$I(r,t) = 1 + \sum_{k=1}^{\infty} A_k(t) \sin(\pi k r). \tag{62}$$

Here, the transmission line wave velocity is $\tilde{c}/\pi$.

Consider the k^{th} standing wave of the transmission line. It has wavelength $2\ell/k$ and thus circular frequency $\omega = (2\pi)(\tilde{c}/\pi)(k/2\ell)$. Since in my units $\omega = \ell = 1$, the resonant architecture requires $\tilde{c}k = 1$, so that $\tilde{c}^{-1}$ is also equal to the total number of half-wavelengths of the standing wave.

Now suppose the junctions are evenly spaced: $r_i - r_{i-1} = \tilde{c}m$, where m is an odd integer, i.e. the spacing equals an odd multiple of half-wavelengths of some transmission line mode. One can readily show that in this case there exists an inphase periodic solution for the junction voltages $\sim \dot{\Phi}_j$. But it turns out this is not an attractor; instead the array forms inphase pairs; the phase relationship between pairs can be anything, depending on the initial conditions. Technically, the attracting set is an $N/2$-dimensional torus foliated by periodic orbits.

Fig. 14 shows the results of a simulation which illustrates the pairing phenomenon. An array of 10 equally spaced junctions with close but different initial conditions were placed at positions corresponding to antinodes of the bare transmission line mode having wavelength 1/5, so that $\tilde{c} = 1/10$ (and $m = 1$). Plotted are the time series of $\dot{\Phi}_j$. After a complicated transient, the system settles into a pairwise synchronized state. All elements oscillate with the same period, but the five paired waveforms are shifted one from another. In Fig. 14 the shifts are roughly uniform, but for different initial conditions the various shifts between paired waveforms will be different from those in Fig. 14.

Actually, the emergence of this dynamical state does not require equally spaced oscillators. The distance between pairs can be significantly altered, but as long as the size of each pair is equal to an odd multiple of $\tilde{c}$, synchronized pairs form and thereafter act independently. In fact, the fully symmetric case (all oscillators equally spaced) can also show far more complicated (non-pairing) dynamics owing to a kind of dynamical frustration effect. No such complications appear when the extra symmetry is removed; an example is shown

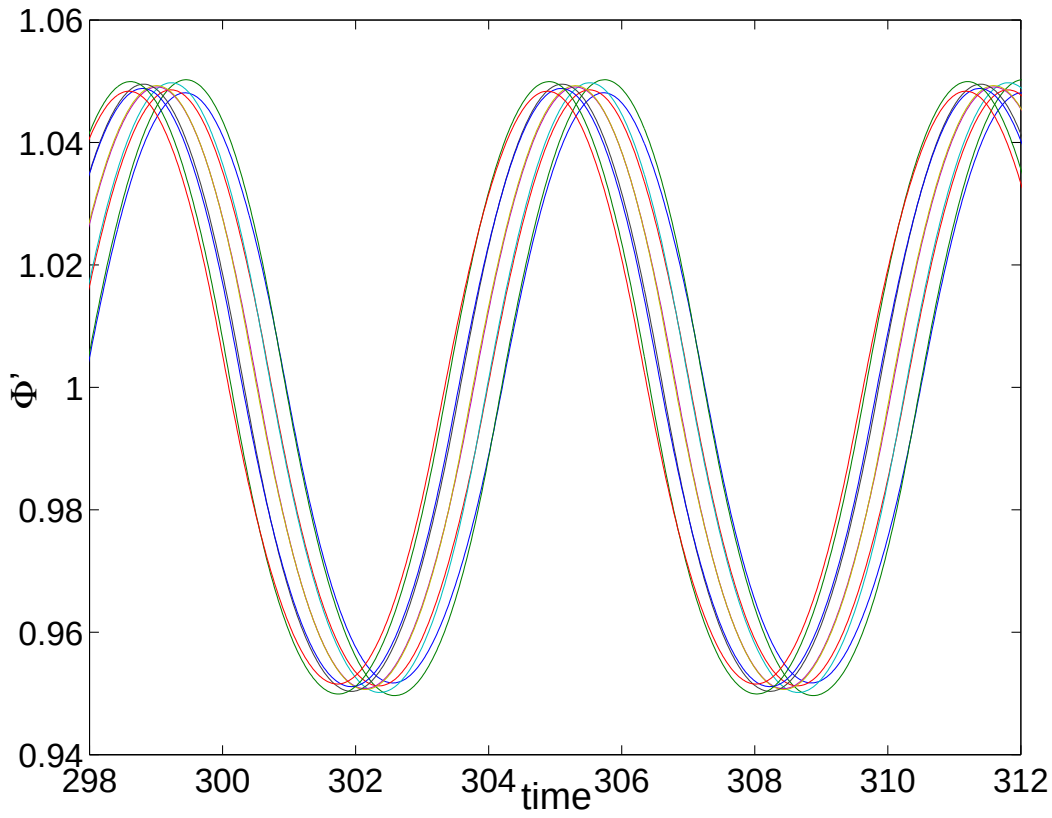

Figure 14: Simulation results of Eqs.(31,32), demonstrating the emergence of the paired state. The synchronized pairs are all nearest neighbors. Plotted are $\dot{\Phi}_j$ vs. t. Parameter values: $b = 0.05, \tilde{\alpha} = 0.05, \tilde{\beta} = 0.5, \tilde{c} = 0.1$.

in Fig. 15, with junction spacing alternating between $\tilde{c}$ and $\tilde{c}/2$. The figure shows a typical time series, as well as histograms generated from the final states for 500 different initial conditions. In almost all runs, the final state has very small phase shifts within each pair (left panel) but virtually arbitrary phase shifts between pairs (right panel).

Now I present an analysis of the problem which ultimately explains this peculiar dynamical state, and establishes the key links between resonant interactions of the transmission line, synchronization of oscillator pairs, and the resulting non-interaction between established pairs. I also find that these links do not rest on the particular nonlinearity of the Josephson junction, at least to first order; consequently, one can expect the same phenomenon for other types of nonlinear oscillator.

Although I will use the same perturbation approach as in the previous section, the calculations are quite different due to the fact that this problem does not have the symmetry

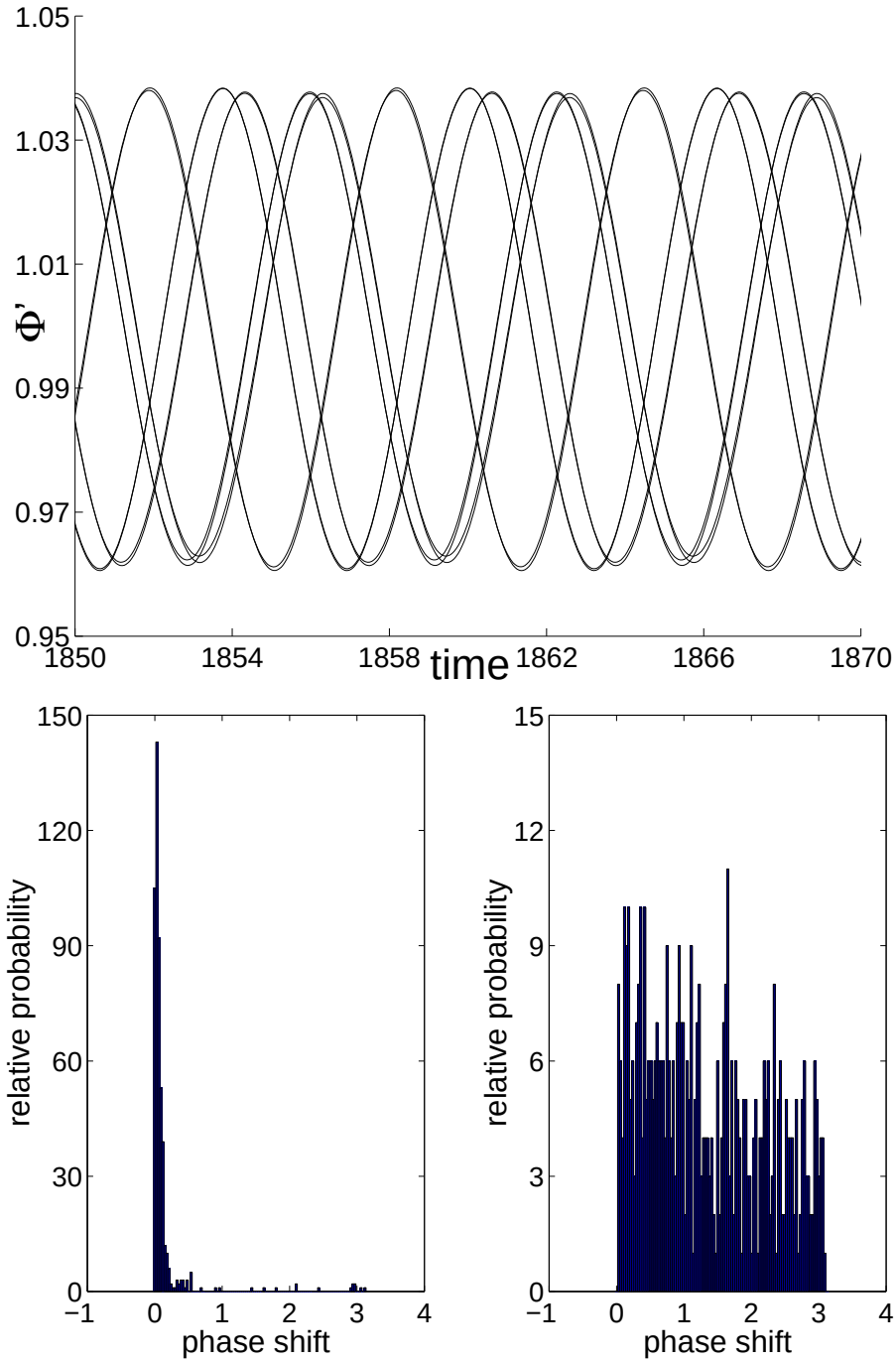

Figure 15: (Top) Same as Fig. 14, but for a system of 10 unevenly spaced junctions. Parameter values: $b = 0.05, \tilde{\alpha} = 0.7, \tilde{\beta} = 0.07, \tilde{c} = 0.1$. (Bottom) Histograms generated from the final states of 500 different initial conditions. Left: phase shift (in radians) between two oscillators a distance $\tilde{c}$ apart. Right: phase shift between oscillators a distance $\tilde{c}/2$ apart.

of equally-spaced junctions.

To lowest order in b the solution was found to be:

$$A_k^{(0)} = 0,$$
$$\Phi_j^{(0)} = t + \theta_j,$$

where the θ_j are constants. The junction phases advance with uniform angular velocity, and the transmission line is inactive.

The first order solution has the form

$$A_k^{(1)} = c_k \sin t + d_k \cos t, \tag{63}$$
$$\Phi_k^{(1)} = a_k \sin t + b_k \cos t,$$

which yields four sets of equations for the coefficients a_j, b_j, c_j, d_j

$$c_k = \tilde{\alpha} \sum_{j=1}^{N} \frac{a_j \sin(\pi k r_j)}{\tilde{c}^2 k^2 - 1},\ d_k = \tilde{\alpha} \sum_{j=1}^{N} \frac{b_j \sin(\pi k r_j)}{\tilde{c}^2 k^2 - 1}, \tag{64}$$

$$-\tilde{\beta} a_j - b_j + \cos\theta_j = -\sum_{i=1}^{N} a_i U_{ij}, \tag{65}$$

$$-\tilde{\beta} b_j + a_j + \sin\theta_j = -\sum_{i=1}^{N} b_i U_{ij}, \tag{66}$$

where

$$U_{ij} = \tilde{\alpha} \sum_{k=1}^{\infty} \frac{\sin(\pi k r_i)\sin(\pi k r_j)}{(1 - \tilde{c}^2 k^2)}. \tag{67}$$

From these equations one sees that U_{ij} plays the role of a coupling constant between junctions i and j.

Formally, the values of U_{ij} are infinite at the resonance $\tilde{c} = 1/K$. Hence, in the following analysis it is assumed that $\tilde{c} = 1/K + \varepsilon$, so that the final equations can be estimated at the resonance by taking the limit $\varepsilon \to 0$.

2.5.1 Single pair analysis

In order to get insight into the pairing phenomenon, I consider first the case of two junctions (N=2), and return to general N later. Then Eqs.(65,66) have the solution

$$\begin{aligned} a_1 &= -\frac{TM + RL}{KM - L^2},\ b_1 = \frac{PM + SL}{KM - L^2}, \\ a_2 &= -\frac{TL + RK}{KM - L^2},\ b_2 = \frac{PL + SK}{KM - L^2}, \end{aligned} \tag{68}$$

where

$$
\begin{aligned}
K &= 1 + U_{12}^2 + (U_{11} - \tilde{\beta})^2, \\
M &= 1 + U_{12}^2 + (U_{22} - \tilde{\beta})^2, \\
L &= U_{12}(2\tilde{\beta} - U_{11} - U_{22}), \\
T &= \sin\theta_1 + (U_{11} - \tilde{\beta})\cos\theta_1 + U_{12}\cos\theta_2, \\
R &= \sin\theta_2 + (U_{22} - \tilde{\beta})\cos\theta_2 + U_{12}\cos\theta_1, \\
P &= \cos\theta_1 - (U_{11} - \tilde{\beta})\sin\theta_1 - U_{12}\sin\theta_2, \\
S &= \cos\theta_2 - (U_{22} - \tilde{\beta})\sin\theta_2 - U_{12}\sin\theta_1.
\end{aligned}
$$

Rather than focus on the (monotonically increasing) phases $\Phi_j(t)$, things are clearer if one considers the time derivatives $\dot{\Phi}_j$ (which are also more physically relevant, being proportional to the voltage across the j^{th} junction). In the notation of the previous section $\dot{\Phi}_j = 1 + b\dot{\Phi}_j^{(1)} + O(b^2) = 1 + be_j \sin(t + f_j) + O(b^2)$, where $e_j^2 = a_j^2 + b_j^2$ and $\tan f_j = -\frac{a_j}{b_j}$. Note in particular that the waveforms generally have different amplitudes e_j as well as different phase-shifts f_j. The oscillations fully and constructively add if these phase-shifts are equal, so I define $f_1 = f_2$ as the synchronization condition. Hence, synchronization is achieved when

$$
\begin{aligned}
0 &= \frac{a_1}{b_1} - \frac{a_2}{b_2} = \frac{TM + RL}{PM + SL} - \frac{TL + RK}{PL + SK} \\
&= \frac{(TM + RL)(PL + SK) - (TL + RK)(PM + SL)}{(PL + SK)(PM + SL)} \\
&= \frac{TSMK + RPL^2 - TSL^2 - RPMK}{(PL + SK)(PM + SL)} \\
&= \frac{(TS - RP)(MK - L^2)}{(PL + SK)(PM + SL)}.
\end{aligned} \tag{69}
$$

Note that

$$\begin{aligned} MK - L^2 &= (1+U_{12}^2)^2 + (1+U_{12}^2)(U_{11}-\tilde{\beta})^2 + (1+U_{12}^2)(U_{22}-\tilde{\beta})^2 \\ &+ (U_{11}-\tilde{\beta})^2(U_{22}-\tilde{\beta})^2 - U_{12}^2(U_{11}-\tilde{\beta}+U_{22}-\tilde{\beta})^2 \\ &= 1 + 2U_{12}^2 + U_{12}^4 + (U_{11}-\tilde{\beta})^2 + (U_{22}-\tilde{\beta})^2 \\ &+ (U_{11}-\tilde{\beta})^2(U_{22}-\tilde{\beta})^2 - 2U_{12}^2(U_{11}-\tilde{\beta})(U_{22}-\tilde{\beta}) \\ &= 1 + 2U_{12}^2 + (U_{11}-\tilde{\beta})^2 + (U_{22}-\tilde{\beta})^2 + [U_{12}^2 - (U_{11}-\tilde{\beta})(U_{22}-\tilde{\beta})]^2. \end{aligned}$$

Therefore, $MK - L^2 - 1$ is the sum of positive values, so that $MK - L^2 \geq 1$. Using (69) I conclude that the synchronization condition can be written as

$$TS - RP = 0.$$

Up until now the oscillator positions have been arbitrary. But in order to get a fully symmetric solution, their spacing cannot be arbitrary. Specifically, if I set $\theta_1 = \theta_2 = \theta$, then the in-phase condition becomes

$$\begin{aligned} 0 &= TS - RP = [\sin\theta + (U_{11} - \tilde{\beta} + U_{12})\cos^2\theta][\cos\theta + (U_{22} - \tilde{\beta} + U_{12})\sin^2\theta] \\ &- [\sin\theta + (U_{22} - \tilde{\beta} + U_{12})\cos^2\theta][\cos\theta + (U_{11} - \tilde{\beta} + U_{12})\sin^2\theta] \\ &= (U_{11} - \tilde{\beta} + U_{12})\cos^2\theta - (U_{22} - \tilde{\beta} + U_{12})\sin^2\theta \\ &- (U_{22} - \tilde{\beta} + U_{12})\cos^2\theta + (U_{11} - \tilde{\beta} + U_{12})\sin^2\theta \\ &= (U_{11} - \tilde{\beta} + U_{12}) - (U_{22} - \tilde{\beta} + U_{12}) = U_{11} - U_{22}, \end{aligned}$$

so that $U_{11} = U_{22} = U$, which is equivalent to $r_2 = r_1 + m\tilde{c}$, where $m = 1, 2, 3, ..., [\frac{1-r_1}{\tilde{c}}]$. That is, the distance between oscillators must be an integer multiple of half-wavelengths of the transmission line's resonant mode. Moreover, in this case $M = K$, and the resonant configuration implies $U_{12} = (-1)^m U$.

If m's are odd integers, then

$$T = R = \sin\theta - \tilde{\beta}\cos\theta,$$

$$P = S = \cos\theta + \tilde{\beta}\sin\theta.$$

Substituting this into Eqs.(68), I obtain

$$a_1 = a_2 = -\frac{T(M+L)}{M^2-L^2} = -\frac{T}{M-L},$$
$$b_1 = b_2 = \frac{P(M+L)}{M^2-L^2} = \frac{P}{M-L},$$

where

$$M - L = 1 + U^2 + (\tilde{\beta} - U)^2 + 2U(\tilde{\beta} - U) = 1 + \tilde{\beta}^2.$$

Finally, for the amplitudes $e_{1,2}$ and phases $f_{1,2}$, I get the following expressions:

$$e_1^2 = e_2^2 = \frac{T^2 + P^2}{(M-L)^2} = \frac{1}{1+\tilde{\beta}^2},$$
$$\tan f_1 = \tan f_2 = \frac{T}{P} = \frac{\tan\theta - \tilde{\beta}}{1 + \tilde{\beta}\tan\theta} = \tan(\theta - \arctan\tilde{\beta}).$$

Similarly, for even m's:

$$T = R = \sin\theta - (\tilde{\beta} - 2U)\cos\theta,$$
$$P = S = \cos\theta + (\tilde{\beta} - 2U)\sin\theta,$$

and

$$M - L = 1 + U^2 + (\tilde{\beta} - U)^2 - 2U(\tilde{\beta} - U) = 1 + (\tilde{\beta} - 2U)^2,$$

so that

$$e_1^2 = e_2^2 = \frac{1}{1 + (\tilde{\beta} - 2U)^2},$$
$$f_1 = f_2 = \theta - \arctan(\tilde{\beta} - 2U).$$

Therefore, there are two types of the synchronized solution: the first one for odd m's, and the second for even m's:

$$[1] \qquad \dot{\Phi}_{1,2} = 1 - b\,\frac{\sin(t + \theta - \arctan\tilde{\beta})}{\sqrt{1+\tilde{\beta}^2}}, \tag{70}$$

$$[2] \qquad \dot{\Phi}_{1,2} = 1 - b\,\frac{\sin(t + \theta - \arctan(\tilde{\beta} - 2U))}{\sqrt{1 + (\tilde{\beta} - 2U)^2}}. \tag{71}$$

However, the even-m solution is extremely sensitive: the amplitude e_{tot} of the total voltage $\dot{\Phi}_1 + \dot{\Phi}_2$ varies wildly depending on the precise position of the pair in the transmission

line. In contrast, for odd m's the amplitude e_{tot} is always equal to the value $\frac{2b}{1+\tilde{\beta}^2}$. For this reason, I robustly observe synchronization for odd m only.

The above assumed that $\theta_1 = \theta_2$. But in fact synchronization is insensitive to small disturbances when the transmission line is driven resonantly. I can readily show that if I introduce perturbations $\theta_i = \theta + \delta\theta_i$, where $\delta\theta_1 \neq \delta\theta_2$ and $|\delta\theta_i| \ll 1$, then in the resonant limit $|U| \to \infty$ the phases are both shifted *but by the same amount*. Note that the resonant condition $|U| \to \infty$ is equivalent to the statement that $1/\tilde{c}$ (or the number of the current standing half-wavelengths in the transmission line without junctions) is an integer number.

I now prove the above statement. Indeed,

$$\begin{aligned}
T &= T_0 + (\cos\theta + (\tilde{\beta} - U)\sin\theta)\delta\theta_1 - (-1)^m U \sin\theta\delta\theta_2, \\
R &= T_0 + (\cos\theta + (\tilde{\beta} - U)\sin\theta)\delta\theta_2 - (-1)^m U \sin\theta\delta\theta_1, \\
P &= P_0 - (\sin\theta - (\tilde{\beta} - U)\cos\theta)\delta\theta_1 - (-1)^m U \cos\theta\delta\theta_2, \\
S &= P_0 - (\sin\theta - (\tilde{\beta} - U)\cos\theta)\delta\theta_2 - (-1)^m U \cos\theta\delta\theta_1,
\end{aligned}$$

where T_0 and P_0 are the unperturbed values. Thus,

$$\begin{aligned}
TM + RL = T_0(M+L) \quad &+ \quad [M(\cos\theta + (\tilde{\beta} - U)\sin\theta) - (-1)^m LU \sin\theta]\delta\theta_1 \\
&+ \quad [L(\cos\theta + (\tilde{\beta} - U)\sin\theta) - (-1)^m MU \sin\theta]\delta\theta_2
\end{aligned}$$

and

$$\begin{aligned}
PM + SL = P_0(M+L) \quad &- \quad [M(\sin\theta - (\tilde{\beta} - U)\cos\theta) + (-1)^m LU \cos\theta]\delta\theta_1 \\
&- \quad [L(\sin\theta - (\tilde{\beta} - U)\cos\theta) + (-1)^m MU \cos\theta]\delta\theta_2.
\end{aligned}$$

To first order in $\delta\theta_{1,2}$

$$\begin{aligned}
\frac{TM + RL}{PM + SL} = \frac{T_0}{P_0}\Bigg[1 \quad &+ \quad \frac{M(\cos\theta + (\tilde{\beta} - U)\sin\theta) - (-1)^m LU \sin\theta}{T_0(M+L)}\delta\theta_1 \\
&+ \quad \frac{L(\cos\theta + (\tilde{\beta} - U)\sin\theta) - (-1)^m MU \sin\theta}{T_0(M+L)}\delta\theta_2 \\
&+ \quad \frac{M(\sin\theta - (\tilde{\beta} - U)\cos\theta) + (-1)^m LU \cos\theta}{P_0(M+L)}\delta\theta_1 \\
&+ \quad \frac{L(\sin\theta - (\tilde{\beta} - U)\cos\theta) + (-1)^m MU \cos\theta}{P_0(M+L)}\delta\theta_2\Bigg],
\end{aligned}$$

which can be written as

$$\frac{TM+RL}{PM+SL} = \frac{T_0}{P_0}\Bigg[1 \quad + \quad \frac{MP_0+(-1)^m(M-L)U\sin\theta}{T_0(M+L)}\delta\theta_1 + \quad \frac{LP_0-(-1)^m(M-L)U\sin\theta}{T_0(M+L)}\delta\theta_2 + \quad \frac{MT_0-(-1)^m(M-L)U\cos\theta}{P_0(M+L)}\delta\theta_1 + \quad \frac{LT_0+(-1)^m(M-L)U\cos\theta}{P_0(M+L)}\delta\theta_2\Bigg].$$

Finally, for odd m's, in the limit $|U| \to \infty$, we have finite T_0 and P_0, and $\lim_{|U|\to\infty} \frac{M}{L} = 1$. Therefore:

$$\tan f_1 = \tan f_2 = \frac{T_0}{P_0}\left(1 + \frac{(T_0^2+P_0^2)(\delta\theta_1+\delta\theta_2)}{2T_0P_0}\right).$$

Having established the link between pair synchronization and resonant modes I now ask why such a pair might be "dynamically inert". Since all interactions are carried by the current oscillations in the transmission line, let's calculate $I(r,t)$. Combining Eqs.(62,63,64) yields

$$I(r,t) = 1 - b\sum_{j=1}^{N}\Phi_j^{(1)}(t)U_j(r) + O(b^2), \tag{72}$$

$$\text{where} \qquad U_j(r) = \tilde{\alpha}\sum_{k=1}^{\infty}\frac{\sin(\pi k r_j)\sin(\pi k r)}{(1-\tilde{c}^2k^2)}. \tag{73}$$

For a perfectly synchronized pair of junctions, with $r_2 - r_1 = m\tilde{c}$ and m odd, the spatial dependence of current is

$$I(r) = b\tilde{\alpha}\sum_k \frac{\sin(\pi k r_1)+\sin(\pi k r_2)}{1-\tilde{c}^2k^2}\sin(\pi k r) \tag{74}$$

$$= \begin{cases} \frac{\pi b\tilde{\alpha}}{2\tilde{c}}\sin\left[\frac{\pi}{\tilde{c}}(r-r_1)\right]; & \text{if } r_1 < r < r_2, \\ 0; & \text{otherwise.} \end{cases}$$

Thus, to leading order the current changes its value only in the piece of transmission line between the two synchronized junctions!

Numerical simulations of the full nonlinear equations show that the current is not strictly zero outside the oscillator pair, but it is very small. It is plausible that one could add another

synchronized pair elsewhere on the transmission line without the two pairs affecting each other; moreover, the precise placement of the second pair (relative to the first) should be irrelevant.

2.5.2 Multi-junction resonant array

These plausibility arguments for the array case ($N > 2$) can be put on a firm analytic footing. Specifically, I now explicitly construct pairwise synchronized solutions and show that these yield a spatially localized current profile which generalizes Eq.(74).

Guided by the single pair analysis, I choose the oscillator positions so that $r_i - r_{i-1} = \tilde{c}m_i$, for $i = 2, 3, \ldots, N$. Thus, the junctions need not be equally spaced, but the distance between any two adjacent elements is an integer multiple of half-wavelengths of a transmission line mode. (This condition is rather restrictive: numerical simulations show that it is enough if it is satisfied for even i only. I use the stronger constraint in order to make the problem analytically tractable.) It follows that (see Eq.(67)) $U_{ij} = (-1)^{i+j}U$, where U is a function of three parameters $\tilde{\alpha}, \tilde{c}$ and r_1. In this case the solution of Eqs.(65,66) is

$$a_j = \frac{-\sin\theta_j + \tilde{\beta}\cos\theta_j}{1+\tilde{\beta}^2} - \frac{U}{(1+\tilde{\beta}^2)[1+(\tilde{\beta}-NU)^2]} \tag{75}$$
$$\times \sum_{i=1}^{N}(-1)^{i+j}\left[\cos\theta_i(1-\tilde{\beta}^2+\tilde{\beta}NU) + \sin\theta_i(2\tilde{\beta}-NU)\right],$$

$$b_j = \frac{\cos\theta_j + \tilde{\beta}\sin\theta_j}{1+\tilde{\beta}^2} - \frac{U}{(1+\tilde{\beta}^2)[1+(\tilde{\beta}-NU)^2]} \tag{76}$$
$$\times \sum_{i=1}^{N}(-1)^{i+j}\left[\sin\theta_i(1-\tilde{\beta}^2+\tilde{\beta}NU) - \cos\theta_i(2\tilde{\beta}-NU)\right].$$

The pairwise synchronized state corresponds to $\theta_1 = \theta_2$, $\theta_3 = \theta_4$, etc., so that $f_1(t) = f_2(t), f_3(t) = f_4(t)$, and so on. To find the current profile $I(r,t)$ for this state, note first that Eqs.(72,73) remain true for an array. It follows that through $O(b^2)$

$$I(r,t) = 1 - b\tilde{\alpha}\sum_{j\,\text{even},k}\Phi_j^{(1)}\frac{\sin(\pi k r_j)+\sin(\pi k r_{j-1})}{1-\tilde{c}^2k^2}\sin(\pi k r),$$

since $\Phi_j = \Phi_{j-1}$ for all even j. The sum over k can be performed as before, with result

$$I(r,t) - 1 = \sum_{j \text{ even}} \Phi_j^{(1)}(t) \times \begin{cases} \frac{\pi b \tilde{\alpha}}{2\tilde{c}} \sin\left[\frac{\pi}{\tilde{c}}(r - r_{j-1})\right]; & \text{if } r_{j-1} < r < r_j, \\ 0; & \text{otherwise,} \end{cases}$$

for $j = 2, 4, \ldots, N$. This generalizes the previous result for $N = 2$: in between each synchronized pair, the current in the transmission line takes on its constant boundary value, as if there were no junctions at all.

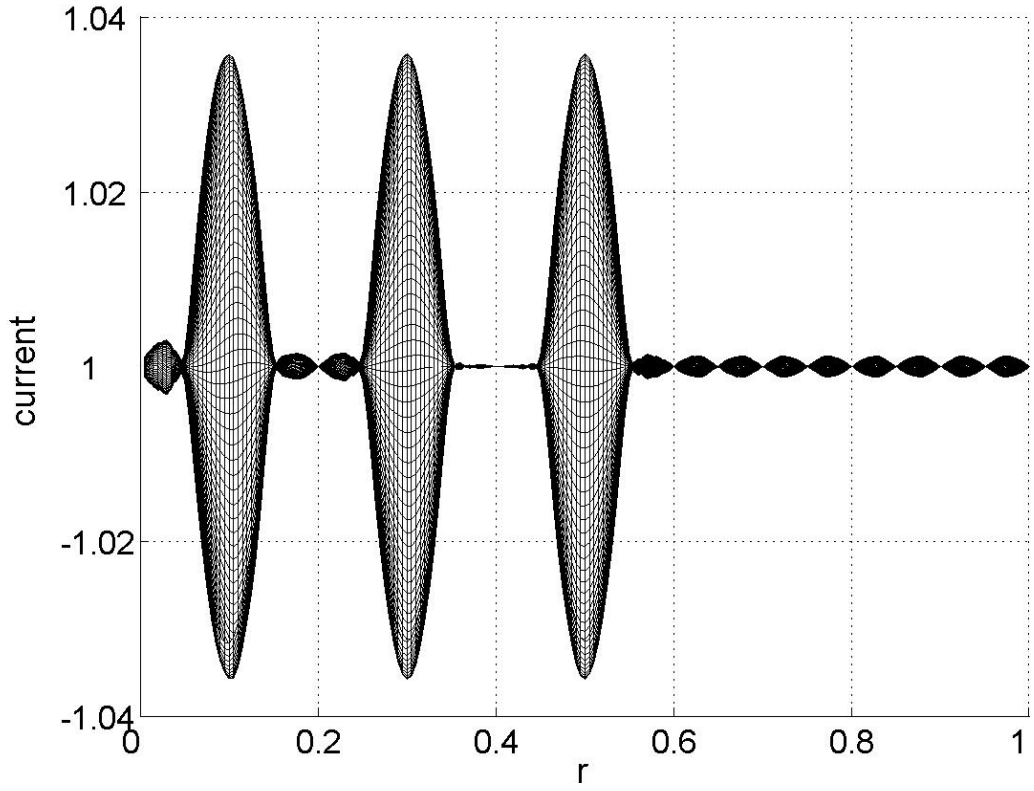

Figure 16: Simulation results for $n = 6$, showing the spatial profile of the transmission line current once the paired state is formed. Parameter values: $b = 0.05, \tilde{\alpha} = 0.05, \tilde{\beta} = 0.5, \tilde{c} = 0.1$.

Fig. 16 shows the actual transmission line current found via direct numerical simulation of Eqs.(4,5) for $N = 6$. The junction positions are self-evident; note that there is no particular symmetry in the placement of the junctions along the transmission line. The current is greatly reduced outside the junction pairs (though not strictly zero) indicating

the pairs are very weakly interacting. Although not shown in the figure, the paired junctions are strongly synchronized, having virtually identical and inphase waveforms.

My analysis suggests that the pairing phenomenon is insensitive to the detailed dynamical properties of Josephson junctions *per se*. Rather, it hinges on the resonant coupling architecture inherent to the transmission line. I was thus led to consider an array of van der Pol oscillators embedded in a transmission line:

$$\ddot{A}_k + \tilde{c}^2 k^2 A_k + \tilde{\alpha} \sum_{j=1}^{N} \dot{V}_j \sin(\pi k r_j) = 0,$$

$$\tilde{\beta}\ddot{V}_j - b_1 \dot{V}_j (1 - \epsilon V^2) + b_2 V_j = \sum_{k=1}^{\infty} \dot{A}_k \sin(\pi k r_j).$$

I set up a simulation just as before, with oscillators spaced at odd-integer multiples of $\frac{1}{2}\lambda$, where λ is the wavelength of some resonant mode of the bare transmission line. The emergence of inert, synchronized oscillator pairs was readily observed.

Fig. 17 shows the results from one run, using 4 oscillators. The spatial profile for the transmission line current shows substantially reduced magnitude outside the two synchronized pairs. The reduction is not as complete as in the Josephson array, indicating that the pair interactions are not as weak. The inset shows the steady state time series for all four oscillators: the waveforms show a fair degree of amplitude meandering. Even so, the pairing behavior is unmistakable.

Perhaps the closest thing in the coupled nonlinear oscillator literature to this pairing behavior is the phenomenon of clustering. The term clustering is actually used to describe a rather broad set of circumstances where one or more subsets of the population display some type of synchronous behavior. In some cases such cluster(s), once formed, effectively decouple from the remaining population. In other cases, synchronized clusters interact strongly with each other, much like domains in a magnetic material. Examples may be found in various dynamical settings, including coupled map lattices, neural networks, and chaotic differential equations [121, 122, 123].

Broadly speaking, the pairing phenomenon in my problem might be viewed as another example of clustering; however, it seems to differ in two fundamental respects from existing examples. First, the pairs have an intrinsic spatial size. This is a consequence of the

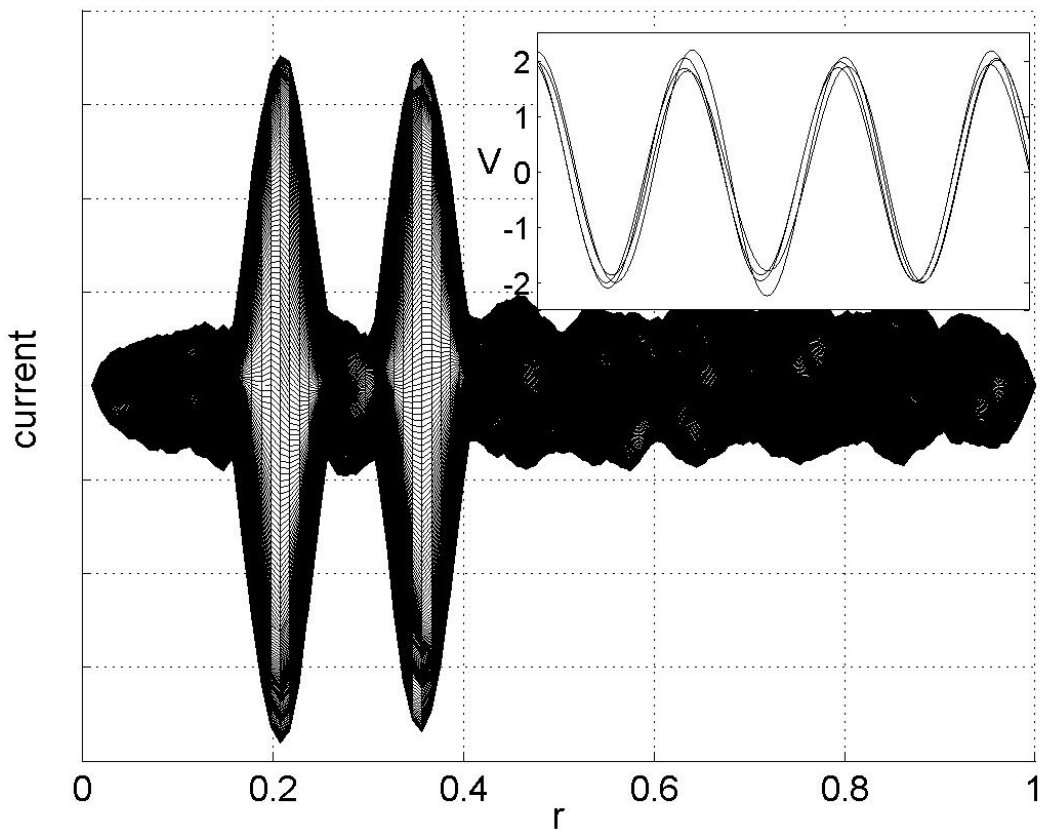

Figure 17: Transmission line current vs. position with Van der Pol oscillators at positions $r_1 = 0.15, r_2 = 0.25, r_3 = 0.3, r_4 = 0.4$. Other system parameters are $b_1 = 0.01, \tilde{\alpha} = 0.05, \tilde{\beta} = b_2 = \epsilon = 1, \tilde{c} = 0.1$. Inset: V_j vs. t for all 4 oscillators.

interaction being mediated by the transmission line rather than direct coupling between elements. The other difference is the nature of the paired state, in which the elements are synchronized in phase. More commonly, when clustered subsets decouple from the remaining population, their phases are staggered in a way which naturally results in a cancelling effect. Perhaps the most famous such case is variously termed splay-phase or anti-phase clustering (an early example of which, as it happens, was reported in a different Josephson junction array [91, 93]). In contrast, an in-phase pairing would normally be expected to reinforce their effect on the remaining population, rather than cancel out.

CHAPTER III

FIBER LASER ARRAYS

The main subject of this chapter is the phenomenon of weak-link synchronization, which is another important example of synchronization due to a nontrivial dynamical coupling. Although this phenomenon will be described in context of coupled fiber lasers, the general idea might be very useful for the study of other array systems, especially those that require avoiding the idealized assumption of identical oscillators.

The first section contains the basic information about individual fiber lasers and amplifiers which is necessary for the development of the model I use later as a tool to investigate the behavior of an array of such lasers.

This model of a specific experimental setup is introduced in the second section. A step by step derivation of the governing equations is provided with a clear statement of all assumptions made.

The next section presents coupled mode theory, which is used to describe the dynamics of electric fields interacting in closely placed waveguiding fibers. The basic results of this theory are fundamental for the model construction.

The results of analytical and numerical analysis of the system are presented in Section 4, which also includes a discussion of the general concept of weak-link synchronization. Since the calculations essential for the understanding of the observed phenomena are quite tedious and lengthy, I have placed them in Appendix.

3.1 Fiber Lasers and Amplifiers

In some sense fiber lasers [124, 125] can be considered as a logical miniaturization of solid-state lasers. In 1963, Koester and Snitzer demonstrated the first fiber amplifier made of a one-meter neodymium-doped fiber wrapped around a flash lamp [126]. Still, the idea of using an optical fiber as a laser medium did not receive much attention until the development

of fiber-optic communication systems came to a point when further progress required new ways to boost signals in extended transmission lines.

However, the concept of optical communication was born a time long ago, in the 1870s, when John Tyndall showed that light can follow a specific path by a series of internal reflections. In the 1880s, Alexander Bell created a so called photophone. It took about 70 years before fiber optics really became useful in applications. In the 1950s an image-transmitting device - the fiberscope - was developed mainly for weld inspections. It used glass-coated glass fiber as a signal transmitter. When (in the 1970s) improved technology of glass fabrication allowed one to satisfy all practical requirements, fiber optics also became a feasible method of communication [127].

The operation of fiber optics is based on the principles of total internal reflection, which means that all of the light gets reflected within the fiber cable. The angle at which light hits the surface is known as the angle of incidence. The critical angle is the angle of incidence at which the angle of refraction is equal to $\pi/2$. Total internal reflection is achieved when the angle of incidence is bigger than the critical angle (see Fig. 18).

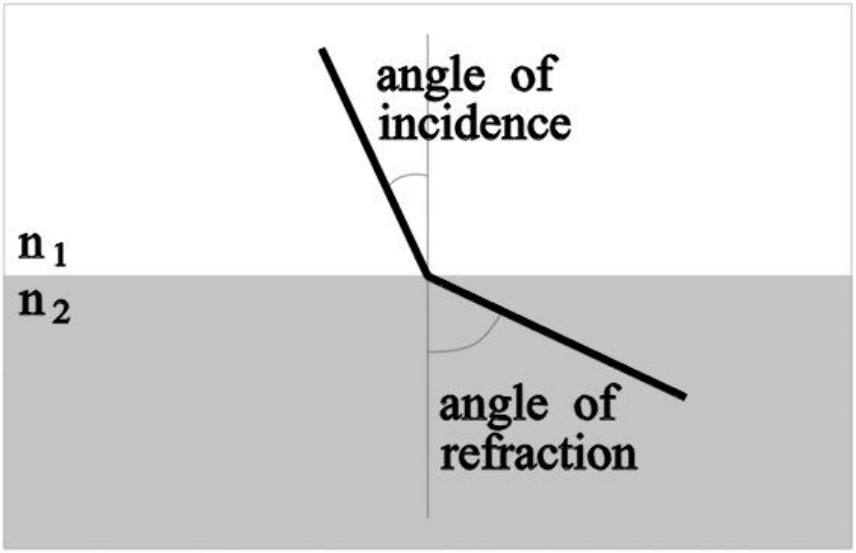

Figure 18: General schematic of refraction.

Fiber-optic cables consist of very thin threads of ultra-pure glass, which are called the cores. The region surrounding the core is known as the cladding. It is the cladding that

is responsible for reflecting the light back into the core. In order to do that, the cladding must have a smaller index of refraction than the refractive index of the core. Protection and strength of the fiber is provided by the outer region called the coating, which can be made of Kevlar, for instance.

There are two basic types of fiber cable. The first commercially available fiber-optic cables were multimode fibers with a relatively large core, allowing hundreds of modes to pass through the fiber simultaneously. The other fiber cables belong to a class of singlemode fibers. These fibers have a smaller core than that of multimode cables, but they allow one to transmit more information by retaining better fidelity of light pulses over long distances.

One should always take into account transmission losses. In the case of fiber optics, these losses come from scattering, absorption, and dispersion, which lead to an overall signal attenuation. To solve this problem, engineers use fiber laser amplifiers to maintain the signal in optical communication systems.

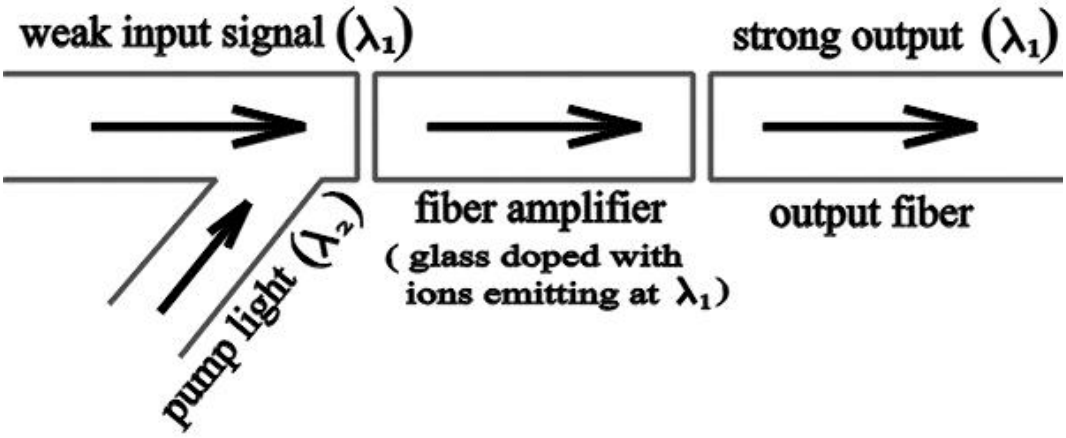

Figure 19: Schematic of a fiber amplifier.

Fig. 19 shows the basic concept of a fiber amplifier. It is made of a solid-state laser material such as glass, doped with ions that emit the light of a desired wavelength, let's

say λ_1. Suppose the fiber has a weak signal with wavelength λ_1 at one end, and it is illuminated by a strong steady beam, which has wavelength λ_2 and excites the doped ions to their upper level. While the weak signal propagates along the amplifier, it stimulates emission of excited ions at λ_1 and, consequently, get amplified. The remaining light from the pump passes through the cable with much stronger attenuation than the amplified signal, so that only the desired signal gets transmitted.

High-performance optical fiber systems utilize mainly two windows of operation. Some cables works at the wavelength $1.3\mu m$, when step-index single-mode fibers have almost zero pulse dispersion. The other operating regime is at $1.55\mu m$, when silica fibers have the lowest attenuation. Scientists have found proper solid-state laser ions for each of these regimes. Neodymium is used for the $1.3\mu m$ fibers, while the $1.54\mu m$ line of erbium is suitable for the longer wavelength signals in silica glasses. However, other materials also have been tested in experiments. In principle, materials such as fluoride-based and phosphate glasses can provide less excited-state absorption, better wavelengths or other features useful in applications.

There are several important advantages of fiber lasers compared to other laser types. Fiber lasers have low losses, simple doping procedures and can be pumped with compact, efficient diodes. Since the fiber itself provides the waveguide, it minimizes the necessity of mechanical alignments and bulk optics. Fiber lasers have different cavity designs such as linear Fabry-Perot, ring or a combination of those two. Another advantage of fiber lasers is a strong nonlinearity of the media because of long interaction lengths and relatively large signal intensities. The nonlinearity is important for the mode-locking mechanism. In the last decades, fiber lasers have motivated a lot of research effort due to their potential implementations as compact fiber-compatible optical sources with a simple diode pumping [128, 129, 130, 131].

3.2 Coupled Fiber Lasers

An important and challenging area of laser physics is coherent combination of laser beams [132, 133, 134, 135, 136, 137, 138, 139]. In many industrial and scientific applications researchers

pursue the goal of obtaining a single high-power output from a number of moderate-power lasers and to control its deflection without mechanical movements.

An array of lasers that has constant relative phases between its elements provides the output with maximum spatial brightness. The brightness of an incoherent array increases in direct proportion to the number of lasers. However, the brightness of a phase-locked array increases as the square of this number, which makes coherent arrays of lasers very attractive from the technological point of view.

Rare-earth-doped fiber lasers are excellent candidates for such coherent arrays for a number of reasons. Although the power of individual fiber lasers is lower than the power of solid-state or gas lasers, fiber lasers have compact transverse dimensions, relative freedom from thermal problems and single-mode beam structure [140, 141, 142, 143, 144, 145, 146, 147].

Recently, researchers have been especially interested in the development of field-coupled multicore fiber laser arrays, when the system exhibits collective mode structures due to the periodic exchange of power between the cores.

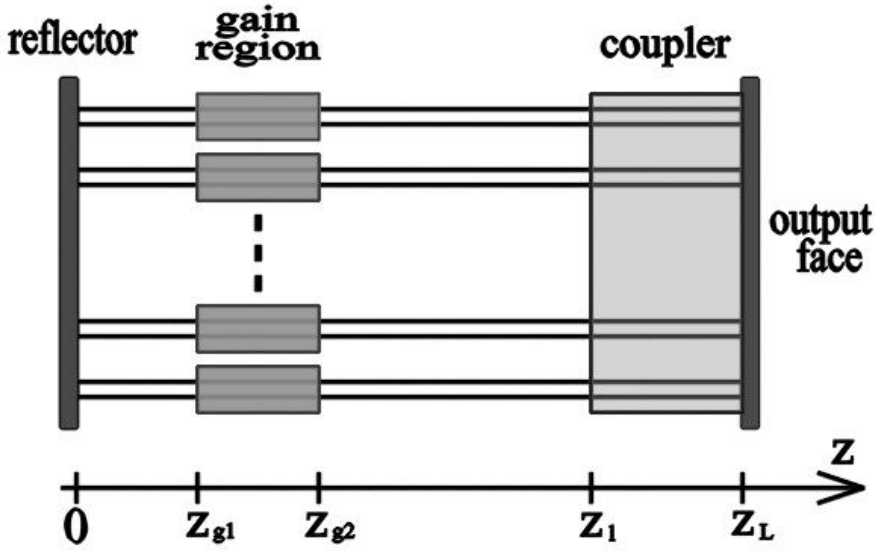

Figure 20: Schematic of the laser array.

Fig. 20 shows an experimental setup that will be studied in the following sections [148, 149, 150]. All N fiber laser are connected to a 100% reflective mirror on one end ($z = 0$) and

to a partially reflective mirror with reflectivity r on the other side ($z = z_L$). The parameter r is assumed to be small (about 0.2), which means that this is a high-loss/high gain system. The lasers are separated and independent everywhere except a relatively small region (from z_l to z_L), where they are placed together in a coupler and allowed to interact through fiber crosstalk (see the next section). Each fiber also has a gain region from z_{g1} to z_{g2}, where the field gets amplified.

In the following subsections I will describe the gain dynamics as well as the changes of the field amplitudes over one round trip (this analysis follows closely that presented in Ref. [149]). These results will provide us with one step of the iterative map that I will use later to study the long-time behavior of the system.

3.2.1 Round trip dynamics of the electric fields

Let $E_i^+(z)$ and $E_i^-(z)$ be the complex amplitude of an electromagnetic plane wave propagating from $z = 0$ to $z = z_L$ and from $z = z_L$ to $z = 0$, respectively. Formally the round trip can be started from an arbitrary point, but I choose the 100% reflective mirror as the starting point for reasons that will become clear later, during the map construction.

Since the left mirror has the 100% reflectivity, at point $z = 0$ the fields satisfy the condition

$$E_i^+(0) = -E_i^-(0),$$

where the minus sign comes from the π phase shift due to the reflection.

When the fields propagate through the gain region, they are amplified by a factor $\exp(G_i/2)$, where G_i are the gain variables that will be determined separately. Hence, passing the gain section the fields change as

$$E_i^+(z_{g2}) = e^{G_i/2} E_i^+(z_{g1}).$$

Similarly, for the left-going wave I obtain:

$$E_i^-(z_{g1}) = e^{G_i/2} E_i^-(z_{g2}).$$

Then, the right-going waves propagate through the coupling region, so that the fields get mixed according to coupled-mode theory [151], which is considered in the next section.

Using the results of this theory I can write that

$$E_i^+(z_L) = \sum_{i=1}^{N} S_{ij}(z_c) E_j^+(z_l),$$

where $z_c \equiv z_L - z_l$. A similar expression is valid for the left-going wave:

$$E_i^-(z_l) = \sum_{i=1}^{N} S_{ij}(z_c) E_j^-(z_L).$$

Hence, taking into account partial reflection at the point $z = z_L$ I find

$$E_i^-(z_L) = -r E_i^+(z_L),$$

and therefore,

$$\begin{aligned} E_i^-(z_l) &= -r \sum_{i=1}^{N} S_{ij}(z_c) E_j^+(z_L) = \\ & -r \sum_{i=1}^{N} S_{ij}(z_c) \sum_{j=1}^{N} S_{jk}(z_c) E_k^+(z_l). \end{aligned}$$

Using the fact that $\mathbf{S} = \mathbf{U}\mathbf{D}\mathbf{U}^{-1}$, where $\mathbf{D}$ is a diagonal matrix with exponents on the diagonal, I immediately obtain

$$\begin{aligned} &\mathbf{S}(z_c)\mathbf{S}(z_c) = \mathbf{U}\mathbf{D}(z_c)\mathbf{U}^{-1}\mathbf{U}\mathbf{D}(z_c)\mathbf{U}^{-1} = \\ &\mathbf{U}\mathbf{D}(z_c)\mathbf{D}(z_c)\mathbf{U}^{-1} = \mathbf{U}\mathbf{D}(2z_c)\mathbf{U}^{-1} = \mathbf{S}(2z_c), \end{aligned}$$

so that

$$E_i^-(z_l) = -r \sum_{i=1}^{N} S_{ik}(2z_c) E_k^+(z_l).$$

Both waves propagate freely between the coupler and the gain region, as well as between the gain region and the left mirror.

Thus, combining all previous expression I find that after one round trip the fields change as

$$E_i'(0) = r e^{G_i/2} \sum_{k=1}^{N} S_{ik} e^{G_k/2} E_k(0). \tag{77}$$

The usual step at this point is to assume that the changes in the field amplitudes over one round trip are very small, which allows one to approximate the discrete map as a differential equation. But I will not make the assumption of slowly varying amplitudes. As

was mentioned earlier, due to the low reflectivity of the output mirror the system operates in the high-gain/high-loss regime. The iterative map is a natural tool for studying such systems.

3.2.2 Dynamics of the gain variables

In this subsection the equation for the evolution of the gain variables will be derived using the Rigrod method [152].

The counterpropagating laser fields have the corresponding intensities:

$$I_i^+(z,t) = |E_i^+(z,t)|^2,$$
$$I_i^-(z,t) = |F_i^-(z,t)|^2.$$

Having 100% reflectivity of the mirror at $z = 0$, one obtains the following boundary condition:

$$I_n^+(0,t) = I_n^-(0,t). \tag{78}$$

The Rigrod analysis for the counter propagating waves is based on two partial differential equations for intensities and one equation for the time evolution of the atomic gain:

$$\frac{\partial I_i^+(z,t)}{\partial z} = N_i(z,t)\sigma I_i^+(z,t), \tag{79}$$
$$\frac{\partial I_i^-(z,t)}{\partial z} = -N_i(z,t)\sigma I_i^-(z,t), \tag{80}$$
$$\frac{\partial N_i(z,t)}{\partial t} = R_i^p(z,t) - \frac{N_i(z,t)}{\tau} - \frac{\sigma}{\hbar\omega}N_i(z,t)\left[I_i^+(z,t) + I_i^-(z,t)\right], \tag{81}$$

where $N_n(z,t)$ is the number of inverted atoms per unit length distributed along the i^{th} fiber, σ is the stimulated emission cross section, τ is the relaxation time, and R_i^p is the pumping rate of the i^{th} fiber. In the Rigrod analysis one ignores time derivatives in Eqs.(79) and (80) assuming that they are small with respect to the exponential spatial dependence of the gains.

These equations allow one to determine the temporal evolution of the gains by integrating $N_i(z,t)$ over the gain section having length z_g;

$$\hat{N}_i(t) = \int_0^{z_g} N_i(z,t)dz.$$

Substituting Eqs. (79) and (80) into Eq.(81) gives

$$\frac{\partial N_i(z,t)}{\partial t} = R_i^p(z,t) - \frac{N_i(z,t)}{\tau} - \frac{1}{\hbar\omega}\left[\frac{\partial I_i^+(z,t)}{\partial z} - \frac{\partial I_i^-(z,t)}{\partial z}\right].$$

After integrating this result over the gain region $z \in [0, z_g]$ one obtains

$$\frac{d\hat{N}_i(t)}{dt} = \hat{R}_i^p(t) - \frac{\hat{N}_i(t)}{\tau} - \frac{1}{\hbar\omega}\left[I_i^+(z_g,t) - I_i^+(0,t) - I_i^-(z_g,t) + I_i^-(0,t)\right], \tag{82}$$

where the total pumping rate $\hat{R}_n^p(t)$ is defined as

$$\hat{R}_i^p(t) = \int_0^{z_g} R_i^p(z,t)dz.$$

Using Eq.(78) I eliminate the intensities at the mirror ($z = 0$) in Eq.(82), so that

$$\frac{d\hat{N}_i(t)}{dt} = \hat{R}_i^p(t) - \frac{\hat{N}_i(t)}{\tau} + \frac{1}{\hbar\omega}\left[I_i^-(z_g,t) - I_i^+(z_g,t)\right]. \tag{83}$$

The next step is to express I_i^- in terms of I_i^+. First, integrate Eq.(80) over the gain region $z \in [0, z_g]$ to find

$$\ln\left[\frac{I_i^-(z_g,t)}{I_i^-(0,t)}\right] = -\sigma\hat{N}_i(t). \tag{84}$$

Then from Eq.(79) one gets

$$\ln\left[\frac{I_i^+(z_g,t)}{I_i^+(0,t)}\right] = \sigma\hat{N}_i(t). \tag{85}$$

Finally, substracting Eq.(85) from Eq.(84) gives

$$\ln\left[\frac{I_i^-(z_g,t)I_i^+(0,t)}{I_i^+(z_g,t)I_i^-(0,t)}\right] = -2\sigma\hat{N}_i(t).$$

Once again using Eq.(78) one can cancel the intensities at the mirror and obtain the following dependence:

$$I_i^-(L,t) = e^{-2\sigma\hat{N}_i(t)}I_i^+(z_g,t). \tag{86}$$

Defining the gain variable as

$$G_i(t) = 2\sigma\hat{N}_i(t),$$

then using Eq.(86), one eliminates $I_i^-(L,t)$ from Eq.(83) and finds the governing differential equations for the gains

$$\frac{dG_i}{dt} = \frac{1}{\tau}\left[G_i^p(t) - G_i(t) + \frac{2}{I_{sat}}\left(e^{-G_i(t)} - 1\right)|E_i(z_g,t)|^2\right], \tag{87}$$

where

$$G_n^p(t) = 2\sigma\tau \hat{R}_n^p(t),$$
$$I_{sat} = \frac{\hbar\omega}{\sigma\tau}.$$

3.2.3 Iterated map for the coupled laser model

Together Eqs.(77) and (87) provide a quantitative description for the dynamics of the fiber laser array. However, in order to use these equations as an iterated map I need to make a few simplifying assumptions.

First, I assume that the round trip times of all fiber lasers in the array are equal. This is a reasonable approximation since in the laboratory fibers are several meters long and can be cut accurately enough. Therefore, I assume all round trip times to be the same to within a negligible error.

The evolution equation for the electric fields (77) can be rewritten as

$$E_i(t+T) = re^{G_i(t)/2} \sum_{k=1}^{N} S_{ik} e^{G_k(t)/2} E_k(t). \tag{88}$$

Then, instead of using a hybrid dynamical system which involves the iterated map Eq.(88) and the differential equation Eq.(87), I can recast the latter into an iterated map. In order to do this, I assume that the gain variables change slowly over intervals comparable to the round trip time T. The pumping parameters G_i^p are assumed to be constants. Hence, integrating Eq. (87) over time T we obtain the following map:

$$G_i(t+T) = G_i(t) + \frac{T}{\tau}\left[G_i^p(t) - G_i(t) - \frac{2}{I_{sat}}\left(1 - e^{-G_i(t)}\right)\langle I_i(t)\rangle\right], \tag{89}$$

where

$$\langle I_i(t)\rangle = \frac{1}{T}\int_t^{t+T} |E_i(t)|^2 dt$$

is a time average of the field intensity in the i^{th} fiber over the round trip.

The best way to approximate the average intensity is to use the value of the field at the 100% reflective mirror $|E^+(z=0)|^2$, because at this point the propagating wave has been amplified one time, so that its intensity is in between the minimum value $|E^-(z_L)|^2$ and

maximum value $|E^+(z_L)|^2$. This explains the choice of starting point I made for the round trip.

Substituting this into Eq.(89) I obtain the final equations of motion,

$$E_i(t+T) = r\sum_{k=1}^{N} e^{G_i(t)/2} S_{ik} e^{G_k(t)/2} E_k(t), \tag{90}$$

$$G_i(t+T) = G_i(t) + \epsilon\left[G_i^p(t) - G_i(t) - 2\left(1 - e^{-G_i(t)}\right)|E_i(t)|^2\right], \tag{91}$$

where I have normalized the field so that $\frac{E_i}{\sqrt{I_{sat}}} \rightarrow E_i$, and introduced the parameter $\epsilon = \frac{T}{\tau}$. Typically the fluorescence time τ is much longer than the round trip time T, so the parameter ϵ is a small number.

3.3 Coupled-Mode Theory (Fiber Crosstalk)

Coupled-mode theory is a mathematical tool useful for the description of electromagnetic waves propagating and interacting with media in optical waveguides. The advantages of the coupled-mode theory are its physical intuitiveness and mathematical simplicity, which help one to understand the behavior of systems with different designs [151, 153, 154, 155, 156, 157, 158, 159].

In the 1950s Pierce and Miller [160, 161] started the development of coupled-mode theory, which received rigorous formulations later, when Schelkunoff and Haus [162, 163] applied, respectively, a mode expansion and a variational principle. Originally, the theory was applied to the problems of microwave propagation. In the 1970s, Snyder et al. applied coupled mode theory to waveguiding optical systems [151, 159].

The coupled-mode equations were used to analyze new optical devices such as distributed feedback lasers and coupler switches, created at Bell Laboratories by Herwig Kogelnik [164, 165]. Moreover, coupled-mode theory was a fruitful approach for the analysis of nonlinear optical phenomena, including modulation instability, second harmonic generation, and parametric amplification.

The operation of some optical devices is based on coupled waveguide systems, which consist of several dielectrical waveguides placed close to each other. These waveguides are not necessarily parallel. They can also have built-in gratings, tapers, nonlinearities, or other

index perturbations as well as losses or gain along their axes.

In some cases, these index perturbations are the result of fabrication or material imperfections, which can be avoided or at least minimized. In other cases, the index perturbations are built intentionally, for example, to produce switching, reflection or modulation of the light in the waveguides.

The conventional approach in the analysis of coupled waveguide systems is, first, to determine the propagation constants and field patterns in the individual uncoupled waveguides. Then the amplitudes of the modes can be found by solving the coupled-mode equations. These equations describe both the mode propagation and coupling in the system. Therefore, combining the results of coupled-mode theory with analysis of the cross sectional field distribution, one gets a rigorous and simple description of electromagnetic wave propagation in the interacting waveguides.

Let me consider a simple model of the coupled waveguide system, which consists of two uniform and parallel waveguides placed close to each other. We can assume that the transverse cross sections of the fibers are arbitrary. Suppose each waveguide has a mode with amplitude $E_i(z)$ and time dependence $\exp(i\omega t)$. Then the modes in the individual wavequides without crosstalk obey the amplitude equations:

$$\frac{dE_1}{dz} + i\beta_1 E_1 = 0,$$
$$\frac{dE_2}{dz} + i\beta_2 E_2 = 0,$$

where β_1 and β_2 are the propagation constants of these independent modes passing through each fiber.

If the waveguides are placed close enough, their fields start to interact with each other, so that the modes are not really independent but coupled and their amplitudes modify each other while propagating along the waveguides. When the coupling is weak, the amplitude equations can be written in the form:

$$\frac{dE_1}{dz} = -i(\beta_1 + C_{11})E_1 - iC_{12}E_2, \tag{92}$$
$$\frac{dE_2}{dz} = -i(\beta_2 + C_{22})E_2 - iC_{21}E_1, \tag{93}$$

where C_{12} and C_{21} are the mutual coupling coefficients, while C_{11} and C_{22} represent the self-coupling of the modes.

In the following analysis I will also assume that this system of coupled waveguides is lossless, which implies power conservation:

$$\frac{d}{dz}P(z) = 0.$$

Since the power of each mode is proportional to the square of its amplitude, the total power in the system is

$$P(z) \sim |E_1|^2 + |E_2|^2.$$

Using Eqs.(92,93) one finds that

$$\begin{aligned}\frac{d}{dz}P(z) \quad \sim \quad & i(C_{11}^* - C_{11})|E_1|^2 + i(C_{22}^* - C_{22})|E_2|^2 + \\ & i(C_{12}^* - C_{21})E_1E_2^* + i(C_{21}^* - C_{12})E_1^*E_2 = 0,\end{aligned}$$

for any z. Therefore, the coefficients C_{11} and C_{22} have to be real, and the mutual coupling coefficients satisfy the condition:

$$C_{12} = C_{21}^* = \kappa.$$

If the coupled waveguides are uniform, then all coupling coefficients and propagation constants are independent of z, so that Eqs.(92,93) can be integrated by the diagonalization method. In order to keep notation simple, it is convenient to introduce the detuning parameter,

$$\delta = \frac{\beta_1 - \beta_2}{2} + \frac{C_{11} - C_{22}}{2}$$

and a common phase factor, so that

$$E_i(z) = \varepsilon_i(z)e^{-i\beta_0 z},$$

where

$$\beta_0 = \frac{\beta_1 + \beta_2}{2} + \frac{C_{11} + C_{22}}{2}.$$

In this notation Eqs.(92,93) can be written as

$$\frac{d\varepsilon_1}{dz} = -i\delta\varepsilon_1 - i\kappa\varepsilon_2, \tag{94}$$

$$\frac{d\varepsilon_2}{dz} = +i\delta\varepsilon_2 - i\kappa\varepsilon_1, \tag{95}$$

or even in more compact vector form

$$\frac{d}{dz}\vec{\varepsilon} = -i\mathbf{C}\vec{\varepsilon}, \tag{96}$$

where

$$\vec{\varepsilon} = \begin{bmatrix} \varepsilon_1 \\ \varepsilon_2 \end{bmatrix},$$

$$\mathbf{C} = \begin{bmatrix} +\delta & \kappa \\ \kappa & -\delta \end{bmatrix}.$$

The matrix $\mathbf{C}$ can be diagonalized by a unitary matrix

$$\mathbf{U} = \begin{bmatrix} \cos(\tilde{q}/2) & -\sin(\tilde{q}/2) \\ \sin(\tilde{q}/2) & \cos(\tilde{q}/2) \end{bmatrix},$$

so that

$$\mathbf{U}^{-1}\mathbf{C}\mathbf{U} = \mathbf{D}.$$

Here I have introduced a parameter $\tilde{q}$, which is defined as

$$\tan(\tilde{q}) = \frac{\kappa}{\delta}.$$

The diagonal matrix $\mathbf{D}$ consists of the propagation constants of the normal modes. Indeed, let

$$\vec{\varepsilon} = \mathbf{U}\vec{\xi},$$

then from Eq.(96) one obtains

$$\mathbf{U}\frac{d}{dz}\vec{\xi} = -i\mathbf{C}\mathbf{U}\vec{\xi},$$

and finally:

$$\frac{d}{dz}\vec{\xi} = -i\mathbf{D}\vec{\xi}, \tag{97}$$

where

$$\mathbf{D} = \begin{bmatrix} \sqrt{\delta^2+\kappa^2} & 0 \\ 0 & -\sqrt{\delta^2+\kappa^2} \end{bmatrix}.$$

Therefore, the vector $\vec{\xi}$ can be considered as a vector of the amplitudes for the composite modes, which are not coupled.

Eq.(97) can be now readily solved, so that

$$\vec{\xi}(z) = \begin{bmatrix} \exp(-i\sqrt{\delta^2+\kappa^2}z) & 0 \\ 0 & \exp(+i\sqrt{\delta^2+\kappa^2}z) \end{bmatrix} \vec{\xi}(0).$$

Hence, one can express the mode amplitudes in terms of the propagation matrix **S** in the following way:

$$\vec{E}(z) = \mathbf{U}\vec{\xi}(z)e^{-i\beta_0 z} = \mathbf{S}\vec{E}(0),$$

where

$$\mathbf{S} = \mathbf{U} \begin{bmatrix} \exp(-i\beta_s z) & 0 \\ 0 & \exp(-i\beta_a z) \end{bmatrix} \mathbf{U}^{-1}.$$

Here the propagation constant of the symmetric normal mode is

$$\beta_s = \beta_0 + \sqrt{\delta^2+\kappa^2},$$

while the propagation constant of the antisymmetric mode is

$$\beta_a = \beta_0 - \sqrt{\delta^2+\kappa^2}.$$

In explicit form the matrix elements of the propagation matrix are

$$S_{11} = S_{22}^* = \cos(p) - i\sin(q)\sin(p), \tag{98}$$

$$S_{12} = S_{21} = -i\cos(q)\sin(p), \tag{99}$$

where the parameter $p = z\sqrt{\delta^2+\kappa^2}$ characterizes the coupling strength, while q is the modified deturning parameter:

$$q = \frac{\pi}{2} - \tilde{q} = \arctan\left(\frac{\delta}{\kappa}\right).$$

3.4 Weak Link Synchronization

Besides its intrinsic interest for the field of nonlinear dynamics, the goal of synchronization is important in many practical contexts. In some cases, the desired behavior can be achieved by so-called injection locking, so that (for example) a generator is entrained by a controlled external signal which is weak but very precise [3]. In contrast to this master-slave situation

there is the problem of mutual synchronization among a population of nominally identical oscillators, of which the Kuramoto model is the archetype[1].

In this section I describe a kind of mutual synchronization which occurs in the model of high-gain/high-loss fiber lasers (90,91). Typically, the search for highly coherent output states considers schemes where the individual elements are as identical as possible, and driven identically. In contrast, I investigate arrays where such uniformity is intentionally avoided by driving some elements more strongly than others. I find that these inhomogeneous arrays can operate in a highly coherent way via a mechanism I call weak link synchronization [166]. The weak link synchronized states, though sub-optimal compared with the uniformly pumped array, is far more robust with respect to parameter mismatch among the individual elements. The practical advantage of weak link synchronization may therefore be especially pronounced for very large arrays.

Weak link synchronization represents a trade-off between optimization in principle and optimization in practice. In principle, a fully symmetric coherent state is ideal. In practice, it may be difficult to achieve the necessary tolerances. I find that employing a strategy of intentionally non-uniform (but patterned) driving yields an attractor with both a high degree of coherence and robustness under parameter mismatch. Our numerical simulations suggest that the scheme can be applied to very large arrays without substantial degradation.

Based on the result of the previous section I describe the system of coupled fiber lasers by the dynamical model (90,91)

$$E_n(t+T) = r\sum_{m=1}^{N} e^{\frac{G_n(t)+G_m(t)}{2}} S_{nm}E_m(t),$$
$$G_n(t+T) = G_n(t) + \epsilon[G_n^p - G_n(t) - 2(1-e^{-G_n(t)})|E_n(t)|^2].$$

The coupling matrix elements S_{nm} were derived in the section 3.3 for the case of two fibers ($N = 2$). In general, to determine the matrix $\mathbf{S}$ for arrays (i.e. $N > 2$), I integrate the equation

$$\frac{dE_n}{dz} = iA_{nm}E_m,$$

where z is the spatial coordinate along the fiber, $A_{nm} = \beta_n\delta_{nm} + C(d_{nm})$, and d_{nm} is the distance between the centers of n^{th} and m^{th} fibers. Integrating over the total coupling

length $2z_c$ yields $E_n(z+2z_c) = S_{nm}E_m(z)$. Typically, I take nearest neighbor coupling:

$$C(d_{nm}) = \begin{cases} 0 & \text{if } d_{nm} > 2R, \\ \kappa & \text{if } d_{nm} = 2R, \end{cases}$$

where R is the radius of each fiber. However, the following results are essentially unchanged for other functions $C(d_{nm})$ provided they decay fast enough. Anyway, the matrix elements C_{nm} depend only on the architecture and properties of the coupler.

Ultimately, one would like to identify the conditions (if any) under which very large arrays will be behave in a highly coherent manner. The most common strategy is to consider a system of identical elements, identically driven and with fully symmetric coupling, then explore the linear stability of the fully symmetric solution in which all elements behave identically [132]. I used a similar strategy in the previous chapter to study the Josephson transmission line, but now I take a different approach, since I want to look more broadly at other types of synchronized solutions and test their sensitivity with respect to disordering effects, such as detuning and parameter mismatch.

In fact, the case of just two elements yields important insight, and my present analytic understanding of weak link synchronization rests on a careful analysis of the $N = 2$ problem. This case yields the simplest incarnation of the weak link idea, and demonstrates the relative pros and cons of weak link synchronized states as compared with the inphase states of the uniformly driven array. Later, I use this insight to design arrays with much larger N, and explore these numerically.

3.4.1 Two laser analysis

The detailed derivation of all possible fixed-point solutions for $N = 2$ is given in the Appendix, which also includes a stability analysis of these solutions. Here, I will discuss the obtained solutions in context of weak-link synchronization.

Let $E_n(t) = \varepsilon_n(t)e^{i\psi_n(t)}$, where ε_n and ψ_n are real. I seek solutions for which $\psi(t) = \psi_1(t) - \psi_2(t)$ is constant. I do not require that the lasers be pumped identically, viewing G_1^p and G_2^p as independent control parameters. Meanwhile, any intrinsic disorder in the system is due to a non-zero value of the detuning parameter q.

Consider first the limit where there is no detuning ($q = 0$). A straightforward calculation yields several constant-ψ solutions. The overall situation is illustrated in Fig. 21. The first branch of solutions exists only within a narrow strip of parameter space corresponding to nearly identically pumped lasers. It is natural therefore to introduce a small parameter ρ to express these solutions: I have

$$\begin{aligned}
\tilde{\psi} &= \arcsin[\rho/\tan p] + O(\rho^2), \\
\tilde{\varepsilon_1}^2 &= \tilde{\varepsilon_2}^2 = I + O(\rho^2), \\
\tilde{G_1} &= G_0 + \rho + O(\rho^2), \\
\tilde{G_2} &= G_0 - \rho + O(\rho^2),
\end{aligned} \tag{100}$$

where $\rho = \frac{G_1^p - G_2^p}{2(1+2rI)}$, $I = \frac{G^p - G_0}{2(1-r)}$, $G^p = \frac{G_1^p + G_2^p}{2}$ and $G_0 = -\ln r$.

This is the synchronized solution corresponding to states where both lasers operate with (nearly) equal and optimal intensity and a constant phase difference. If the lasers are identically pumped, these states are the familiar inphase and antiphase states $\tilde{\psi} = 0, \pi$, respectively, described e.g. for coupled semiconductor lasers in Ref. [134].

A careful analysis (see Appendix) shows that this solution is attracting in its narrow region of existence as long as

$$\begin{aligned}
&0 < I < I_m \equiv 1/\sqrt{4-6r} \quad ; \quad (G_0 < G^p < G_m \equiv G_0 + \frac{1-r}{2-3r}), \\
&p\,|\cos\tilde{\psi}| < \sqrt{\frac{\epsilon}{2}\left(1 - \frac{I}{I_m}\right)}.
\end{aligned}$$

Now suppose I allow for a small amount of detuning ($q \neq 0$), to find the corresponding corrections to this solution. Of particular importance is the correction to the relative phase, which is

$$\sin(\psi) = \frac{G_1^p - G_2^p}{2p(1+2rI)} - \frac{q(G^p - G_0)}{p(1+2rI)\cos\tilde{\psi}}.$$

Recall that p represents the coupling strength, which is a small quantity. It is evident that

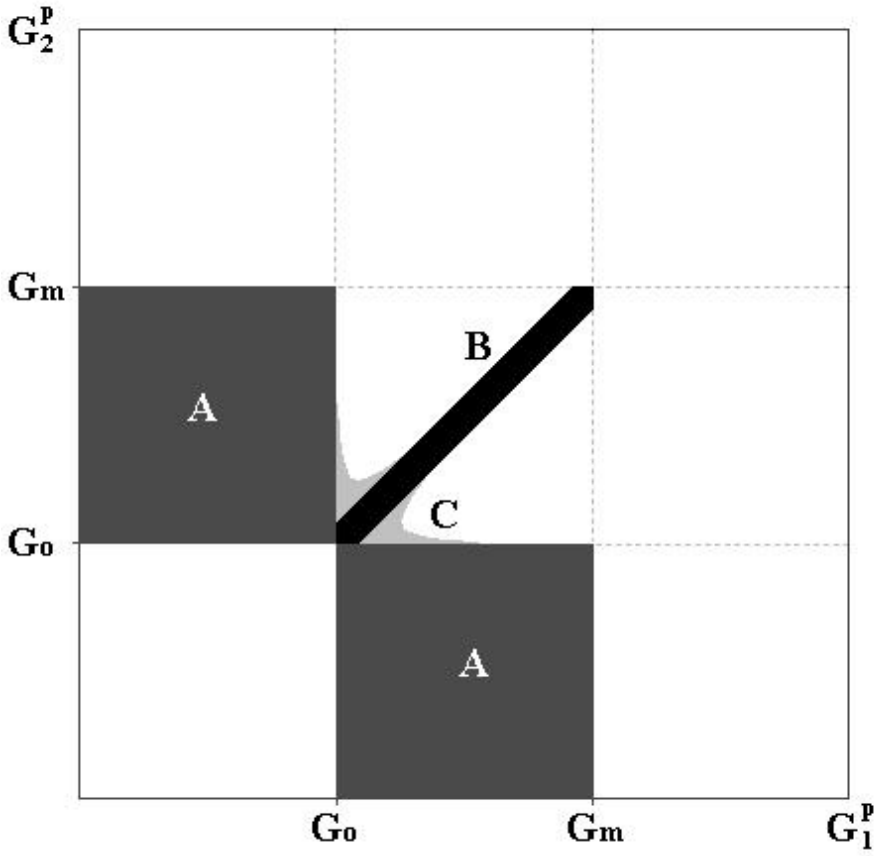

Figure 21: Schematic summarizing the regions of stability for the various fixed point solutions: A – weak link solutions, B – well-pumped solutions Eq. (100), C – near-threshold transitional solutions.

these solutions are very sensitive to parameter mismatch, and might be difficult to observe in practice. All of the foregoing refers to the fixed points labelled "B" in Fig. 21.

Now consider another set of fixed point solutions, labelled "A" in Fig. 21. These are given by (in the limit of zero detuning)

$$\begin{aligned}
&\tilde{\psi} = \pi/2, && && \tilde{\psi} = -\pi/2,\\
&\tilde{\varepsilon_1} = \sqrt{I_1} + O(p^2), && && \tilde{\varepsilon_1} = p\frac{\sqrt{rI_2 \exp G_1^p}}{1 - r\exp G_1^p} + O(p^2),\\
&\tilde{\varepsilon_2} = p\frac{\sqrt{rI_1 \exp G_2^p}}{1 - r\exp G_2^p} + O(p^2), && \text{and} && \tilde{\varepsilon_2} = \sqrt{I_2} + O(p^2),\\
&\tilde{G_1} = G_0 + O(p^2), && && \tilde{G_1} = G_1^p + O(p^2),\\
&\tilde{G_2} = G_2^p + O(p^2) && && \tilde{G_2} = G_0 + O(p^2)\ .
\end{aligned}$$

The corresponding regions of stability are, respectively

$$G_0 < G_1^p < G_m, \qquad \text{and} \qquad 0 < G_1^p < G_0,$$
$$0 < G_2^p < G_0 \qquad\qquad G_0 < G_2^p < G_m'.$$

These solutions correspond to a state where one laser is well pumped ($G^p > G_0$) and operates with relatively large intensity, while the other laser is under-pumped ($G^p < G_0$) and has a very small amplitude (of order of p). Even so, these are synchronized states because the two lasers maintain a constant $\frac{\pi}{2}$-phase shift. For reasons that will become clear when I turn to larger arrays, I call this the "weak link solution". The fact that the under-pumped laser has non-zero intensity is important, because it is how phase information is transmitted across larger arrays.

Although the total intensity of the weak link solution is less than the intensity of the "fully pumped" branch of solutions, the weak link solution has significant benefits: 1) it has a very broad region of existence and stability; and 2) it is extraordinarily robust with respect to parameter mismatch. Corrections to first order in q do not have any serious influence on this solution, in contrast to the fully pumped solution. In particular, the phase difference is only slightly modified

$$\tilde{\psi} = \pm\left(\frac{\pi}{2} + \frac{rpq}{\exp\left(-G^p\right) - r}\right).$$

There is yet one more fixed point solution, which is labelled "C" in Fig. 21. However, its region of stable existence is extremely small and I don't consider it further. It may hold some mathematical interest, in some sense providing a continuous transition between the other solution branches. (See Appendix)

3.4.2 Many laser analysis

The situation that I have just described suggests a scheme for how one might try to synchronize a large array of lasers if the uniformly pumped configuration is too sensitive to be successfully synchronized. Suppose I have three lasers, with the outer two well-pumped and the middle under-pumped. If each of the well-pumped lasers easily synchronizes with the under-pumped one, then they will synchronize with each other. Thus, by sacrificing the

intensity of one laser, one might robustly and effectively synchronize the other two through a weak link, which would be otherwise fail.

To test this idea, I consider first a linear array of coupled fiber lasers, and compare the configuration when all the lasers are well-pumped against the configuration when every other laser is under-pumped. For this and other large arrays to follow, I use near-neighbor coupling to generate the matrix elements S_{nm}, as described in the Appendix. As a convenient quantitative measure of the output, I use the power spectrum of the total electric field:

$$P(\omega) = \left| \int_{-\infty}^{\infty} E_{tot}(t) e^{i\omega t} dt \right|^2 ,$$

where

$$E_{tot} = \sum_n \varepsilon_n(t) e^{i\psi_n(t)}$$

.

Figure 22 shows the results for an array of $N = 19$ lasers. There I have introduced a small amount of intrinsic disorder ($\delta \sim 10^{-4}$). The upper panel is the result when all lasers are pumped with $G^p = 1.9$; the lower panel is the result when I reduce the pump for 9 of the lasers to $G^p = 0.4$, a value below the single-laser threshold value. The other parameters are listed in the figure caption. Repeated trials indicate that these results are independent of initial conditions. The uniformly pumped configuration doesn't generate a coherent output; consequently, the contrast is considerably lower than for the corresponding weak-link pumping scheme, whose power spectrum has a single sharp line.

There are other strategies one can try to get the fully pumped array to synchronize. For example, one can individually trim the pump parameters of each laser in the hope of somehow compensating for the intrinsic disorder. I tried this: I was unable to get anything even approaching the clean output of the weak-link synchronized state; there are reasons to suspect that it is impossible in practice.

Yet another strategy is to change the topology of the array, e.g. by introducing periodic boundary conditions. This strategy works: a one-dimensional ring of these lasers can robustly synchronize. On the other hand, using a ring architecture begs the question of still

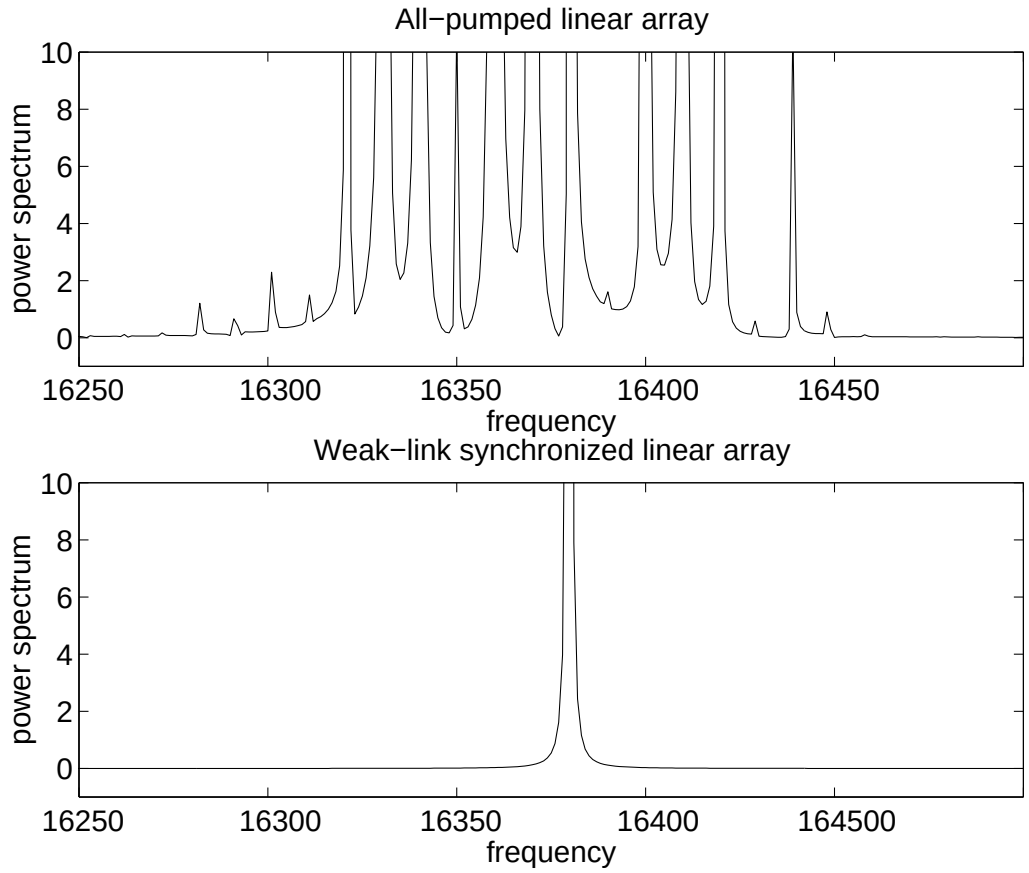

Figure 22: Power spectrum $P(\omega)$ for a linear array of 19 lasers with near-neighbor coupling, with $r = 0.2$, $\epsilon = 0.005$, $\delta \sim 10^{-4}$, $\kappa = 0.015$, and $z_c = 1$. Initial conditions were chosen randomly with $\epsilon_n \in (0, 1), \psi_n \in (0, 2\pi)$, and $G_n \in (1.6, 2.3)$. The upper plot is for the case when all lasers are strongly pumped, with $G^p = 1.9$. The lower plot is for the case when instead every other laser is under-pumped, with $G^p = 0.4$ (weak link synchronization).

larger arrays. After all, a large ring takes up a large cross-sectional area, most of which is empty space. From the perspective of total power, a more attractive possibility is to use a large bundle of fiber lasers. I consider, therefore, a bundle comprising four concentric rings of $1, 6, 12$, and 18 lasers. The resulting arrangement of 37 lasers is illustrated in Fig. 23. In view of the robust synchronization of a single ring, I choose for my weak-link configuration one where every other ring is under-pumped. I compare the output against the output of the corresponding fully-pumped configuration, as shown in Fig. 24. In the well-pumped array I find no synchronization; the other array readily falls into the weak-link synchronized attractor.

The same strategy works for even larger arrays. I have observed robust weak link

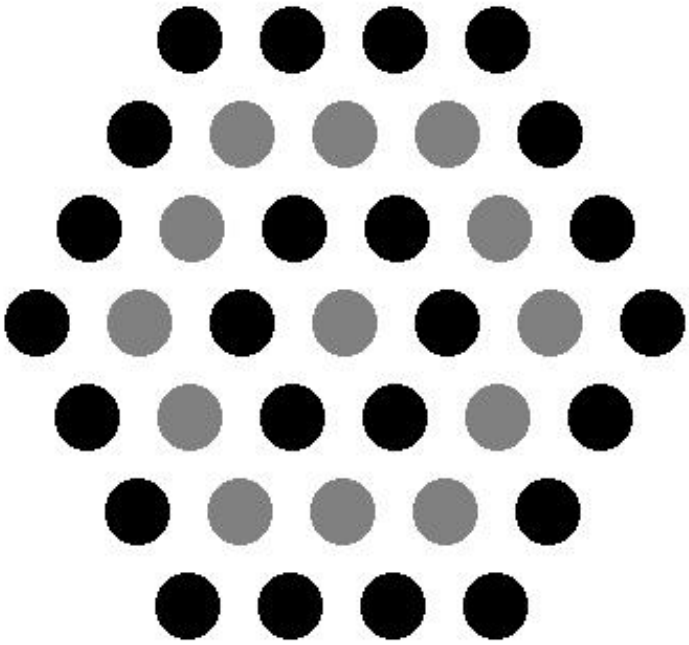

Figure 23: Cross section of the 37-fiber system and the pumping scheme used to achieve weak link synchronization. Black and gray circles represent the well-pumped and under-pumped lasers, respectively.

synchronization in simulations with as many as 91 elements (comprising 6 concentric rings) with no apparent degradation.

3.4.3 General oscillator analysis

Is the behavior of the fiber laser array unique, or is weak-link synchronization a more general phenomenon? Most of the principle ingredients of the laser system can be observed in an archetypical model which describes a broad range of physical problems. Consider the general equations of a chain of coupled Hopf oscillators with slowly varying complex amplitudes [3, 167]:

$$\dot{A}_i = i\omega_i A_i + \mu_i A_i - (\gamma_i + i\alpha_i)|A_i|^2 A_i + \sum_j S_{ij}(A_j - A_i).$$

For simplicity I restrict myself to nearest-neighbor coupling: $S_{ij} = i\kappa(\delta_{j,i+1}+\delta_{j,i-1})$, with the same nonlinear frequency shift $\frac{\alpha_i}{\gamma_i} \equiv \alpha$ for all oscillators. Introducing real amplitudes and phases according to $A_i = \frac{r_i}{\sqrt{\gamma_i}} e^{i\theta_i}$, I get:

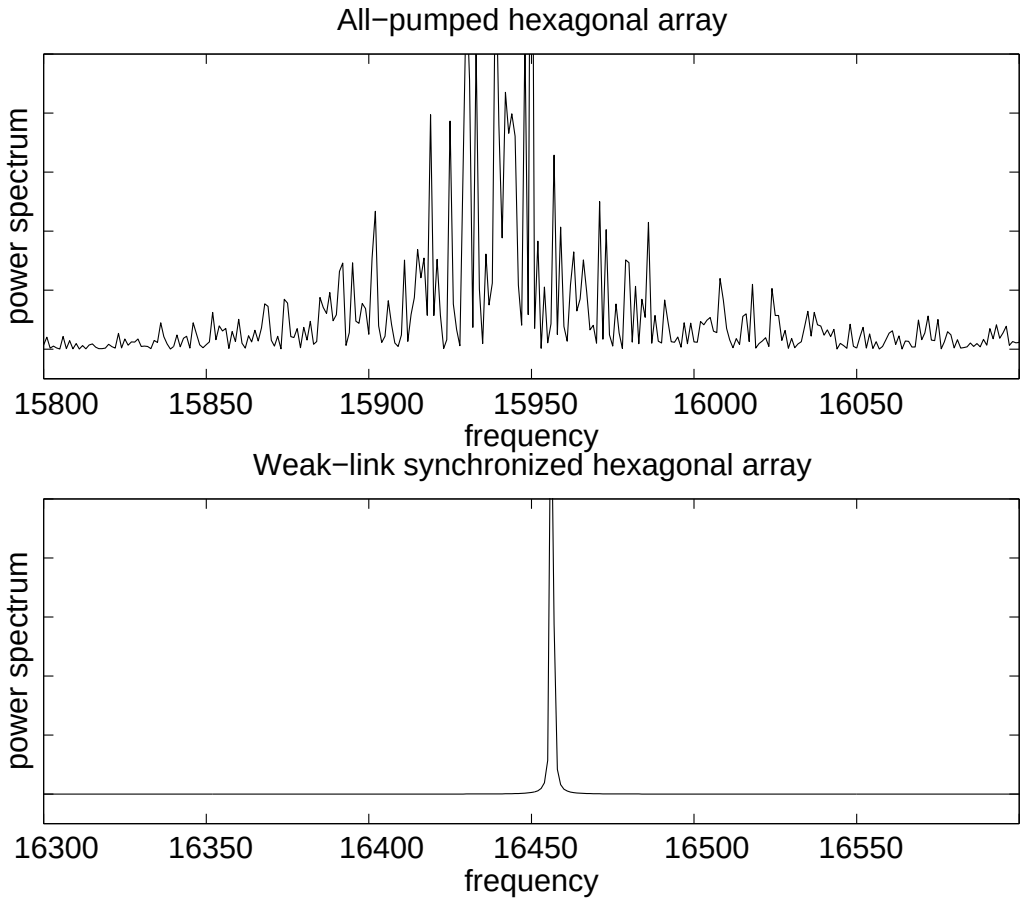

Figure 24: Same as Fig. 22 but for a two dimensional ($N = 37$) array. Upper plot is for the all-pumped configuration; lower plot is for the weak link arrangement.

$$\dot{r_i} = \mu_i r_i - r_i^3 + \kappa r_{i-1} \sin(\theta_i - \theta_{i-1}) - \kappa r_{i+1} \sin(\theta_{i+1} - \theta_i),$$
$$\dot{\theta_i} = \omega_i - \alpha r_i^2 - 2\kappa + \kappa \frac{r_{i-1}}{r_i} \cos(\theta_i - \theta_{i-1}) + \kappa \frac{r_{i+1}}{r_i} \cos(\theta_{i+1} - \theta_i).$$

Note that without coupling ($\kappa = 0$), each oscillator obeys the normal form equation for a supercritical Hopf bifurcation: when $\mu < 0$ the origin $r = 0$ is a stable spiral; when $\mu > 0$ there is an unstable spiral at the origin and a stable circular limit cycle at $r = \sqrt{\mu}$.

For $N = 2$ these equations show similar behavior to two fiber lasers: if both oscillators are "turned on" (i.e. $\mu_{1,2} > 0$) then they synchronize to each other in terms of frequency entraining and constant phase difference only if the detuning $\Delta\omega = |\omega_1 - \omega_2|$ and mismatch $\Delta\mu = |\mu_1 - \mu_2|$ are small enough; but if one of them is turned off (so $\mu_1 < 0$ and $\mu_2 > 0$)

then they synchronize regardless of $\Delta\omega$ and $\Delta\mu$, with the first oscillator having very small (but non-zero) amplitude.

What happens to a linear array of these oscillators with every other one under-pumped, i.e. taking $\mu_{2i} < 0$ and $\mu_{2i+1} > 0$, and some distribution of ω_i? Such a system indeed synchronizes, though there are significant differences with the laser system. First of all, even in the case of the weak-link configuration the Hopf array is still sensitive to the width of natural frequency distribution, $\Delta\omega$. Moreover, for some small $\Delta\omega$ the configuration of all-turned-on oscillators with close positive μ's also readily synchronizes, which was not the case for the fiber lasers. This means that although weak-link synchronization occurs in the Hopf array, it does not provide the obvious benefit of superior robustness when compared against the conventional strategy of using uniformly pumped arrays.

That said, one sees that weak-link synchronization is not a peculiar property of the fiber-laser system, and may provide a useful alternative scheme for synchronizing other nonlinear oscillator arrays where conventional synchronization is troublesome or elusive.

CHAPTER IV

CONCLUSIONS

This thesis considered examples of nonlinear oscillator arrays with a coupling which is a dynamical unit by itself. Each of the two systems analyzed in the thesis led to the discovery of new and interesting phenomena, and also might have promising scientific applications.

It was shown that taking advantage of proper positioning of oscillating elements in a distributed array can provide a resonant architecture and a situation when weak physical coupling is effectively amplified, increasing the degree of coherence. I set up the problem of synchronization in the load-free Josephson transmission line and analyzed the effects of the coupling, which is intrinsically distributed. A somewhat peculiar phenomenon of the formation of inert oscillating pairs was observed and explained from both physical and mathematical points of view.

Despite the progress I made in the understanding of the properties of this system, there are still open questions concerning the frustration behavior among equally-spaced junctions and possible simultaneous effects of a transmission line and a load on the synchronization in general, and the paired state in particular.

By considering van der Pol oscillators instead of Josephson junctions I have confirmed that the paring phenomenon does not come from some special characteristics of single Josephson junctions or its nonlinearity type, which implies that the problem can be viewed from a much broader fundamental perspective.

The study of a different system of coupled nonlinear oscillators, namely an array of interacting fiber lasers, disclosed an even more promising phenomenon that I called weak-link synchronization. Such arrays can also take an advantage of coupling through a dynamical object, though this time the mechanism is quite different. In this case the coupling is provided by oscillators of the same nature but driven in a different way than the ones contributing most to the total coherent field.

The important feature of this system is that conventional direct coupling of equally driven oscillators does not provide a robust synchronized state, contrary to the weak-link configuration, which not only makes the coherence possible, but also guarantees its robustness with respect to frequency detuning or other parameter mismatch.

Testing the idea of the weak-link synchronization on oscillators of a more general type supported my expectation that this phenomena can be observed in other physical or biological systems. However, determination of the conditions for the robustness or other desired properties require additional research and deeper understanding of the underlying mechanisms.

Hopefully, my work will motivate other scientists to explore structurally similar systems in regard to these or other interesting phenomena. As was described in the Introduction, synchronization phenomena already have been implemented in many useful applications. Therefore, theoretical discoveries of new aspects in technologically motivated problems such as arrays of Josephson junctions or fiber lasers have potential importance for future engineering developments.

APPENDIX A

DETAILED ANALYSIS OF THE TWO COUPLED SINGLE-MODE LASER MODEL

In this appendix I present a thorough mathematical analysis of the equations which were discussed in Chapter 3. Since these equation are strongly nonlinear and have 5 degrees of freedom, finding even the fixed point solutions is not trivial.

The method of solution is the following. First, I rewrite the equations in a convenient form, so that I can find all possible interactions of some nonlinear functions, which allows me to determine the number of solutions in each parameter regime. Moreover, the asymptotic behavior of these functions provides an initial guess for the solution values. Then, having a knowledge of the leading terms of all solutions, I find the corresponding corrections up to second order in the small parameter of the problem, namely the coupling parameter p.

The stability of the solutions is also an important issue, which is addressed in Section (A.2).

Since the motivation for the analysis of this model was to consider the effects of non-zero detuning ($q \neq 0$), I have found the q-corrections to the solution as well (Appendix A.3).

According to Eqs.(90) with Eqs.(98,99)

$$E_1(t+T) = re^{G_1+i\phi_1} S_{11} E_1(t) + re^{\frac{G_1+G_2}{2}} S_{12} E_2(t),$$
$$E_2(t+T) = re^{G_2+i\phi_2} S_{22} E_2(t) + re^{\frac{G_1+G_2}{2}} S_{21} E_1(t),$$

where

$$S_{11} = S_{22}^* = \cos(p) - i\sin(q)\sin(p),$$
$$S_{12} = S_{21} = -i\cos(q)\sin(p).$$

Let $E_n(t) = \varepsilon_n(t)e^{i\psi_n(t)}$, where $\varepsilon_n \equiv |E_n|$ and $\psi_n \equiv \arg(E_n)$, then

$$\begin{aligned}
\varepsilon_1(t+T)\cos[\psi_1(t+T)] &= re^{G_1}\varepsilon_1(t)\cos(p)\cos[\psi_1(t)] \\
&+ re^{G_1}\varepsilon_1(t)\sin(q)\sin(p)\sin[\psi_1(t)] \\
&+ re^{\frac{G_1+G_2}{2}}\varepsilon_2(t)\cos(q)\sin(p)\sin[\psi_2(t)], \qquad (101) \\
\varepsilon_1(t+T)\sin[\psi_1(t+T)] &= re^{G_1}\varepsilon_1(t)\cos(p)\sin[\psi_1(t)] \\
&- re^{G_1}\varepsilon_1(t)\sin(q)\sin(p)\cos[\psi_1(t)] \\
&- re^{\frac{G_1+G_2}{2}}\varepsilon_2(t)\cos(q)\sin(p)\cos[\psi_2(t)], \qquad (102) \\
\varepsilon_2(t+T)\cos[\psi_2(t+T)] &= re^{G_2}\varepsilon_2(t)\cos(p)\cos[\psi_2(t)] \\
&- re^{G_2}\varepsilon_2(t)\sin(q)\sin(p)\sin[\psi_2(t)] \\
&+ re^{\frac{G_1+G_2}{2}}\varepsilon_1(t)\cos(q)\sin(p)\sin[\psi_1(t)], \qquad (103) \\
\varepsilon_2(t+T)\sin[\psi_2(t+T)] &= re^{G_2}\varepsilon_2(t)\cos(p)\sin[\psi_2(t)] \\
&+ re^{G_2}\varepsilon_2(t)\sin(q)\sin(p)\cos[\psi_2(t)] \\
&- re^{\frac{G_1+G_2}{2}}\varepsilon_1(t)\cos(q)\sin(p)\cos(\psi_1(t)). \qquad (104)
\end{aligned}$$

I consider two lasers synchronized if the phase difference of the fields is a constant in time. Thus, in order to explore synchronization I have to rewrite the last equations in terms of phase difference $\psi(t) = \psi_1(t) - \psi_2(t)$.

From (101)*(103)+(102)*(104), one gets

$$\begin{aligned}
&\varepsilon_1(t+T)\varepsilon_2(t+T)\cos[\psi(t+T)] = r^2e^{G_1+G_2}\varepsilon_1(t)\varepsilon_2(t)\cos^2(q)\sin^2(p)\cos[\psi(t)] \\
&+r^2e^{G_1+G_2}\varepsilon_1(t)\varepsilon_2(t)[\cos^2(p) - \sin^2(q)\sin^2(p)]\cos[\psi(t)+\phi] \\
&+2r^2e^{G_1+G_2}\varepsilon_1(t)\varepsilon_2(t)\sin(q)\sin(p)\cos(p)\sin[\psi(t)] \\
&+re^{\frac{G_1+G_2}{2}}[re^{G_1}\varepsilon_1^2(t) - re^{G_2}\varepsilon_2^2(t)]\sin(q)\cos(q)\sin^2(p). \qquad (105)
\end{aligned}$$

(102)*(103)-(101)*(104):

$$\varepsilon_1(t+T)\varepsilon_2(t+T)\sin[\psi(t+T)] = -r^2 e^{G_1+G_2}\varepsilon_1(t)\varepsilon_2(t)\cos^2(q)\sin^2(p)\sin[\psi(t)]$$
$$+r^2 e^{G_1+G_2}\varepsilon_1(t)\varepsilon_2(t)[\cos^2(p)-\sin^2(q)\sin^2(p)]\sin[\psi(t)]$$
$$-2r^2 e^{G_1+G_2}\varepsilon_1(t)\varepsilon_2(t)\sin(q)\sin(p)\cos(p)\cos[\psi(t)+\phi]$$
$$+re^{\frac{G_1+G_2}{2}}[re^{G_1}\varepsilon_1^2(t)-re^{G_2}\varepsilon_2^2(t)]\cos(q)\cos(p)\sin(p). \quad (106)$$

(101)*(101)+(102)*(102):

$$\varepsilon_1^2(t+T) = r^2 e^{2G_1}\varepsilon_1^2(t)[\cos^2(p)+\sin^2(q)\sin^2(p)]$$
$$+r^2 e^{G_1+G_2}\varepsilon_2^2(t)\cos^2(q)\sin^2(p)$$
$$+2r^2 e^{\frac{3G_1+G_2}{2}}\varepsilon_1(t)\varepsilon_2(t)\sin(q)\cos(q)\sin^2(p)\cos[\psi(t)]$$
$$-2r^2 e^{\frac{3G_1+G_2}{2}}\varepsilon_1(t)\varepsilon_2(t)\cos(q)\cos(p)\sin(p)\sin[\psi(t)]. \quad (107)$$

(103)*(103)+(104)*(104):

$$\varepsilon_2^2(t+T) = r^2 e^{2G_2}\varepsilon_2^2(t)[\cos^2(p)+\sin^2(q)\sin^2(p)]$$
$$+r^2 e^{G_1+G_2}\varepsilon_1^2(t)\cos^2(q)\sin^2(p)$$
$$-2r^2 e^{\frac{G_1+3G_2}{2}}\varepsilon_1(t)\varepsilon_2(t)\sin(q)\cos(q)\sin^2(p)\cos[\psi(t)]$$
$$+2r^2 e^{\frac{G_1+3G_2}{2}}\varepsilon_1(t)\varepsilon_2(t)\cos(q)\cos(p)\sin(p)\sin[\psi(t)]. \quad (108)$$

In this form the equations are still quite complicated. Hence, I will start with a simple particular case of equal modes ($\beta_1 = \beta_2$), before considering the general situation (in Appendix A.3).

Let $\delta = 0$, so that $p = 2z_c\kappa$ and $q = 0$, then one can rewrite Eqs.(105,106,107,108) as

$$\varepsilon_1(t+T)\varepsilon_2(t+T)\cos[\psi(t+T)] = r^2 e^{G_1(t)+G_2(t)}\varepsilon_1(t)\varepsilon_2(t)\cos[\psi(t)], \tag{109}$$

$$\varepsilon_1(t+T)\varepsilon_2(t+T)\sin[\psi(t+T)]$$
$$= r^2 e^{G_1+G_2}\varepsilon_1(t)\varepsilon_2(t)[\cos^2(p)-\sin^2(p)]\sin[\psi(t)]$$
$$+re^{\frac{G_1+G_2}{2}}[re^{G_1}\varepsilon_1^2(t) - re^{G_2}\varepsilon_2^2(t)]\sin(p)\cos(p), \tag{110}$$

$$\varepsilon_1^2(t+T) = r^2 e^{2G_1}\varepsilon_1^2(t)\cos^2(p) + r^2 e^{G_1+G_2}\varepsilon_2^2(t)\sin^2(p)$$
$$-2r^2 e^{\frac{3G_1+G_2}{2}}\varepsilon_1(t)\varepsilon_2(t)\sin(p)\cos(p)\sin[\psi(t)], \tag{111}$$

$$\varepsilon_2^2(t+T) = r^2 e^{2G_2}\varepsilon_2^2(t)\cos^2(p) + r^2 e^{G_1+G_2}\varepsilon_1^2(t)\sin^2(p)$$
$$+2r^2 e^{\frac{G_1+3G_2}{2}}\varepsilon_1(t)\varepsilon_2(t)\sin(p)\cos(p)\sin[\psi(t)], \tag{112}$$

$$G_1(t+T) = G_1(t) + \epsilon[G_1^p - G_1(t) - 2(1-e^{-G_1(t)})\varepsilon_1^2(t)], \tag{113}$$

$$G_2(t+T) = G_2(t) + \epsilon[G_2^p - G_2(t) - 2(1-e^{-G_2(t)})\varepsilon_2^2(t)], \tag{114}$$

where I have also added Eqs.(91).

A.1 Fixed point solutions

Let me denote the fixed point solution as ($\tilde{\psi}$, $\tilde{\varepsilon_1}$, $\tilde{\varepsilon_2}$, $\tilde{G_1}$, and $\tilde{G_2}$). From now on I will assume that $\tilde{\varepsilon_1}$, $\tilde{\varepsilon_2}$, $\tilde{G_1}$, and $\tilde{G_2}$ are strictly positive. Then Eq.(109) gives:

$$\cos(\tilde{\psi})[1 - r^2 e^{\tilde{G_1}+\tilde{G_2}}] = 0,$$

and I have two possible cases:

Case 1$(\cos(\tilde{\psi}) \neq 0)$

In this case $r^2 e^{\tilde{G_1}+\tilde{G_2}} = 1$ and from Eqs.(110-114) I have:

$$2\sin(p)\sin(\tilde{\psi}) - r\cos(p)\left[\frac{\tilde{\varepsilon_1}}{\tilde{\varepsilon_2}}e^{\tilde{G_1}} - \frac{\tilde{\varepsilon_2}}{\tilde{\varepsilon_1}}e^{\tilde{G_2}}\right] = 0, \tag{115}$$

$$r^2 e^{2\tilde{G_1}}\cos^2(p) + \left(\frac{\tilde{\varepsilon_2}}{\tilde{\varepsilon_1}}\right)^2 \sin^2(p) - 2r\frac{\tilde{\varepsilon_2}}{\tilde{\varepsilon_1}}e^{\tilde{G_1}}\sin(p)\cos(p)\sin(\tilde{\psi}) = 1, \tag{116}$$

$$r^2 e^{2\tilde{G_2}}\cos^2(p) + \left(\frac{\tilde{\varepsilon_1}}{\tilde{\varepsilon_2}}\right)^2 \sin^2(p) + 2r\frac{\tilde{\varepsilon_1}}{\tilde{\varepsilon_2}}e^{\tilde{G_2}}\sin(p)\cos(p)\sin(\tilde{\psi}) = 1, \tag{117}$$

$$\tilde{\varepsilon_1}^2 = \frac{G_1^p - \tilde{G_1}}{2(1-e^{-\tilde{G_1}})},\ \ \tilde{\varepsilon_2}^2 = \frac{G_2^p - \tilde{G_2}}{2(1-e^{-\tilde{G_2}})}. \tag{118}$$

Substituting $\sin(\tilde{\psi})$ from Eq.(115) into Eqs.(116, 117) gives the following result:

$$\tilde{\varepsilon_1} = \tilde{\varepsilon_2},$$

so that

$$\sin(\tilde{\psi}) = \frac{r(e^{\tilde{G_1}} - e^{\tilde{G_2}})}{2\tan(p)}, \tag{119}$$

$$\frac{G_1^p - \tilde{G_1}}{1-e^{-\tilde{G_1}}} = \frac{G_2^p - \tilde{G_2}}{1-e^{-\tilde{G_2}}}. \tag{120}$$

In order to find $\tilde{G_1}$ and $\tilde{G_2}$, let me use the following notation:

$$x = e^{-\tilde{G_1}},\ \ y = e^{-\tilde{G_2}},\ \ x_p = e^{-G_1^p},\ \ y_p = e^{-G_2^p},$$

so that $xy = r^2$ and from Eq.(120)

$$\frac{\ln x - \ln x_p}{1-x} = \frac{\ln y - \ln y_p}{1-y},$$

where $x, y, x_p, y_p \in (0,1)$.

Actually, since $\tilde{\varepsilon_1}$ and $\tilde{\varepsilon_2}$ are positive, then $x_p < x$ and $y_p < y$, so that $x_p y_p < xy = r^2$. Substituting $y = r^2/x$ into the last expression I get

$$\frac{\ln x - \ln x_p}{1-x} = \frac{\ln r^2 - \ln x - \ln y_p}{1-r^2/x},$$

which is equivalent to

$$\frac{\ln(x/x_p)}{1-x} = \frac{\ln[r^2/(x_p y_p)] - \ln(x/x_p)}{1-r^2/x}.$$

The next step is to right this as

$$\frac{1-r^2/x}{1-x} = \frac{\ln[r^2/(x_p y_p)] - \ln(x/x_p)}{\ln(x/x_p)} = \frac{\ln[r^2/(x_p y_p)]}{\ln(x/x_p)} - 1,$$

or

$$\frac{\ln[r^2/(x_p y_p)]}{\ln(x/x_p)} = 1 + \frac{1 - r^2/x}{1-x} = \frac{2 - x - r^2/x}{1-x} = \frac{2x - x^2 - r^2}{x(1-x)},$$

and finally

$$\frac{\ln(x/x_p)}{\ln(r/\sqrt{x_p y_p})} = \frac{2x(1-x)}{(1-r^2) - (1-x)^2}. \tag{121}$$

The right-hand side of Eq.(121) decreases from 0 to $-\infty$, when $x \in (0, x_0)$, and decreases from $+\infty$ to 0, when $x \in (x_0, 1)$, where $x_0 = 1 - \sqrt{1-r^2}$. Since $x_p y_p < r^2$, then the left-hand side of Eq.(121) increases from $-\infty$ to 0, when $x \in (0, x_p)$, and continues to increase from 0 to $\frac{\ln(1/x_p)}{\ln(r/\sqrt{x_p y_p})}$, when $x \in (x_p, 1)$. Hence, there are two solution of Eq.(121): $x_- \in (0, x_p)$ and $x_+ \in (x_p, 1)$. Therefore, the physically meaningful solution is x_+.

Now, since $|\sin(\tilde{\psi})| \leq 1$, then from Eq.(119) I find that

$$|e^{\tilde{G}_1} - e^{\tilde{G}_2}| \leq \frac{2\tan(p)}{r} \ll 1.$$

On the other hand from Eq.(120) I find that $\tilde{G}_1 = \tilde{G}_2$ if and only if $G_1^p = G_2^p$, which means that a fixed point solution exists only for small values of $|x_p - y_p|$.

Let me first consider the special case when $y_p = x_p = e^{-G^p}$, then simply by inspection I find that the solution of Eq.(119) is $x_+ = r$, and thus, the fixed point solution is

$$\tilde{\psi} = 0, \pi, \tag{122}$$

$$\tilde{\varepsilon_1}^2 = \tilde{\varepsilon_2}^2 = \frac{G^p + \ln r}{2(1-r)}, \tag{123}$$

$$\tilde{G}_1 = \tilde{G}_2 = \ln\frac{1}{r}. \tag{124}$$

Now I can find the corrections to this solution assuming that $|G_1^p - G_2^p|$ is small enough (the explicit expression for this condition must be also derived).

So let $x = r(1-\rho)$, where $\rho \ll 1$, then from Eq.(119) I get

$$\begin{aligned}
&\frac{\ln(r/x_p) + \ln(1-\rho)}{\ln(r/\sqrt{x_p y_p})} = \frac{2r(1-\rho)(1-r+r\rho)}{(1-r^2) - (1-r+r\rho)^2} \\
&= \frac{2r(1-r+2r\rho-\rho) + O(r^2\rho^2)}{(1-r^2) - (1-r)^2 - 2(1-r)r\rho + O(r^2\rho^2)} = \frac{1 - \rho\frac{1-2r}{1-r} + O(\rho^2))}{1 - \rho + O(\rho^2)} \\
&= (1 - \rho\frac{1-2r}{1-r})(1+\rho) + O(\rho^2) = 1 + \rho\frac{r}{1-r} + O(\rho^2).
\end{aligned}$$

Hence, to first order in ρ,

$$\ln(r/x_p) - \rho = (1 + \rho\frac{r}{1-r})\ln(r/\sqrt{x_p y_p}),$$

and therefore,

$$\begin{aligned}
\rho &= \frac{\ln(\sqrt{y_p/x_p})}{1 + \frac{r\ln(r/\sqrt{x_p y_p})}{1-r}} = \frac{(G_1^p - G_2^p)/2}{1 + \frac{r(G^p + \ln r)}{1-r}}, \\
\tilde{\psi} &= \arcsin\left[\frac{\rho}{\tan(p)}\right] + O(\rho^2), \\
{\tilde{\varepsilon_1}}^2 &= {\tilde{\varepsilon_2}}^2 = \frac{G^p + \ln r}{2(1-r)} + O(\rho^2), \\
\tilde{G_1} &= \ln\frac{1}{r} + \rho + O(\rho^2), \\
\tilde{G_2} &= \ln\frac{1}{r} - \rho + O(\rho^2),
\end{aligned}$$

where $G^p = \frac{G_1^p + G_2^p}{2}$.

Case 2 $(\cos(\tilde{\psi}) = 0)$

In this case $\sin(\tilde{\psi}) = \pm 1 \equiv g_0$, so that Eqs.(110,111,112) give the following equations for a fixed point:

$$\begin{aligned}
&g_0 = g_0 r^2 e^{\tilde{G_1}+\tilde{G_2}}[\cos^2(p) - \sin^2(p)] + r^2 e^{\frac{\tilde{G_1}+\tilde{G_2}}{2}}\left[\frac{\tilde{\varepsilon_1}}{\tilde{\varepsilon_2}}e^{\tilde{G_1}} - \frac{\tilde{\varepsilon_2}}{\tilde{\varepsilon_1}}e^{\tilde{G_2}}\right]\sin(p)\cos(p) = 0, \\
&r^2 e^{2\tilde{G_1}}\cos^2(p) + r^2 e^{\tilde{G_1}+\tilde{G_2}}\left(\frac{\tilde{\varepsilon_2}}{\tilde{\varepsilon_1}}\right)^2\sin^2(p) - 2g_0 r^2 e^{\tilde{G_1}} e^{\frac{\tilde{G_1}+\tilde{G_2}}{2}}\left(\frac{\tilde{\varepsilon_2}}{\tilde{\varepsilon_1}}\right)\sin(p)\cos(p) = 1, \\
&r^2 e^{2\tilde{G_2}}\cos^2(p) + r^2 e^{\tilde{G_1}+\tilde{G_2}}\left(\frac{\tilde{\varepsilon_1}}{\tilde{\varepsilon_2}}\right)^2\sin^2(p) + 2g_0 r^2 e^{\tilde{G_2}} e^{\frac{\tilde{G_1}+\tilde{G_2}}{2}}\left(\frac{\tilde{\varepsilon_1}}{\tilde{\varepsilon_2}}\right)\sin(p)\cos(p) = 1.
\end{aligned}$$

I can write this result in the earlier introduced notations as

$$\begin{aligned}
&\frac{r^2}{xy}[\cos^2(p) - \sin^2(p)] + g_0 r\cos(p)\left[\frac{r\sin(p)\tilde{\varepsilon_1}}{x\tilde{\varepsilon_2}\sqrt{xy}} - \frac{r\sin(p)\tilde{\varepsilon_2}}{y\tilde{\varepsilon_1}\sqrt{xy}}\right] = 1, \qquad (125) \\
&\left(\frac{r\cos(p)}{x} - g_0\frac{r\sin(p)\tilde{\varepsilon_2}}{\tilde{\varepsilon_1}\sqrt{xy}}\right)^2 = 1, \\
&\left(\frac{r\cos(p)}{y} + g_0\frac{r\sin(p)\tilde{\varepsilon_1}}{\tilde{\varepsilon_2}\sqrt{xy}}\right)^2 = 1.
\end{aligned}$$

From the last two expressions I find that

$$g_0 \frac{r\sin(p)\tilde{\varepsilon_2}}{\tilde{\varepsilon_1}\sqrt{xy}} = \frac{r\cos(p)}{x} - g_1, \tag{126}$$

$$g_0 \frac{r\sin(p)\tilde{\varepsilon_1}}{\tilde{\varepsilon_2}\sqrt{xy}} = g_2 - \frac{r\cos(p)}{y}, \tag{127}$$

where $g_1 = \pm 1$ and $g_2 = \pm 1$.

Substituting Eq.(126,127) into Eq.(125) I get

$$1 + \frac{r^2}{xy} = r\cos(p)\left[\frac{g_2}{x} + \frac{g_1}{y}\right],$$

so that

$$g_1 x = r\frac{g_2 y\cos(p) - r}{g_1 y - r\cos(p)}.$$

Dividing Eq.(127) by Eq.(126) I obtain

$$\frac{y\tilde{\varepsilon_1}^2}{x\tilde{\varepsilon_2}^2} = \frac{g_2 y - r\cos(p)}{r\cos(p) - g_1 x}.$$

Finally using the fact that

$$r\cos(p) - g_1 x = r\cos(p) - r\frac{g_2 y\cos(p) - r}{g_1 y - r\cos(p)} = r\frac{(g_1 - g_2)y\cos(p) + r\sin^2(p)}{g_1 y - r\cos(p)},$$

I find

$$\frac{y\tilde{\varepsilon_1}^2}{x\tilde{\varepsilon_2}^2} = \frac{(g_1 y - r\cos(p))(g_2 y - r\cos(p))}{(g_1 - g_2)ry\cos(p) + r^2\sin^2(p)}.$$

On the other hand from Eqs.(113,114) I have

$$\frac{\tilde{\varepsilon_1}^2}{\tilde{\varepsilon_2}^2} = \frac{\ln(x/x_p)(1-y)}{\ln(y/y_p)(1-x)},$$

so that I get two equations with two variables (x,y):

$$\frac{\ln(x/x_p)(1-y)y}{\ln(y/y_p)(1-x)x} = \frac{(g_1 y - r\cos(p))(g_2 y - r\cos(p))}{(g_1 - g_2)ry\cos(p) + r^2\sin^2(p)}, \tag{128}$$

$$x = r\frac{g_2 y\cos(p) - r}{y - g_1 r\cos(p)}. \tag{129}$$

Let me define functions $L(y, x_p, y_p)$ and $R(y)$ as:

$$L(y, x_p, y_p) = \frac{\ln[x(y)/x_p](1-y)y}{\ln(y/y_p)[1-x(y)]x(y)},$$
$$R(y) = \frac{[g_1 y - r\cos(p)][g_2 y - r\cos(p)]}{(g_1 - g_2)ry\cos(p) + r^2\sin^2(p)}.$$

Now I have to consider 3 different cases: $g_1 = g_2 = +1$, $g_1 = -g_2 = \pm 1$ and $g_1 = g_2 = -1$.

Case 2.1 ($g_1 = g_2 = +1$)

In this case

$$L(y, x_p, y_p) = \frac{\ln[x(y)/x_p](1-y)y}{\ln(y/y_p)[1-x(y)]x(y)},$$
$$R(y) = \frac{[y - r\cos(p)]^2}{r^2\sin^2(p)},$$
$$x(y) = r\frac{y\cos(p) - r}{y - r\cos(p)}.$$

Note that $x(y)$ increases from Y_2 to 1, when $y \in (0, Y_1)$, where $Y_1 = r\frac{\cos(p)-r}{1-r\cos(p)} < r\cos(p)$ and $Y_2 = \frac{r}{\cos(p)} > Y_1$, and it increases from 0 to Y_1, when $y \in (Y_2, 1)$. For $y \in (Y_1, Y_2)$, $x(y) < 0$ or $x(y) > 1$, which is beyond physical values, because $x = e^{-\tilde{G}}$. If $\cos(p) < r$, then $Y_1 < 0$, $Y_2 > 1$ and there can be no solutions at all, so that p must be less then $\arccos(r)$. Moreover if both x_p and y_p bigger than Y_1, then there are no solutions. And the last remark is that $x(y, p) = x_p$ at $y = Y_3 = r\frac{x_p\cos(p)-r}{x_p - r\cos(p)}$. Since I restricted myself to $\cos(p) > r$, then $Y_3 \in (0, Y_1)$ for $x_p > Y_2$ and $Y_3 \in (Y_2, 1)$ for $x_p < Y_1$.

Hence, the function $L(y, x_p, y_p)$ has four characteristic points, Y_1, Y_2, Y_3 and y_p, and I have to consider five different possibilities:

$$\begin{array}{lccc}
(1) & 0 < x_p < Y_1 & \text{and} & 0 < y_p < Y_1, \\
(2) & 0 < x_p < Y_1 & \text{and} & Y_1 < y_p < Y_2, \\
(3) & 0 < x_p < Y_1 & \text{and} & Y_2 < y_p < 1, \\
(4) & Y_1 < x_p < Y_2 & \text{and} & 0 < y_p < Y_1, \\
(5) & Y_2 < x_p < 1 & \text{and} & 0 < y_p < Y_1.
\end{array}$$

The function R(y,p) is a parabola, which is positive and symmetrical with respect to $y = Y_2$, where it is zero.

So, let me first consider the **possibility (1)**. We have $y_p < Y_1 < Y_2 < Y_3$, $L(y, x_p, y_p) \to +\infty$ at $y \to (y_p)^+$ and at $y \to (Y_1)^-$, and $L(y, x_p, y_p) \to -\infty$ at $y \to (Y_2)^+$. Hence, $L(y, x_p, y_p)$ has a positive minimum on $y \in (y_p, Y_1)$ and positive maximum on $y \in (Y_3, 1)$.

When p and y_p are small enough, $R(y,p) > \min[L(y,p)]$ and I have two solutions, y_1 and y_2, on $y \in (y_p, Y_1)$. Similarly, when p and x_p are small enough, $R(y,p) < \max[L(y,p)]$ and I have two more solutions, y_3 and y_4, on $y \in (Y_2, 1)$. In the limit $p \to 0$, $y_1 \approx y_p$ and $y_2 \approx y_3 \approx y_4 \approx r$.

Let

$$\Delta_1(x_p, y_p) = \min_{y \in (y_p, Y_1)} [L(y, x_p, y_p) - R(y)],$$

$$\Delta_2(x_p, y_p) = \max_{y \in (Y_3, 1)} [L(y, x_p, y_p) - R(y)],$$

then the equations $\Delta_{1,2}(x_p, y_p) = 0$ produce two bifurcation curves in the (x_p, y_p)-parameter space, so that I have:

4 solutions (y_1, y_2, y_3, y_4), when $\Delta_1(x_p, y_p) < 0$ and $\Delta_2(x_p, y_p) > 0$;

2 solutions (y_1 and y_2), when $\Delta_1(x_p, y_p) < 0$ and $\Delta_2(x_p, y_p) < 0$;

2 solutions (y_3 and y_4), when $\Delta_1(x_p, y_p) > 0$ and $\Delta_2(x_p, y_p) > 0$;

and 0 solutions, when $\Delta_1(x_p, y_p) > 0$ and $\Delta_2(x_p, y_p) < 0$.

Now for the **possibility (2)**, I have $Y_1 < y_p < Y_2 < Y_3$, so that I can have solutions only for $y \in (Y_2, 1)$, where the function $L(y, x_p, y_p)$ has a positive maximum. Therefore I find two solutions, y_3 and y_4, for $\Delta_2(x_p, y_p) > 0$ and no solutions for $\Delta_2(x_p, y_p) < 0$. Note that $L(y, x_p, y_p)$ changes continuously on $y \in (Y_3, 1)$, when the parameter y_p passes Y_1. Hence, the curve $\Delta_2(x_p, y_p)$ is continuous at $y_p = Y_1$, as well as the solutions y_3 and y_4.

My next step is to find solutions for the **possibility (3)**, when both Y_3 and y_p bigger then Y_2. Let

$$\Delta_3(x_p, y_p) = y_p - Y_3 = y_p - \frac{r x_p \cos(p) - r^2}{x_p - r\cos(p)}.$$

If $\Delta_3(x_p, y_p) > 0$, then $L(y,p) \to +\infty$ at $y = (y_p)^+$ and I have only one solution, y_5,

for $y \in (y_p, 1)$. In the limit $p \to 0$, $y_5 \approx y_1 \approx y_p$. If $\Delta_3(x_p, y_p) < 0$, then $L(y, p) \to -\infty$ at $y = (y_p)^+$ and $L(Y_3, x_p, y_p) = L(1, x_p, y_p) = 0$, so that $L(y, x_p, y_p)$ has a positive maximum on $y \in (y_p, 1)$. Hence I obtain two solutions, y_3 and y_4, when $\Delta_3(x_p, y_p) < 0$ and $\Delta_2(x_p, y_p) > 0$, and zeros solutions when $\Delta_3(x_p, y_p) < 0$ and $\Delta_2(x_p, y_p) < 0$. Note that $\Delta_3(x_p, y_p) < 0$ at $y_p = Y_2$ for $0 < x_p < Y_1$ and $L(y, x_p, y_p)$ changes continuously on $y \in (Y_3, 1)$, when the parameter y_p passes Y_2. Therefore, the curve $\Delta_2(x_p, y_p)$ is continuous at $y_p = Y_2$.

Here is a good place to recall that Eqs.(109-114) stay the same if I exchange indices 1 and 2. This means that if (x, y) is a solution for parameters (x_p, y_p), then (y, x) is also a solution for parameters (y_p, x_p). Thus, the bifurcation curves $\Delta_{1,2,3}(x_p, y_p)$ are symmetric in the (x_p, y_p)-parameter space with respect to the line $x_p = y_p$. So that I don't even need to consider separately the **possibilities (4) and (5)**.

I can estimate the values of y_1, y_2, y_3 and y_4 in the limit $p \to 0$, where $y_1 \approx y_p$ and $y_2 \approx y_3 \approx y_4 \approx r$. In this limit $L(y_2, p) = L(y_4, p) = \frac{\ln(r/x_p)}{\ln(r/y_p)} + O(p)$, so that $\frac{y_{2,4} - r + O(p^2)}{rp} = \mp\sqrt{\frac{\ln(r/x_p)}{\ln(r/y_p)}} + O(p)$; and $L(y_3, p) = 0 + O(p)$, so that $\frac{y_3 - r + O(p^2)}{rp} = O(p)$. Now let $y_1 = y_p + \delta$, then $L(y_1, p) \sim \frac{1}{\delta_1}$ and $R(y_1, p) \sim \frac{1}{p^2}$. Hence $\delta_1 = O(p^2)$ and finally

$$
\begin{aligned}
y_1 &= y_p + O(p^2), \\
y_2 &= r\left(1 - p\sqrt{\frac{\ln(r/x_p)}{\ln(r/y_p)}}\right) + O(p^2), \\
y_3 &= r + O(p^2), \\
y_4 &= r\left(1 + p\sqrt{\frac{\ln(r/x_p)}{\ln(r/y_p)}}\right) + O(p^2).
\end{aligned}
$$

The easiest way to find the corresponding x's is to realize that I could start from the beginning by expressing y as a function of x, so that

$$
\begin{aligned}
L(x, x_p, y_p) &= \frac{\ln[y(x)/y_p](1-x)x}{\ln(x/x_p)[1 - y(x)]y(x)}, \\
R(x) &= \frac{[x - r\cos(p)]^2}{r^2 \sin^2(p)}, \\
y(x) &= r\frac{x\cos(p) - r}{x - r\cos(p)};
\end{aligned}
$$

and, therefore,

$$
\begin{aligned}
x_1 &= r + O(p^2), \\
x_2 &= r\left(1 + p\sqrt{\frac{\ln(r/y_p)}{\ln(r/x_p)}}\right) + O(p^2), \\
x_3 &= x_p + O(p^2), \\
x_4 &= r\left(1 - p\sqrt{\frac{\ln(r/y_p)}{\ln(r/x_p)}}\right) + O(p^2).
\end{aligned}
$$

The symmetry arguments at $x_p = y_p$ assure the proper matching.

Case 2.2 ($g_1 = -g_2 = \pm 1$)

In this case

$$
\begin{aligned}
L(y, x_p, y_p) &= \frac{\ln[x(y)/x_p](1-y)y}{\ln(y/y_p)[1-x(y)]x(y)}, \\
R(y) &= \frac{r^2\cos(p)^2 - y^2}{r^2\sin^2(p) \pm 2ry\cos(p)}, \\
x(y) &= r\frac{y\cos(p) \pm r}{r\cos(p) \mp y}.
\end{aligned}
$$

These equations have the same topological structure in (x_p, y_p)-parameter space as the equations in the previous case, only now $Y_1 = r\frac{\cos(p)-r}{1+r\cos(p)} < r\frac{1-r}{1+r}$ and $Y_3 = r\frac{x_p\cos(p)-r}{x_p+r\cos(p)}$. So that, there is no solution unless G_1^p or G_2^p is bigger than $\ln\frac{1+r}{r-r^2}$ (which is 2.015 for $r = 0.2$).

Case 2.3 ($g_1 = g_2 = -1$)

In this case $x(y) = -r\frac{y\cos(p)+r}{r\cos(p)+y} < 0$ for any positive $\cos(p)$, so that we find no solutions at all.

This completes consideration of all possible solutions in both cases, $\cos(\tilde{\psi}) = 0$ and $\cos(\tilde{\psi}) \neq 0$, for the case of identical modes ($\beta_1 = \beta_2$).

A.2 Linear stability of the solutions

I start the stability analysis with the case: $\cos(\tilde{\psi}) \neq 0$, when Eqs.(109-114) can be written as

$$\begin{aligned}
\psi(t+T) &= \arctan\Big([\cos^2(p)-\sin^2(p)]\tan[\psi(t)] \\
&\quad + \left[\frac{\sqrt{y(t)}\varepsilon_1(t)}{\sqrt{x(t)}\varepsilon_2(t)} - \frac{\sqrt{x(t)}\varepsilon_2(t)}{\sqrt{y(t)}\varepsilon_1(t)}\right]\frac{\sin(p)\cos(p)}{\cos[\psi(t)]}\Big), \qquad (130)\\
\varepsilon_1(t+T) &= \frac{r\varepsilon_1(t)}{x(t)}\left(\cos^2(p) + \frac{x(t)\varepsilon_2^2(t)}{y(t)\varepsilon_1^2(t)}\sin^2(p)\right. \\
&\quad \left. - 2\frac{\sqrt{x(t)}\varepsilon_2(t)}{\sqrt{y(t)}\varepsilon_1(t)}\sin(p)\cos(p)\sin[\psi(t)]\right)^{1/2}, \qquad (131)\\
\varepsilon_2(t+T) &= \frac{r\varepsilon_2(t)}{y(t)}\left(\cos^2(p) + \frac{y(t)\varepsilon_1^2(t)}{x(t)\varepsilon_2^2(t)}\sin^2(p)\right. \\
&\quad \left. + 2\frac{\sqrt{y(t)}\varepsilon_1(t)}{\sqrt{x(t)}\varepsilon_2(t)}\sin(p)\cos(p)\sin[\psi(t)]\right)^{1/2}, \qquad (132)\\
x(t+T) &= x(t)\left(\frac{x(t)}{x_p}\right)^{-\epsilon} e^{2\epsilon[1-x(t)]\varepsilon_1^2(t)}, \qquad (133)\\
y(t+T) &= y(t)\left(\frac{y(t)}{y_p}\right)^{-\epsilon} e^{2\epsilon[1-y(t)]\varepsilon_2^2(t)}. \qquad (134)
\end{aligned}$$

The corresponding fixed point solution was found in the previous section:

$$\begin{aligned}
&\tilde{\varepsilon_1} = \tilde{\varepsilon_2} = \tilde{\varepsilon} = \left[\frac{\ln(r/\sqrt{x_p y_p})}{2(1-r)}\right]^{1/2} + O(p^2),\\
&\tilde{x} = r(1 - p\ \sin(\tilde{\psi})) + O(p^2),\\
&\tilde{y} = r(1 + p\ \sin(\tilde{\psi})) + O(p^2),\\
&\sin(\tilde{\psi}) = \frac{\ln(y_p/x_p)}{p\ (1+2r\tilde{\varepsilon})}(1 + O(p^2)).
\end{aligned}$$

The Jacobi matrix at this point is

$$J = \begin{pmatrix}
1 & \frac{2p}{\tilde{\varepsilon}}\cos(\tilde{\psi}) & -\frac{2p}{\tilde{\varepsilon}}\cos(\tilde{\psi}) & -\frac{p}{r}\cos(\tilde{\psi}) & \frac{p}{r}\cos(\tilde{\psi}) \\
-p\tilde{\varepsilon}\cos(\tilde{\psi}) & 1+p\sin(\tilde{\psi}) & -p\sin(\tilde{\psi}) & -\frac{\tilde{\varepsilon}}{r}[1+\frac{3p}{2}\sin(\tilde{\psi})] & \frac{p\tilde{\varepsilon}}{2r}\sin(\tilde{\psi}) \\
p\tilde{\varepsilon}\cos(\tilde{\psi}) & p\sin(\tilde{\psi}) & 1-p\sin(\tilde{\psi}) & -\frac{p\tilde{\varepsilon}}{2r}\sin(\tilde{\psi}) & -\frac{\tilde{\varepsilon}}{r}[1-\frac{3p}{2}\sin(\tilde{\psi})] \\
0 & 4\epsilon\tilde{\varepsilon}r(1-r) & 0 & 1-\epsilon(1+2r\tilde{\varepsilon}^2) & 0 \\
0 & 0 & 4\epsilon\tilde{\varepsilon}r(1-r) & 0 & 1-\epsilon(1+2r\tilde{\varepsilon}^2)
\end{pmatrix},$$

where I have omitted all terms of the order ϵp, p^2, and higher. In order to make a quantitative estimate I keep only the leading terms of the equation $\det(J-\lambda E)=0$, so that

$\lambda_1 = \lambda_2 = \lambda_3 = 1$ and

$$\lambda_{4,5} = 1 - \epsilon(1 + 2r\tilde{\varepsilon}^2) \pm i\sqrt{8\epsilon\tilde{\varepsilon}^2(1-r) + 4p^2\cos^2(\tilde{\psi})}.$$

Hence the fixed point solution is stable as long as

$$p\,|\cos(\tilde{\psi})| < \sqrt{\frac{\epsilon}{2}\left(1 - \frac{\tilde{\varepsilon}^2}{\varepsilon_m^2}\right)},$$

where $\varepsilon_m = 1/\sqrt{4-6r}$, and which is consistent with direct numerical calculations.

The next step is to consider the case $\cos(\tilde{\psi}) = 0$. Let me for a moment assume that $\psi(t) = \pm\frac{\pi}{2} + \delta\psi(t)$, where $\delta\psi(t)$ is a small perturbation, then from Eq.(109) I find

$$\delta\psi(t+T) = \frac{r^2}{\tilde{x}\tilde{y}}\,\delta\psi(t),$$

so that one of the eigenvalues is

$$\lambda_1 = \begin{cases} \frac{r}{y_p} & \text{for solution} \quad (x_1, y_1), \\ 1 - p\left[\sqrt{\frac{\ln(r/y_p)}{\ln(r/x_p)}} - \sqrt{\frac{\ln(r/x_p)}{\ln(r/y_p)}}\right] & \text{for solution} \quad (x_2, y_2), \\ \frac{r}{x_p} & \text{for solution} \quad (x_3, y_3), \\ 1 - p\left[\sqrt{\frac{\ln(r/x_p)}{\ln(r/y_p)}} - \sqrt{\frac{\ln(r/y_p)}{\ln(r/x_p)}}\right] & \text{for solution} \quad (x_4, y_4). \end{cases}$$

The other eigenvalues are determined by the Jacobi matrix of Eqs.(131-134), which is

$$\begin{pmatrix} 1 \mp \frac{p\tilde{\varepsilon_2}}{\tilde{\varepsilon_1}} & \pm p & -\frac{\tilde{\varepsilon_1}}{r} \pm \frac{3p\tilde{\varepsilon_2}}{2r} & \mp\frac{p\tilde{\varepsilon_2}}{2r} \\ \mp p & 1 \pm \frac{p\tilde{\varepsilon_1}}{\tilde{\varepsilon_2}} & \pm\frac{p\tilde{\varepsilon_1}}{2r} & -\frac{\tilde{\varepsilon_2}}{r} \mp \frac{3p\tilde{\varepsilon_1}}{2r} \\ 4\epsilon\tilde{\varepsilon_1}r(1-r) & 0 & 1 - \epsilon(1 + 2r\tilde{\varepsilon_1}^2) & 0 \\ 0 & 4\epsilon\tilde{\varepsilon_2}r(1-r) & 0 & 1 - \epsilon(1 + 2r\tilde{\varepsilon_2}^2) \end{pmatrix}$$

for the solutions (x_2, y_2) and (x_4, y_4), where

$$\tilde{\varepsilon_1} = \sqrt{\frac{\ln(r/x_p)}{2(1-r)}} + O(p^2), \quad \tilde{\varepsilon_2} = \sqrt{\frac{\ln(r/y_p)}{2(1-r)}} + O(p^2).$$

The solution (x_1, y_1) corresponds to the fixed point

$$\tilde{\varepsilon_1} = \sqrt{\frac{\ln(r/x_p)}{2(1-r)}} + O(p^2), \quad \tilde{\varepsilon_2} = \frac{p\,\tilde{\varepsilon_1}\sqrt{ry_p}}{y_p - r} + O(p^2),$$
$$\tilde{x} = r + O(p^2), \quad \tilde{y} = y_p + O(p^2), \quad \sin(\tilde{\psi}) = 1,$$

so that the Jacobi matrix at this point is

$$\begin{pmatrix} 1 & -p\frac{\sqrt{r}}{\sqrt{y_p}} & -\frac{\tilde{\varepsilon_1}}{r} & 0 \\ p\frac{\sqrt{r}}{\sqrt{y_p}} & \frac{r}{y_p} & -\frac{p\tilde{\varepsilon_1}}{2\sqrt{ry_p}} & -\frac{p\tilde{\varepsilon_1}\sqrt{r}}{2\sqrt{y_p^3}}\frac{y_p+r}{y_p-r} \\ 4\epsilon\tilde{\varepsilon_1}r(1-r) & 0 & 1-\epsilon(1+2r\tilde{\varepsilon_1}^2) & 0 \\ 0 & 0 & 0 & 1-\epsilon \end{pmatrix}$$

Thus, to the first order in p, $\lambda_2 = 1-\epsilon$, $\lambda_3 = \frac{r}{y_p}$ and $|\lambda_{4,5}|^2 = 1-\epsilon\left(1-\frac{\tilde{\varepsilon_1}^2}{\varepsilon_m^2}\right)$, and for small p the stability region is

$$\begin{cases} 1 > y_p > r, \\ r > x_p > r_m \equiv e^{\frac{1-r}{3r-2}}, \end{cases}$$

where $x_p = r_m$ when $\tilde{\varepsilon_1} = \varepsilon_m$. (For $r = 0.2$, $r_m \approx 0.113$.)

I get similar results for the solution (x_3, y_3):

$$\tilde{\varepsilon_1} = \frac{p\,\tilde{\varepsilon_2}\sqrt{rx_p}}{x_p - r} + O(p^2) \quad \tilde{\varepsilon_2} = \sqrt{\frac{\ln(r/y_p)}{2(1-r)}} + O(p^2),$$
$$\tilde{x} = x_p + O(p^2), \quad \tilde{y} = r + O(p^2), \quad \sin(\tilde{\psi}) = -1.$$

$\lambda_2 = 1-\epsilon$, $\lambda_3 = \frac{r}{x_p}$, $|\lambda_{4,5}|^2 = 1-\epsilon\left(1-\frac{\tilde{\varepsilon_1}^2}{\varepsilon_m^2}\right)$, and the stability region is:

$$\begin{cases} 1 > x_p > r, \\ r > y_p > r_m. \end{cases}$$

A.3 Non-identical modes

In this section I will consider the situation when the modes have a slightly different propagation constants, $\beta_1 \neq \beta_1$, so that q is small but finite. Since I have analytical expressions for the fixed point solutions only to first order in p, it makes sense to ignore the terms of the order qp^2 and higher in Eqs.(105-108). Then the modified equations for a fixed point

are

$$\cos(\psi)\left(\frac{xy}{r^2}-1\right)=2q\sin(p)\cos(p)\sin(\psi), \tag{135}$$

$$\sin(\psi)\left(\frac{xy}{r^2}-1+2\sin^2(p)\right)-\left(\frac{\varepsilon_1\sqrt{y}}{\varepsilon_2\sqrt{x}}-\frac{\varepsilon_2\sqrt{x}}{\varepsilon_1\sqrt{y}}\right)\sin(p)\cos(p)$$
$$=-2q\sin(p)\cos(p)\cos(\psi), \tag{136}$$

$$\frac{x^2}{r^2}=\cos^2(p)+\frac{\varepsilon_2^2 x}{\varepsilon_1^2 y}\sin^2(p)-2\frac{\varepsilon_2\sqrt{x}}{\varepsilon_1\sqrt{y}}\sin(p)\cos(p)\sin(\psi), \tag{137}$$

$$\frac{y^2}{r^2}=\cos^2(p)+\frac{\varepsilon_1^2 y}{\varepsilon_2^2 x}\sin^2(p)+2\frac{\varepsilon_1\sqrt{y}}{\varepsilon_2\sqrt{x}}\sin(p)\cos(p)\sin(\psi), \tag{138}$$

$$\frac{\varepsilon_1^2}{\varepsilon_2^2}=\frac{\ln(x/x_p)}{\ln(y/y_p)}\frac{(1-y)}{(1-x)}. \tag{139}$$

I can find new fixed point solutions as corrections to the ones found:

$$\begin{aligned}
\psi &= \tilde{\psi}+\alpha_\psi q,\\
x &= \tilde{x}(1+\alpha_x q),\\
y &= \tilde{y}(1+\alpha_y q),\\
\tfrac{\varepsilon_1}{\varepsilon_2} &= \frac{\tilde{\varepsilon_1}}{\tilde{\varepsilon_2}}(1+\alpha_\varepsilon q).
\end{aligned}$$

As usual I start with the case $\cos(\tilde{\psi})\neq 0$, when $\tilde{\varepsilon_1}=\tilde{\varepsilon_2}$, $\tilde{x}\tilde{y}=r^2$ and Eqs.(135-138) become

$$(\alpha_x+\alpha_y)\cos(\tilde{\psi})=2\sin(p)\cos(p)\sin(\tilde{\psi}), \tag{140}$$

$$(\alpha_x+\alpha_y)\sin(\tilde{\psi})+2\alpha_\psi\cos(\tilde{\psi})\sin^2(p)$$
$$=(2\alpha_\varepsilon-\alpha_x+\alpha_y)\frac{\tilde{x}+\tilde{y}}{2r}\sin(p)\cos(p)-2\sin(p)\cos(p)\cos(\tilde{\psi}), \tag{141}$$

$$\alpha_x=\left(\alpha_\varepsilon-\frac{\alpha_x-\alpha_y}{2}\right)\left[\frac{\sqrt{\tilde{y}}}{\sqrt{\tilde{x}}}\sin(p)\cos(p)\sin(\tilde{\psi})-\sin^2(p)\right]$$
$$-\alpha_\psi\frac{\sqrt{\tilde{y}}}{\sqrt{\tilde{x}}}\sin(p)\cos(p)\cos(\tilde{\psi}), \tag{142}$$

$$\alpha_y=\left(\alpha_\varepsilon-\frac{\alpha_x-\alpha_y}{2}\right)\left[\frac{\sqrt{\tilde{x}}}{\sqrt{\tilde{y}}}\sin(p)\cos(p)\sin(\tilde{\psi})+\sin^2(p)\right]$$
$$+\alpha_\psi\frac{\sqrt{\tilde{x}}}{\sqrt{\tilde{y}}}\sin(p)\cos(p)\cos(\tilde{\psi}). \tag{143}$$

It is convenient to introduce the following notation:

$$\alpha_+ = \alpha_x + \alpha_y,$$

$$\alpha_- = \alpha_x - \alpha_y.$$

Using this notation Eqs.(140-143) are

$$\alpha_+ = 2\sin(p)\cos(p)\frac{\sin(\tilde{\psi})}{\cos(\tilde{\psi})}, \tag{144}$$

$$\alpha_+ \sin(\tilde{\psi}) + 2\alpha_\psi \cos(\tilde{\psi})\sin^2(p) - (2\alpha_\varepsilon - \alpha_-)\frac{\tilde{x}+\tilde{y}}{2r}\sin(p)\cos(p)$$
$$= -2\sin(p)\cos(p)\cos(\tilde{\psi}), \tag{145}$$

$$\alpha_+ = (\alpha_\varepsilon - \alpha_-/2)\left[\frac{\tilde{x}+\tilde{y}}{r}\sin(p)\cos(p)\sin(\tilde{\psi})\right]$$
$$-\alpha_\psi \frac{\tilde{y}-\tilde{x}}{r}\sin(p)\cos(p)\cos(\tilde{\psi}), \tag{146}$$

$$\alpha_- = (\alpha_\varepsilon - \alpha_-/2)\left[\frac{\tilde{y}-\tilde{x}}{r}\sin(p)\cos(p)\sin(\tilde{\psi}) - 2\sin^2(p)\right]$$
$$-\alpha_\psi \frac{\tilde{x}+\tilde{y}}{r}\sin(p)\cos(p)\cos(\tilde{\psi}). \tag{147}$$

Substituting α_+ from Eq.(144) into Eqs.(145-146) I find

$$\sin(p)\left[\frac{2\cos(p)}{\cos(\tilde{\psi})} + 2\alpha_\psi \sin(p)\cos(\tilde{\psi}) - (2\alpha_\varepsilon - \alpha_-)\frac{\tilde{x}+\tilde{y}}{2r}\cos(p)\right] = 0,$$

where I have used the fact that $(\tilde{y}-\tilde{x}) = rp\sin(\tilde{\psi}) + O(p^2)$. Hence, to the first order in p I have

$$\frac{2}{\cos(\tilde{\psi})} + 2\alpha_\psi p\cos(\tilde{\psi}) = 2\alpha_\varepsilon - \alpha_-. \tag{148}$$

Eq.(147) to first order in p gives

$$\alpha_- = -2\alpha_\psi p\cos(\tilde{\psi}). \tag{149}$$

Hence, from Eqs.(148) and (149) I obtain

$$\alpha_\varepsilon = \frac{1}{\cos(\tilde{\psi})}, \tag{150}$$

and from Eqs.(144) and (149) I find

$$\alpha_x = p\frac{\sin(\tilde{\psi})}{\cos(\tilde{\psi})} - \alpha_\psi p\cos(\tilde{\psi}), \tag{151}$$

$$\alpha_y = p\frac{\sin(\tilde{\psi})}{\cos(\tilde{\psi})} + \alpha_\psi p\cos(\tilde{\psi}). \tag{152}$$

The last step is to use Eq.(139), which gives

$$\begin{aligned} 2\alpha_\varepsilon &= \frac{\alpha_x}{\ln(\tilde{x}/x_p)} - \frac{\alpha_y}{\ln(\tilde{y}/y_p)} + \frac{\tilde{x}\alpha_x}{1-\tilde{x}} - \frac{\tilde{y}\alpha_y}{1-\tilde{y}} \\ &= p\frac{\sin(\tilde{\psi})}{\cos(\tilde{\psi})}\left[\frac{1}{\ln(r/x_p)} - \frac{1}{\ln(r/y_p)} + O(p)\right] \\ &- \alpha_\psi p\cos(\tilde{\psi})\left[\frac{1}{\ln(r/x_p)} + \frac{1}{\ln(r/y_p)} + \frac{2r}{1-r} + O(p)\right], \end{aligned}$$

where I have also used Eqs.(151,152).

Taking into account the fact that $[\ln(r/x_p) - \ln(r/\sqrt{x_p y_p})] \sim \rho$ and $[\ln(r/y_p) - \ln(r/\sqrt{x_p y_p})] \sim -\rho$, we find that

$$\alpha_\psi = \frac{-1}{p\cos^2(\tilde{\psi})}\frac{\ln(r/\sqrt{x_p y_p})}{1+2r\tilde{\varepsilon}^2}, \tag{153}$$

and finally

$$\sin(\psi) = \frac{\ln(\sqrt{y_p}/\sqrt{x_p})}{p(1+2r\tilde{\varepsilon}^2)} - \frac{q\ln(r/\sqrt{x_p y_p})}{p\cos(\tilde{\psi})(1+2r\tilde{\varepsilon}^2)}.$$

Since $|\sin(\psi)| \le 1$, fixed point solutions exist only if

$$|\ln(y_p/x_p) - q\frac{\ln(r^2/x_p y_p)}{\cos(\tilde{\psi})}| \le 2p(1+2r\tilde{\varepsilon}^2).$$

Let $G_1^p = G^p + \Delta G^p$ and $G_1^p = G^p + \Delta G^p$, then I obtain the following condition

$$q\frac{G^p + \ln(r)}{\cos(\tilde{\psi})} - p(1+2r\tilde{\varepsilon}^2) \le \Delta G^p \le q\frac{G^p + \ln(r)}{\cos(\tilde{\psi})} + p(1+2r\tilde{\varepsilon}^2). \tag{154}$$

Although the derivation in this section implies that $\alpha_\psi q$ is small, which leads to the requirement $q \ll p$, a direct numerical solution of Eqs.(105-108,113,114) shows that the stable fixed point solution exists if ΔG^p is close enough to $q\frac{G^p+\ln(r)}{\cos(\tilde{\psi})}$, in conformity with condition (154), even when $q \gg p$. This result suggests that unavoidable discrepancies in mode propagation constants can be "compensated" in principle by a proper tuning of the

pumping parameters, G_1^p and G_2^p. In contrast, the weak-link synchronization described in Chapter 3 allows one to avoid fine tuning and still have $q \gg p$.

Now let $\cos(\tilde{\psi}) = 0$, then

$$\sin(\psi) = \pm 1 + O(q^2),$$
$$\cos(\psi) = \mp \alpha_\psi q + O(q^2).$$

Therefore, in this case Eqs(136-139) have no terms of the order less then q^2, which actually means that to first order q

$$\alpha_x = \alpha_y = \alpha_\varepsilon = 0.$$

The last unknown, α_ψ, can be found immediately from Eq.(135):

$$\alpha_\psi = -\frac{2r^2 \sin(p)\cos(p)}{\tilde{x}\tilde{y} - r^2}. \tag{155}$$

Thus,

$$\alpha_\psi = \begin{cases} -\frac{2rp}{y_p - r} & \text{for solution} \quad (x_1, y_1), \\ \frac{2\sqrt{\ln(r/x_p)\ln(r/y_p)}}{\ln(y_p/x_p)} & \text{for solution} \quad (x_2, y_2), \\ -\frac{2rp}{x_p - r} & \text{for solution} \quad (x_3, y_3), \\ \frac{2\sqrt{\ln(r/x_p)\ln(r/y_p)}}{\ln(x_p/y_p)} & \text{for solution} \quad (x_4, y_4). \end{cases}$$

REFERENCES

[1] Kuramoto, D., *Chemical Oscillations, Waves, and Turbulences*. Springer, New York, 1984.

[2] Guckenheimer, J., and Holmes, P., *Nonlinear Oscillations, Dynamical Systems and Bifurcations of Vector Felds*. Springer Verlag, New York, 1983.

[3] Pikovsky, A., Rosenblum, M., and Kurths, J., *Synchronization - A Universal Concept in Nonlinear Sciences*. Cambridge University Press, 2001.

[4] Van der Pol, B., and Van der Mark, J., "Frequency Demultiplication", *Nature*, vol. 120, pp. 363–364, 1927.

[5] Thompson, J. M. T., and Stewart, H. B., *Nonlinear Dynamics and Chaos*. Wiley, Second ed., 2002.

[6] Lakshmana, M., and Murali, K., *Chaos in Nonlinear Oscillators, Controlling and Synchronization*. World Scientific, Singapore, 1996.

[7] Palacios, A., Carretero-González, R., Longhini, P., Renz, N., In, V., Kho, A., Neff, J. D., Meadows, B. K. and Bulsara A. R. "Multifrequency Synthesis Using two Coupled Nonlinear Oscillator Arrays", *to appear in Phys. Rev. E* , 2005.

[8] Buono, P.–L., Golubitsky, M. and Palacios, A., "Heteroclinic Cycles in Rings of Coupled Cells", *Physica D*, vol. 143, pp. 74–108, 2000.

[9] May, R. M., "Biological Populations with Non-overlapping Generations: Stable Points, Stable Cycles and Chaos", *Science*, vol. 186, pp. 645–647, 1974.

[10] Halow, J. S., Boyle, E. J., Daw C. S. and Finney, C. E. A., *PC-based, Near-real-time, 3-dimensional Simulation of Fluidized Beds*. Fluidization IX Durango, Colorado, May, 1998.

[11] Szucs, A., Varona, P., Volkovskii, A. R. , Abarbanel, H. D. I., Rabinovich, M. I. and Selverston, A. I., "Interacting Biological and Electronic Neurons Generate Realistic Oscillatory Rhythms", *Neuroreport*, vol. 11, no. 3, pp. 563–569, 2000.

[12] Meadows, B. K., Heath, T. H., Neff, J. D., Brown, E. A., Fogliatti, D. W., Gabbay, M, In, V., Hasler, P., Deweerth, S. P. and Ditto, W.L. "Nonlinear Antenna Technology", *Proccedings of the IEEE*, vol. 90, no. 5, pp. 882–897, 2002.

[13] Heath, T., "Difference Pattern Beam Steering of Coupled, Nonlinear Oscillator Arrays", *IEEE Microwave Wireless Comp. Lett.*, vol. 11, no. 8, pp. 343–345, 2001.

[14] Heath, T., "Beam shaping of coupled, nonlinear oscillator arrays", *Proc. SPIE–Radar Sensor Technology VI*, vol. 4374, pp. 114-122, 2001.

[15] Carlson, J. M., Langer, J. S. and Shaw, B. E., "Dynamics of Earthquake Faults", *Reviews of Modern Physics*, vol. 66, no. 2, pp. 657–670, 1994.

[16] Ferguson, C. D., Klein, W., and Rundle J. B., "Long Range Earthquake Fault Models", *Computers in Physics*, vol. 12, pp. 34–40, 1998.

[17] Xia, J., Gould, H., and Klein, W., *Simulations of the Burridge-Knopoff Model*. 3rd APEC Cooperation for Earthquake Simulation (ACES) Workshop, Maui, Hawaii, May 2002.

[18] Hähner, P., and Drossinos, Y., "Nonlinear Dynamics of a Continuous Spring-Block Model of Earthquake Faults", *J. Phys. A: Math. Gen.*, vol. 31, pp. L185–L191, 1998.

[19] Burridge, R., and Knopoff, L., "Model and Theoretical Seismicity", *Bull. Seism. Soc. Am.*, vol. 57, pp. 341–371, 1967.

[20] Bak, P., Tang, C., and Wiesenfeld, K., "Self-organized Criticality: An Explanation of the 1/f Noise", *Phys. Rev. Lett.*, vol. 59, pp. 381–384, 1987.

[21] Sornette, D., *Critical Phenomena in Natural Sciences, Chaos, Fractals, Self-organization and Disorder: Concepts and Tools*. Springer Series in Synergetics, 2000,

[22] Epstein, I. R., and Pojman, J. A., *An Introduction to Nonlinear Chemical Dynamics: Oscillations, Waves, Patterns, and Chaos*. Oxford University Press, New York, 1998.

[23] Degn, H., "Effect of Bromine Derivatives of Malonic Acid on the Oscillating Reaction of Malonic Acid, Cerium Ions and Bromate", *Nature*, vol. 213, pp. 589–590, 1967.

[24] Lakshmanan, M., and Muruganandam, P., "Spatiotemporal Patterns in Array of Coupled Nonlinear Oscillators", *PINSA*, vol. 66A, pp. 393–413, 2000.

[25] Zaikin, A. N., and Zhabotinsky A. M., "Concentration Wave Propagation in Two-dimensional Liquid-phase Self-oscillating Systems", *Nature*, vol. 225, pp. 535–537, 1970.

[26] Winfree, A. T., "Spiral Waves of Chemical Activity", *Science*, vol. 175, pp. 634–686, 1972.

[27] Winfree, A. T., "Rotating Chemical reactions", *Sci. Am.*, vol. 230, pp. 82–95, 1974.

[28] Reddy, D.V.R., Sen, A. and Johnston, G. L., "Experimental Evidence of Time-Delay-Induced Death in Coupled Limit-Cycle Oscillators", *Phys. Rev. Lett.*, vol. 85, pp. 3381–3384, 2000.

[29] Ozden, I., Venkataramani, S., Long, M. A. , Connors, B. W., and Nurmikko, A. V., "Strong Coupling of Nonlinear Electronic and Biological Oscillators: Reaching the 'Amplitude Death' Regime", *Phys. Rev. Lett.*, vol. 93, 158102(4), 2004.

[30] Strogatz, S., *Sync: The Emerging Science of Spontaneous Order*. New York: Hyperion, 2003.

[31] Moore-Ede, M. C., Sulzman, F. M. and Fuller C. A., *The Clocks that Time Us: Physiology of the Circadian Timing System*. Harvard University Press, Cambridge, Massachusetts, 1982.

[32] Winfree, A. T, *The Timing of Biological Clocks*. Scientific American Books, 1987.

[33] Glass, L., "Synchronization and Rhythmic Processes in Physiology", *Nature*, vol. 410, pp. 277–284, 2001.

[34] Niijima, S., Takahashi, K., Onishi, M., Arii, N., Saito, M., Kuremoto, K., and Yamashiro, Y., "Clinical electroencephalographic study of nine pediatric patients with convulsion induced by the TV animation, Pocket Monster", *Acta Paediatr. Jpn.*, vol. 40, no. 6, pp. 544–549, 1998.

[35] Enoki, H., Akiyama, T., Hattori, J., and Oka, E., "Photosensitive Fits Elicited by TV Animation: an Electroencephalographic Study", *Acta Paediatr. Jpn.*, vol. 40, no. 6, pp. 626–630, 1998.

[36] Takahashi, T., and Tsukahara, Y., "Pocket Monster incident and low luminance visual stimuli: special reference to deep red flicker stimulation", *Acta Paediatr. Jpn.*, vol. 40, no. 6, pp. 631–637, 1998.

[37] http://epilepsytoronto.org/photo.html

[38] Schechter, B., "Now the Brain Gets Rhythm", *Science*, vol. 274, pp. 339–340, 1996.

[39] Buck, J. B., "Synchronous Rhythmic Flashing of Fireflies", *Quarterly Review of Biology*, vol. 13, pp. 301–314, 1938.

[40] Buck, J. B., "Synchronous Rhythmic Flashing of Fireflies. II", *Quarterly Review of Biology*, vol. 63, pp. 265–289, 1988.

[41] Michaels, D. C., Matyas, E. P., and Jalife, J., "Mechanisms of Sinoatrial Pacemaker Synchronization: A New Hypothesis", *Circulation Research*, vol. 61, pp. 704-714, 1987.

[42] Goles, E., Schulz, O., and Markus, M., "Prime Number Selection of Cycles in a Predator-prey Model", *Complexity*, vol. 6, pp. 33-38, 2001.

[43] Backwell, P. R. Y., Jennions, M. D., Passmore, N. I. and Christy, J.H., "Synchronous Waving in a Fiddler Crab", *Nature*, vol. 391, pp. 31–32, 1998.

[44] McClintock, M. K., "Menstrual Synchrony and Suppression", *Nature*, vol. 229, pp. 244–245, 1971.

[45] Russel, M. J., Switz, G.M. and Thompson, K., "Olfactory Influences on the Human Menstrual Cycle", *Pharm. Biochem. Behav.*, vol. 13, pp. 737–738, 1980.

[46] Stern, K., and McClintock, M. K., "Regulation of Ovulation by Human Pheromones", *Nature*, vol. 392, pp. 177–179, 1998.

[47] Bennett, M., Schatz, M. F., Rockwood, H. and Wiesenfeld, K., "Huygens's Clock", *Proc. R. Soc. Lond. A*, vol. 458, pp. 563–579, 2002.

[48] Klarreich, E., "Huygens's Clock Revisited", *Am. Sci.*, vol. 90, pp. 322–323, 2002.

[49] Rayleigh, L., *The Theory of Sound*. Dover Publishers, Mew York, 1945.

[50] Eccles, W.H., and Vincent, J.H., *British Patent Spec. clxiii.* p. 462, 1920.

[51] Appleton, E. V., "The Automatic Synchronization of Triode Oscillator", *Proc. Cambridge Phil. Soc. (Math. and Phys. Sci)*, vol. 21, pp. 231–248, 1922.

[52] Van der Pol, B., "Forced Oscillations in a Circuit with Non-linear Resistance. (Reception with Reactive Triod)", *Phil. Mag.*, vol. 3, pp. 64–80, 1927.

[53] Milonni, P. W., and Eberly, J.H., *Lasers.* Wiley-Interscience, New York, 1988.

[54] Bardeen, J., Cooper, L. N., and Schrieffer, J. R., "Theory of Superconductivity", *Phys. Rev.*, vol. 108, pp. 1175–1204, 1957.

[55] Clarke, J., "SQUIDs", *Sci. Am.*, vol. 271, pp. 46–53, 1994.

[56] Bergen, A. R., *Power Systems Analysis.* Prentice-Hall, 1986.

[57] Overbye, T. J., "Reengineering the Electric Grid", *Am. Sci.*, vol. 88, pp. 220–229, 2000.

[58] Bergquist, J. C., Jefferts, S. R., and Wineland, D. J., "Time Measurement at the Millennium", *Phys. Today*, vol. 54, no. 3, pp. 37–42, 2001.

[59] Hering, T. A., "The Global Positioning System", *Sci. Am.*, vol. 274, pp. 44–50, 1996.

[60] Josephson, B. D., "Possible New Effects in Superconductive Tunnelling", *Phys. Lett.*, vol. 1, pp. 251–253, 1962.

[61] Josephson, B. D., "The Discovery of Tunneling Supercurrents", *Science*, vol. 184, pp. 527–530, 1974.

[62] Anderson, P. W., "How Josephson Discovered His Effect", *Phys. Today*, vol. 23, pp. 23–28, 1970.

[63] Golubov, A. A., Kuprianov, M. Yu., and Il'ichev, E., "The Current-phase Relation in Josephson Junctions", *Rev. Mod. Phys.*, vol. 76, pp. 411–470, 2004.

[64] Anderson, P. W., and Rowell, J. M., "Probable Observation of Josephson Superconducting Tunneling Effect", *Phys. Rev. Lett.*, vol. 10, pp. 230–322, 1963.

[65] Likharev, K. K., *Dynamics of Josephson Junctions and Circuits.* Gordon and Breach, New York, 1986.

[66] Feynman, R. P., Leighton, R. B. and Sands, M., *The Feynman Lectures on Physics, Volume III: Quantum Mechanics.* Addison-Wesley, 1965.

[67] Van Duzer, T., and Turner, C. W., *Principles of Superconductive Devices and Circuits.* Elsevier North Holland, Second Edition, 1999.

[68] Josephson, B. D., *Weakly Coupled Superconductors.* Superconductivity, Vol. 1 (Parks, R. D. ed.), Marcel Dekker, 1969.

[69] Tinkham, M., *Introduction to Superconductivity.* McGraw-Hill, New York, 1975.

[70] Ambegaokar, V., and Baratoff, A., "Tunneling Between Superconductors", *Phys. Rev. Lett.*, vol. 11, p. 104, 1963.

[71] Zappe, H. H., "Memory Cell Design in Josephson Technology", *IEEE Trans. Electron Devices*, vol. ED-27, pp. 1870–1882, 1980.

[72] Kohlmann, J., Behr, R., and Funck, T., "Josephson voltage standards", *Meas. Sci. Technol.*, vol. 14, pp. 1216–1228, 2003.

[73] Likharev, K. K., and Semenov, V. K., "RSFQ logic/memory family: A new Josephson-junction technology for sub-terahertz-clock-frequency digital systems", *IEEE Trans. on Appl. Supercond.*, vol. 1, pp. 3–28, 1991.

[74] Nakajima, K., Mizusawa, H., Sugahara, H., and Sawada, Y., "Phase mode Josephson computer system", *IEEE Trans. on Appl. Supercond.*, vol. 1, pp. 29–36, 1991.

[75] Kadin, A. M., "Duality and fluxonics in superconducting devices", *J. Appl. Phys.*, vol. 68, no. 11, pp. 5741–5749, 1990.

[76] Ciria, J. C., Pacetti, P., Paoluzi, L., and Giovannella, C., "Photofluxonic Detection in Ladders and 2D Arrays of Josephson Junctions", *Nucl. Inst. and Meth. in Phys. Res. A*, vol. 370, pp. 128–130, 1996.

[77] Mygind, J., and Pedersen, N. F., "Microwave radiation from superconducting arrays of Josephson junctions", *Macroscopic Quantum Phenomena and Coherence in Superconducting Networks*, (Giovanella, C. and Tinkham, M., eds.), pp. 339–350, Singapore: World Scientific, 1995.

[78] Davidson, B. A., Granata, V., Sarnelli, E., and Pagano, S., "Dynamic properties of asymmetric discrete vortex-flow transistors", *Supercond. Sci. Technol.*, vol. 12, pp. 970-973, 1999.

[79] Winfree, A. T., "Biological Rhythms and the Behavior of Populations of Coupled Oscillators", *J. Theor. Biol.*, vol. 16, pp. 15–42, 1967.

[80] Kuramoto, Y., *International Symposium on Mathematical Problems in Theoretical Physics*. Lecture Notes in Physics, Vol. 39, p. 420 (Arakai, H., ed.), Springer, 1975.

[81] Strogatz, S. H., *Norbert Wiener's brain waves, in Frontiers in Mathematical Biology*. Lecture Notes in Biomathematics Vol. 100, pp. 122–138 (Levin, S.A., ed.), Springer, 1994.

[82] Strogatz, S. H., "From Kuramoto to Crawford: Exploring the Onset of Synchronization in Populations of Coupled Oscillators", *Physica D*, vol. 143, pp. 1–20, 2000.

[83] Wiesenfeld, S. H., Colet, P, and Strogatz, S. H., "Synchronization Transitions in a Disordered Josephson Series Array", *Phys. Rev. Lett.*, vol. 76, no. 3, pp. 404–407, 1996.

[84] Hadley, P., and Beasley, M. R., "Dynamical States and Stability o Linear Arrays of Josephson Junctions", *Appl. Phys. Lett.*, vol. 50, no. 10, pp. 621–623, 1987.

[85] Wiesenfeld, S. H., Benz, S.P., and Booi, P. A. A., "Phase-locked Oscillator Optimization for Arrays of Josephson Junctions", *J. Appl. Phys.*, vol. 76, no. 6, pp. 3835–3846, 1994.

[86] Wiesenfeld, S. H., and Swift, J. W., "Averaged Equations for Josephson Junction Series Arrays", *Phys. Rev. E*, vol. 51, no. 2, pp. 1020–1025, 1995.

[87] Schwartz, I. B., and Tsang, K. Y., "Antiphase Switching in Josephson Junction Arrays", *Phys. Rev. Lett.*, vol. 73, no. 21, pp. 2797–2800, 1994.

[88] Nichols, S., and Wiesenfeld, K., "Ubiquitous Neutral stability of Splay-phase States", *Phys. Rev. A*, vol. 45, no. 12, pp. 8430–8435, 1992.

[89] Chandra, P., and Ioffe, L. B., "A superconducting associative memory that is defect tolerant", *J. Phys.: Condens. Matter*, vol. 13, no. 29, pp. L697–L703, 2001.

[90] Tsang, K. Y., Mirollo, R. E., Strogatz, S. H., and Wiesenfeld, K., "Dynamics of a Globally Coupled Oscillator Array", *Physica D*, vol. 48, pp. 102–112, 1991.

[91] Hadley, P., Beasley, M. R., and Wiesenfeld, K., "Phase Locking of Josephson Junction Arrays", *Appl. Phys. Lett.*, vol. 52, pp. 1619–1621, 1988.

[92] Chernikov, A., and Schmidt, G., "Adiabatic Chaos in Josephson-junction Arrays", *Phys. Rev. E*, vol. 50, no. 5, pp. 3436–3445, 1994.

[93] Watanabe, S., and Strogatz, S. H., "Constants of Motion for Superconducting Josephson Arrays", *Physica D*, vol. 74, pp. 197–253, 1994.

[94] Jain, A. K., Likharev, K. K., Lukens, J. E., and Sauvegau, J. E., "Mutual Phase-locking in Josephson Junction Arrays", *Phys. Rep.*, vol. 109, no. 6 pp. 309–426, 1984.

[95] Chernikov, A., and Schmidt, G., "Conditions for Synchronization in Josephson-junction Arrays", *Phys. Rev. E*, vol. 52, no. 4, pp. 3415–3419, 1995.

[96] Olyslager, F., *Electromagnetic Wavequides and Transmission Lines.* Clarendon, Oxford, 1999.

[97] Wadell, B. C., *Transmission Line Design Handbook.* Artech House, Boston, 1991.

[98] *Encyclopædia Britanica.* vol. 21, pp. 764-771, Benton, Chicago, 1967.

[99] Nahin, P. J., *Oliver Heaviside: Sage in Solitude, the life, Work and Times of an Electrical Genius of the Victorian Age.* IEEE Press, New York, 1988.

[100] Maxwell, J. C., *A Treatise on Electricity and Magnetism.* vol. 1 & 2, Third Edition, Dover Publications, 1954.

[101] Denniston, F. J., and Runge, P. K., "The Glass Necklace [FLAG Submarine Fibre-optic Link]", *IEEE Spectrum*, vol. 32, pp. 24–27, 1995.

[102] Cawthorne, A. B., Barbara, P., Shitov, S. V., Lobb. C. J., Wiesenfeld, K. and Zangwill, A., "Synchronized oscillations in Josephson Junction arrays: the Role of Distributed Coupling", *Phys. Rev. B*, vol. 60, no. 10, pp. 7575–7578, 1999.

[103] Barbara, P., Cawthorne, A. B., Shitov, S. V., and Lobb. C. J., "Stimulated Emission and Amplification in Josephson Junction Arrays", *Phys. Rev. Lett.*, vol. 82, no. 9, pp. 1963–1966, 1999.

[104] Vasilić, B., Shitov, S. V., Lobb. C. J., and Barbara, P., "Josephson-junction Arrays as High-efficiency Sources of Coherent Millimeter-wave Radiation", *Appl. Phys. Lett.*, vol. 78, no. 8, pp. 1137–1139, 2001.

[105] Almaas, E., and Stroud, D., "Theory of Two-Dimensional Josephson Arrays in a Resonant Cavity", *Phys. Rev. B*, vol. 67, 064511(12), 2003.

[106] Blackburn, J. A., Smith, H. J. T., and Gronbech-Jensen, N., "Resonant Steps in the Characteristics of a Josephson Junction Coupled to a Transmission Line", *J. Appl. Phys.*, vol. 70, no. 4, pp. 2395–2401, 1991.

[107] Smith, H. J. T., Blackburn, J. A., and Gronbech-Jensen, N., "Dynamical Properties of Josephson Junctions Coupled by a Transmission Line", *J. Appl. Phys.*, vol. 74, no. 8, pp. 5101–5107, 1993.

[108] Han, S., Bi, B., Zhang, W. and Lukens, J. E., "Demonstration of Josephson Effect Submillimeter Wave Sources with Increased Power", *Appl. Phys. Lett.*, vol. 64, no. 11, pp. 1424–1426, 1994.

[109] Booi, P. A. A., and Benz, S. P., "High Power Generation with Distributed Josephson-junction Arrays", *Appl. Phys. Lett.*, vol. 68, no. 26, pp. 3799–3801, 1996.

[110] Gronbech-Jensen, N., Parmentier, R. D., and Pedersen, N. F., "Phase-locking of Fluxon Oscillations in Long Josephson Junctions Coupled Through a Resonator", *Phys. Lett. A*, vol. 142, pp. 427–430, 1989.

[111] Filatrell, G., Rotoli, G., Gronbech-Jensen, N., Parmentier, R. D., and Pedersen, N. F., "Model Studies of Long Josephson Junction Arrays Coupled to a High-Q Resonator", *J. Attl. Phys.*, vol. 72, no. 7, pp. 3179–3185, 1992.

[112] Bennett, M., and Wiesenfeld, K., "Averaged Equations for Distributed Josephson Junction Array", *Physica D*, vol. 192, pp. 196–214, 2004.

[113] Tsygankov, D., and Wiesenfeld, K., "Spontaneous Synchronization in a Josephson Transmission Line", *Phys. Rev. E*, vol. 66, 036215(9), 2002.

[114] Dhamal, M., and Wiesenfeld, K., "Generalized Stability Law for Josephson Series Arrays", *Phys. Lett. A*, vol. 292, pp. 269–274, 2002.

[115] York, R. A., "Nonlinear Analysis of Phase Relationships in Quasi-optical Oscillator Arrays", *IEEE Trans. Microwave Theory Tech., special issue on quasi-optical techniques*, vol. MTT-41, pp. 1799–1809, 1993.

[116] York, R. A., and Itoh, T., "Injection- and Phase-locking Techniques for Beam Control", *IEEE Trans. Microwave Theory Tech.*, vol. 46, pp. 1920–1929, 1998.

[117] Heath, T., Wiesenfeld, K., and York, R. A., "Manipulated Synchronization: Beam Steering in Phased Arrays", *Int. J. Bifurcation Chaos Appl. Sci. Eng.*, vol. 10, no. 11, pp. 2619–2627, 2000.

[118] Pogorzelski, R. J., "A Two-dimensional Coupled Oscillator Array", *IEEE Trans. Microwave Guided Wave Lett.*, vol. 10, pp. 478–480, 2000.

[119] Pogorzelski, R. J., "Experimental Confirmation of the Dynamics of Coupled-oscillator Arrays and Implications for Angle-based Modulation", *IEEE Trans. Microwave Theory Tech.*, vol. 10, no. 1, pp. 143–149, 2002.

[120] Tsygankov, D., and Wiesenfeld, K., "Spontaneous Formation of Inert Oscillator Pairs", *Phys. Lett. A*, vol. 325, pp. 51–56, 2004.

[121] Kaneko, K., "Clustering, Coding, Switching, Hierarchical Ordering, and Control in a Network of Chaotic Elements", *Physica D*, vol. 41, pp. 137–172, 1990.

[122] Li, Y.-X., "Clustering in Neural Networks with Heterogeneous and Asymmetrical Coupling Strengths", *Physica D*, vol. 180, pp. 210–234, 2003.

[123] Maza, D., Boccaletti, S., and Mancini, H., "Phase Clustering and Collective Behaviors in Globally Coupled Map Lattices due to Mean Field Effects", *Int. J. Bifurcation Chaos Appl. Sci. Eng.*, vol. 10, no. 4, pp. 829–833, 2000.

[124] France, P. W., *Optical Fibre Lasers and Amplifiers*. Blackie, Glasgow, 1991.

[125] Hecht, J., *The Laser Guidebook*. Second Edition, McGraw-Hill, New York, 1992.

[126] Koester, C.J., and Snitzer, E., "Amplification in a Fiber Laser", *Appl. Optics*, vol. 3, no. 10, pp. 1182–1186, 1964.

[127] Snell, G., "An Introduction to Fiber Optics and Broadcasting, tutorial", *SMPTE J.*, vol. 105, no. 4, 1996.

[128] Fermann, M. E., Galvanauskas, A., Sucha, G., and Harter, D., "Fiber-lasers for Ultrafast Optics", *Appl. Phys. B*, vol. 65, pp. 259–275, 1997.

[129] Nelson, L. E., Jones, D. J., Tamura, K., Haus, H. A. and Ippen, E. P., "Ultrashort-puls fiber ring lasers", *Appl. Phys. B*, vol. 65, pp. 277–294, 1997.

[130] Waarts, R. G., Makki, S., and Yuan, J., "Fiber Lasers at JDS Uniphase", *Proc. of SPIE*, vol. 5335, pp. 217–228, 2004.

[131] Durvasula, L. N., ed., "Advances in Fiber Lasers", *Proc. of SPIE* vol. 4974, 2003.

[132] Wang, S. S., and Winful, H. G., "Dynamics of phase-locked semiconductor laser arrays", *Appl. Phys. Lett.*, vol. 52, no. 21, pp. 1774–1778, 1988.

[133] Mehuys, D., Mitsunaga, K., Eng, L., Marshall, W.K., and Yariv, A., "Supermode Control in Diffraction-coupled semiconductor Laser Array", *Appl. Phys. Lett.*, vol. 53, no. 13, pp. 1165–1167, 1988.

[134] Winful, H. G., and Wang, S. S., "Stability of Phase Locking in Loupled Semiconductor Laser Arrays", *Appl. Phys. Lett.*, vol. 53, no. 20, pp. 1894–1896, 1988.

[135] Roy, R., Murphy, T. W., Jr., Maier, T. D., and Gills, Z., "Dynamical Control of a Chaotic Laser: Experimental Stabilization of a Globally Coupled System", *Phys. Rev. Lett.*, vol. 68, no. 9, pp. 1259–1262, 1992.

[136] Colet, P., Roy, R., and Wiesenfeld, K., "Controlling Hyperchaos in a Multimode Laser Model", *Phys. Rev. E*, vol. 50, no. 5, pp. 3453–3457, 1994.

[137] Braiman, Y., Kennedy, T.A.B., Wiesenfeld, K., and Khibnik, A., "Entrainment of Solid-State Laser Arrays", *Phys. Rev. A*, vol. 52, no. 2, pp. 1500–1506, 1995.

[138] Thornburg, K. S., Jr., Möller, M., Roy, R., Carr, T. W., Li, R.-D., and Erneux, T., "Chaos and Coherence in Coupled Lasers", *Phys. Rev. E*, vol. 55, no. 4, pp. 3865–3869, 1997.

[139] Terry, J. R., Thornburg, K. S., De Shazer, D. J., Van Wiggeren, G. D., Zhu, S., Ashwin, P., and Roy, R., "Synchronization of Chaos in an Array of Three Lasers", *Phys. Rev. E*, vol. 59, no. 4, pp. 4036–4043, 1999.

[140] Kozlov, V. A., Hernandez-Cordero, J., and Morse, T. F., "All-fiber Coherent Beam Combining of Fiber Lasers", *Optics. Lett.*, vol. 24, no. 2, pp. 1814–1816, 1999.

[141] Lewis, C. T., Aberbanel, H. D. I., Kennel, M. B., Buhl, M., and Illing, L., "Synchronization of Chaotic Oscillations in Doped Fiber Ring Lasers", *Phys. Rev. E.*, vol. 63, 016215(15), 2001.

[142] Choma, M. A., Yang, C., and Izatt, J. A., "Instantaneous Quadrature Low-coherence Interferometry with 3x3 Fiber-optic Couplers", *Optics. Lett.*, vol. 28, no. 22, pp. 2162–2164, 2003.

[143] Cheo, P. K., Liu, A., and King, G. G., "A high-brightnees Laser Beam from a Phase-locked multicore Yb-doped Fiber Laser Array", *IEEE Photon. Tech. Lett.*, vol. 13, no. 5, pp. 439–441, 2001.

[144] Shirakawa, A., Saitou, T., Sekiguchi, T., and Ueda, K.-I., "Coherent Addition of Fiber Lasers by Use of a Fiber Coupler", *Optics Express*, vol. 10, no. 21, pp. 1167–1172, 2002.

[145] Sabourdy, D., Kermène, V., Desfargas-Berthelomot, A., Lefort, L., Barthélémy, A, Mahodaux, C, and Pureur, D., "Power Scaling of fiber Lasers with All-fibre interferometric Cavity", *Electronics Lett.*, vol. 38, no. 14, pp. 692–693, 2002.

[146] Bochove, E. J., Cheo, P. K., and King, G. G., "Self-orgaization in a Multicore Fiber Laser Array", *Optics Lett.*, vol. 28, no. 14, pp. 1200–1202, 2003.

[147] Huo, Y., Cheo, P. K., and King, G. G., "Fundamental Mode Operation of a 19-core Phase-locked Yb-doped Fiber", *Optics Express*, vol. 12, no. 25, pp. 6230–6239, 2004.

[148] Minden, M. L., Bruesselbach, H., Rogers, J. L., Mangir, M. S., Jones, D. C., Dunning, G. J., Hammon, D. L., Solis, A. J., and Vaughan, L., "Self-organized Coherence in Fiber Laser Arrays", *Proc. SPIE*, vol. 5335, pp. 89–97, 2004.

[149] Rogers, J. L., Peleš, S., and Wiesenfeld, K., "Dynamics of High Gain Fiber Laser Arrays", *IEEE J. Quant. Electr.*, vol. 41, no. 6, pp. 767–773, 2005.

[150] Peleš, S., Rogers, J. L., and Wiesenfeld, K., "Synchrony in Fiber Laser Arrays", *preprint*, 2005.

[151] Snyder, A. W., and Love, J. D., *Optical Waveguide Theory.* Chapman and Hall, New York, 1983.

[152] Sigman, A. E., *Lasers.* University Science Books, Mill Valley, 1986.

[153] Huang, W. P., "Coupled-mode Theory for Optical Waveguides: an Overview", *J. Opt. Soc. Am. A*, vol. 11, no. 3, pp. 963–983, 1994.

[154] Engan, H. E., "Analysis of Polarization-mode Coupling by Acoustic Torsional Waves in Optical Fiber", *J. Opt. Soc. Am. A*, vol. 13, no. 1, pp. 112–117, 1996.

[155] Shama, Y., Hardy, A. A., and Marom, E., "Multimode Coupling of Unidentical Waveguides", *J. Lightwave Tech.*, vol. 7, no. 2, pp. 420–425, 1989.

[156] Hardy, A., and Streifer, W., "Coupled Modes of Multiwaveguide Systems and Phase Arrays", *J. Lightwave Tech.*, vol. LT-4, no. 1, pp. 90–99, 1986.

[157] Donnelly, J. P., Haus, H. A., and Molter, L. A., "Cross Power and Crosstalk in Waveguide Couplers", *J. Lightwave Tech.*, vol. 6, no. 2, pp. 257–268, 1988.

[158] Jan, H.-T., Chi, S., and Yeh, P., "Theory of Mode Coupling in a Photorefractive Crystal Waveguide", *J. Opt. Soc. Am. B*, vol. 17, no. 7, pp. 176–182, 2000.

[159] Marcuse, D., *Theory of Dielectric Optical Waveguides.* Academic Press, Second Edition, 1991.

[160] Pierce, J. R., "Coupling of Modes of Propagation", *J. Appl. Phys.*, vol. 25, no. 2, pp. 179–183, 1954.

[161] Miller, S. E., "Coupled Wave Theory and Waveguide Applications", *Bell. Syst. Tech. J.*, vol. 33, pp. 661–719, 1954.

[162] Schelkunoff, S. A., "Conversion of Maxwell's Equations into Generalized Telegraphist's Equations", *Bell. Syst. Tech. J.*, vol. 34, pp. 995–1043, 1955.

[163] Haus, H. A., "Electron beam waves in microwave tubes", *Proc. Symp. Electronic Waveguides*, Polytechnic Institute of Brooklyn, April 8-10, 1958.

[164] Kogelnik, H., "Switched Directional Couplers with Alternating $\Delta\beta$", *IEEE J. Quant. Electr.*, vol. QE-12, pp. 396–401, 1976.

[165] Kogelnik, H., and Shank, C. U., "Coupled-wave Theory of Distributed Feedback Lasers", *J. Appl. Phys.*, vol. 43, pp. 2327–2335, 1972.

[166] Tsygankov, D., and Wiesenfeld, K., "Weak-link Synchronization", *submitted to Phys. Rev. E.*, 2005.

[167] Strogatz, S. H., *Nonlinear Dynamics and Chaos: with Applications to Physics, Biology, Chemistry and Engineering.* Reading, MA: Perseus Books, Cambridge MA., 1994.